Thermal comfort in non-uniform environments: real-time coupled CFD and human thermal-regulation modelling

by
Francesco Babich

A Doctoral Thesis

Submitted in partial fulfilment of the requirements for the award of
Doctor of Philosophy of Loughborough University

August 2017

© by Francesco Babich 2017

Acknowledgements

This study was financially supported by the Engineering and Physical Sciences Research Council (EPSRC) as part of the activities carried out by the London-Loughborough Centre for Doctoral Training in Energy Demand, a partnership between University College London (UCL) and Loughborough University, for what the author expresses his gratitude.

The author would like to thank the supervisors and mentors Professors Malcolm Cook and Dennis Loveday, from Loughborough University (Loughborough, UK), for their availability and guidance during the development of this PhD research.

Ahmedabad, India - March 2016 (From the left: Dennis Loveday, Francesco Babich, Malcolm Cook).

Then, Professor Rajan Rawal and Mr. Yash Shukla from CEPT University (Ahmedabad, India), and Dr. Paul Cropper from De Montfort University (Leicester, UK) have to be mentioned and acknowledged for their support and collaboration throughout this PhD research, as demonstrated by our joint publications (including the paper pre-

sented at IBPSA Italy conference in February 2017, which won the "best conference paper" award).

This PhD research was closely linked with a wider research project that involved Loughborough University, University of California Berkeley (Berkeley, USA), CEPT University and De Montfort University (UK), and was led by Professor Dennis Loveday. The author would like to thank all the researchers and academics from these institutions that contributed to this research with advices, and with support during the visits in India and the USA. This includes Dr. Lynda Webb (Loughborough University), Ms. Sanyogita Manu, Dr. Keyur Valodaria, Ms. Purnima Verma (CEPT University), Dr. Hui Zhang, Professors Edward Arens and Gail Brager, and Dr. Veronika Földvary (University of California Berkeley).

Lastly, for their irreplaceable administrative support, the author would like to thank Mrs. Karen Holmes and Mrs. Karen Chadwick from Loughborough University.

Abstract

Energy consumption in buildings contributes more greenhouse gas emissions than either the industrial or transportation sectors, primarily due to space cooling and heating energy use, driven by the basic human need for thermal comfort and good indoor air quality. In recent years, there has been a proliferation of air conditioning in both residential and commercial buildings especially in the developing economic areas of the world, and, due to the warming climate and the growing disposable income in several densely populated developing countries, the energy demand for space cooling is dramatically increasing.

Although several previous studies focused on thermal comfort, there are only a few works on asymmetrical environments or transient conditions, such as those expected when mixed mode ventilation or other low energy techniques such as elevated air movement generated by ceiling fans are adopted in the residential sector. Moreover, even fewer studies addressed the accuracy of computer predictions of human thermal comfort in non-uniform environmental conditions. However, focusing on non-uniform thermal environments is important because the space conditioning systems that generate them are often likely to be less energy consuming than those which provide more homogeneous conditions. This is due to the fact that these less energy-intensive space conditioning systems tend to condition the occupants, and not the entire room.

The aim of this research was to investigate human thermal comfort in non-uniform transient environmental conditions, focusing in particular on the capability of predicting human thermal comfort in such conditions in residential buildings. Furthermore,

this research investigated the energy savings that can be achieved in residential buildings when the same level of thermal comfort is delivered using less conventional, but lower-energy, approaches.

In this research, a combination of computer based modelling, experimental work in controlled environments, and data from field studies was used. Computer modelling comprised CFD coupled with a model of human thermal physiology and human thermal comfort, and dynamic thermal modelling. In the experimental work, environmental chambers were used to collect data to validate the coupled CFD model. The data from field studies on real domestic buildings in India and in the UK was used to identify the most relevant configurations to be modelled using the coupled system.

This research led to three main conclusions concerning thermal comfort in non-uniform environments: (i) the coupled model is able to predict human thermal comfort in complex non-uniform indoor configurations, as long as the environment around the human body is accurately modelled in CFD, and is superior to the traditional PMV model as both temporal and spatial variation and non-uniform conditions can be taken into account; (ii) dynamic thermal simulation completed using a dynamic cooling set-point showed that the energy demand for space cooling can be reduced by as much as 90% in mixed mode buildings by using ceiling fans, without jeopardising occupants' thermal comfort; and (iii) the accurate and validated transient three-dimensional CFD model of a typical Indian ceiling fan developed in this research can be used for any study that requires the air flow generated by a ceiling fan to be modelled in CFD.

List of publications

Publications - main contributor:

- Babich F, Cook M, Loveday D and Cropper P. 2016. "Numerical modelling of thermal comfort in non-uniform environments using real-time coupled simulation models". In: Proceedings of Building Simulation and Optimisation 2016: 3rd IBPSA-England Conference. Newcastle upon Tyne. 4-11.

- Babich F, Cook M, Loveday D, Rawal R and Shukla Y. 2017. "A new methodological approach for estimating energy savings due to air movement in mixed mode buildings". In: Proceedings of Building Simulation Applications 2017: 3rd IBPSA-Italy conference. Bolzano. 1-8.

- Babich F, Cook M, Loveday D, Rawal R and Shukla Y. 2017. "Transient three-dimensional CFD modelling of ceiling fans". Building and Environment. 123:37-49.

Other publications:

- Loveday D, Webb L, Verma P, Cook M, Rawal R, Valodaria K, Cropper P, Brager G, Zhang H, Foldvary V, Arens E, Babich F, Cobb R, Ariffin R, Kamm S and Toledo L. 2016. "The role of air motion for providing thermal comfort in residential/mixed mode buildings: a multi-partner global innovation initiative (GII) project". In: proceedings of 9th Windsor Conference Making Comfort Relevant NCEUB. 947-962.

All publications are freely available (open access), and can be downloaded using the following link to Google Scholar: https://scholar.google.com/citations?user=pKIwzgMAAAAJ&hl=it

Index

List of Figures xiv

List of Tables xx

List of Abbreviations xxii

1 INTRODUCTION **1**

1.1 Background and context 1

1.2 Research hypothesis, aim and objectives 3

1.3 Structure of the thesis 5

2 LITERATURE REVIEW **7**

2.1 Introduction and international standards 7

2.1.1 Thermal comfort 7

2.1.2 International standards on thermal comfort 10

2.2 Field studies based research 11

2.2.1 Non-domestic buildings 11

2.2.2 Domestic buildings 15

2.3 Physical and numerical models 19

2.3.1 Environmental chamber studies 19

2.3.2 Biophysical principles of fan use 23

2.3.3 Human thermal regulation models 27

2.3.4 Computational fluid dynamics modelling 32

2.3.5 Dynamic thermal modelling 44

2.4 Justification for the research 46

3 INITIAL TESTING OF THE COUPLED SYSTEM: ENVIRONMENTAL CHAMBER STUDY 48

3.1 Overview of the experimental chapters 48

3.1.1 CFD and IESD-Fiala coupled model: key features 49

3.2 Initial testing of the coupled system: environmental chamber study . 51

3.2.1 Experimental set-up 52

3.2.2 Modelling approach and assumptions 56

3.3 Results and discussion 65

3.3.1 CFD models validation 65

3.3.2 Required computational power 70

3.3.3 Thermal comfort results 71

3.3.4 Heat transfer and air movement: how the coupled system models the variations of convective and evaporative heat transfer due to air speed changes 74

3.4 Summary 78

4 CEILING FAN CFD MODEL 81

4.1 Identification of suitable realistic residential indoor scenarios in the UK and in India 82

4.2 Indian ceiling fan CFD model: methodology 86

4.2.1 Experimental set-up 86

4.2.2 Modelling approach and assumptions 89

4.2.3 Model validation - criteria for agreement 94

4.3 Results and discussion 95

4.3.1 Qualitative analysis of the air flow generated by the ceiling fan 95

4.3.2 Quantitative validation of the CFD model 99

4.3.3 The importance of the choice of the turbulence model 103

4.3.4 Required computational power 106
4.3.5 Usability of the developed model 107
4.4 Summary 109

5 APPLICATION OF THE COUPLED SYSTEM TO REAL DOMESTIC BUILDINGS 112

5.1 Methodology 113
5.1.1 Modelling approach and assumptions 113
5.1.2 Development of an "Indian sari" clothing for the IESD-Fiala model 120
5.2 Results and discussion 123
5.2.1 CFD results: air flow generated in the room by ceiling fans . 123
5.2.2 Thermal comfort results 129
5.2.3 Required computational power 136
5.3 Summary 138

6 ESTIMATE OF THE POTENTIAL ENERGY SAVINGS IN A TYPICAL INDIAN HOUSE 141

6.1 Methodology 142
6.1.1 Cooling set-point definition 142
6.1.2 Dynamic cooling set-point implementation 144
6.1.3 The case study building 145
6.1.4 Extension of the analysis to other locations in India 148
6.2 Results and discussion 153
6.2.1 Effect of using air temperature or operative temperature . . . 154
6.2.2 Energy savings - Ahmedabad 158
6.2.3 Energy savings - extension of the analysis to Mumbai, Delhi, and Bangalore 161
6.3 Summary 167

7 CONCLUSIONS **169**

7.1 Key findings of this research and contribution to knowledge 170

7.2 Wider significance of this research: impact on academia, industry, and policy 173

7.3 Limitations of this research 175

References **178**

List of Figures

2.1 Overall air movement preference and air velocity range (Cândido et al., 2010). 14

2.2 Draught chart developed by Fanger and Christensen (1986). 20

2.3 Bidirectional comfort scale (Zhang et al., 2010b), which has been adopted in most recent research at University of California, Berkeley (UCB). 21

2.4 Overall thermal sensation vs. comfort (Zhang et al., 2010b). 21

2.5 Thermal sensation votes for optional (user selected) air speed (Huang et al., 2013). 22

2.6 Relationship between TSV and SET* in different experiments (Huang et al., 2014). 23

2.7 Thermal Interaction of Human Body and Environment (ASHRAE, 2013b). 24

2.8 Schematic diagram of the model developed by Wissler (1964) 28

2.9 Diagram of the model developed by Stolwijk and Hardy (1966) . . . 29

2.10 A schematic diagram of the passive system (Fiala et al., 1999). . . . 31

2.11 Process of achieving a reliable CFD model of indoor environment (Hajdukiewicz et al., 2013a). 33

2.12 Comparison between simulated and measured values (Hajdukiewicz et al., 2013b). 34

2.13 A schematic diagram of the information exchange between the two models. 35
2.14 The clothed body geometry within the CFD mesh (Cropper et al., 2010). 36

3.1 The experimental facilities. 52
3.2 The experimental facilities. In brackets, the measured quantities in each location (with Dantec, air temperature and air speed were measured at three heights, namely 0.1 m, 0.6 m, and 1.1 m from the floor). 53
3.3 Position of U12 Hobo sensors (Onset, 2015) during the preliminary measurements. 54
3.4 Shell mesh. 57
3.5 Volume mesh. 57
3.6 Detailed volume mesh close to Victoria's head. 57
3.7 Configuration without fan: simulated and measured air temperatures. 66
3.8 Configuration without fan: air temperature field. 66
3.9 Configuration with fan: simulated and measured air speeds. 67
3.10 Configuration with fan: air speed field. 69
3.11 Configuration with fan: simulated and measured air temperatures. . . 69
3.12 Configuration with fan: air temperature field. 69
3.13 Configuration without fan: DTS and PPD. 72
3.14 DTS with and without the fan. 73
3.15 DTS with different fan status: always off ("no fan"), always on ("simulation 3"), and on only in the second half of the simulation ("simulation 5"). 74
3.16 Convective heat transfer coefficient with the fan switched off (time 0 to 300), and then on (time 301 to 600) (data from "simulation 5"). . 76
3.17 Virtual manikin surface moisture mass fraction - with the fan (data from "simulation 3"). 77

3.18 Virtual manikin surface moisture mass fraction - without the fan (data from "simulation - no fan"). 77

4.1 Detailed thermal comfort measurements using the Dantec Comfort-Sense kit (Dynamics Dantec, 2015) in one of the UK houses. 83
4.2 Indian participants in their drawing room. 85
4.3 Drawing room with three ceiling fans. 85
4.4 Environmental chamber at CEPT University, Ahmedabad, India. . . . 87
4.5 Plan view of the environmental chamber with the measurement locations. 89
4.6 CFD model of the environmental chamber (yellow marks represent the 36 monitoring points). 90
4.7 Detail of the fan simplified geometry (ring highlighted in yellow, central element in purple). 91
4.8 Volume mesh generated using Delaunay algorithm. 92
4.9 Flow regions identified by Jain et al. (2004). 96
4.10 Air flow generated by the ceiling fan (SST k-ω turbulence model) – side view. 97
4.11 The swirling air movement generated by the ceiling fan 10 cm below the blades (SST k-ω turbulence model) – plan view. 97
4.12 Air flow field generated by the ceiling fan at different time steps (top, middle, bottom) (SST k-ω turbulence model). 98
4.13 Measurements and CFD results comparison at increasing distance from the axis of the ceiling fan (SST k-ω turbulence model). 100
4.14 Measurements and CFD results comparison at increasing distance from the axis of the ceiling fan (RNG k-ε turbulence model). 101
4.15 Measurements and CFD results comparison at increasing distance from the axis of the ceiling fan (k-ω turbulence model). 101
4.16 Measurements and CFD results comparison at increasing distance from the axis of the ceiling fan (k-ε turbulence model). 101

4.17 Measurements and CFD results comparison – perimeter points (SST k-ω turbulence model). 102
4.18 Measurements and CFD results comparison – perimeter points (RNG k-ε turbulence model). 102
4.19 Measurements and CFD results comparison – perimeter points (k-ω turbulence model). 102
4.20 Measurements and CFD results comparison – perimeter points (k-ε turbulence model). 102

5.1 Floor plan of the chosen Indian apartment (highlighted in green the part modelled in CFD). 114
5.2 Model of the drawing room with three ceiling fans - version 1. 115
5.3 Plan view of part of the model. 115
5.4 Model of the drawing room with three ceiling fans - version 2. 115
5.5 Description of the ensembles tested by Indraganti et al. (2014b) (highlighted in green the ensemble used in this research to develop the "Indian sari" option). 122
5.6 Three-dimensional view of the model with the two planes used to show the air speed field in Figures 5.7 to 5.12. 125
5.7 Air speed field - plane passing for F2 (OFF - simulation 10) and M2. 126
5.8 Air speed field - plane passing for F1 (ON - simulation 10) and M2. . 126
5.9 Air speed field - plane passing for F2 (ON - simulation 11) and M2. . 127
5.10 Air speed field - plane passing for F1 (OFF - simulation 11) and M2. 127
5.11 Air speed field - plane passing for F2 (ON - simulation 12) and M2. . 128
5.12 Air speed field - plane passing for F1 (ON - simulation 12) and M2. . 128
5.13 DTS in the first eight simulation scenarios (y-axis: full 7-point thermal sensation scale from -3 to +3). 130
5.14 DTS in the first eight simulation scenarios (y-axis: enlarged scale). . 130

5.15 DTS in scenarios 9 to 12: T_{air} = MRT = 30.0°C, RH = 30% (y-axis: full 7-point thermal sensation scale from -3 to +3). 132
5.16 DTS in scenarios 13 to 16: T_{air} = MRT = 28.0°C, RH = 30% (y-axis: full 7-point thermal sensation scale from -3 to +3). 132
5.17 DTS in scenarios 9 to 12: T_{air} = MRT = 30.0°C, RH = 30% (y-axis: enlarged scale). 132
5.18 DTS in scenarios 13 to 16: T_{air} = MRT = 28.0°C, RH = 30% (y-axis: enlarged scale). 132
5.19 DTS in scenarios 17 to 20: T_{air} = MRT = 50.0°C, RH = 30% (y-axis: full 7-point thermal sensation scale from -3 to +3). 134
5.20 DTS in scenarios 17 to 20: T_{air} = MRT = 30.0°C, RH = 50% (y-axis: enlarged scale). 134
5.21 DTS in scenarios 10 and 21 to 23: T_{air} = MRT = 30.0°C, RH = 30% (y-axis: full 7-point thermal sensation scale from -3 to +3). . . 135
5.22 DTS in scenarios 10 and 21 to 23: T_{air} = MRT = 30.0°C, RH = 30% (y-axis: enlarged scale). 135
5.23 Virtual manikin surface temperature - Indian sari. 136
5.24 Virtual manikin surface temperature - Western summer clothing. . . 136

6.1 Floor plan (the red dashed line indicates an adiabatic party-wall). . . 145
6.2 Schematic section view (the red dashed line indicates adiabatic surfaces). 145
6.3 Internal wall. 145
6.4 External wall. 145
6.5 Floor and ceiling. 145
6.6 Map of Indian climatic regions (ECBC, 2009). 148
6.7 Distribution of the Indian population across the five climatic regions (Census, 2011). 150
6.8 Distribution of the Indian geographical area across the five climatic regions (Census, 2011). 150

6.9 Total number of hours in which the air conditioning system is ON. . 155
6.10 Energy used by the air conditioning system. 156
6.11 Example of T_{air} and T_o profiles in a bedroom over four generic days in April (Control type: T_{air}). 157
6.12 Number of hours in which the air conditioning system, the fan, or both are ON (Control type: T_{air}). 160
6.13 Number of hours in which the air conditioning system, the fan, or both are ON (Control type: T_o). 160

List of Tables

2.1 Measurements taken to replicate an environment in a model in order to predict IEQ using CFD (Hajdukiewicz et al., 2013a,b). 15

3.1 Measurement equipment characteristics 55

3.2 Momentum source values used in this study 62

3.3 Discretization error calculation (Celik, 2008) 64

3.4 Duration of the simulations 70

4.1 Use of cooling devices in UK houses (15 houses). 84

4.2 Use of cooling devices in Indian houses (20 houses). 85

4.3 Measurement equipment characteristics. 89

4.4 Discretization error calculation (Celik, 2008) 94

4.5 Comparison between previous qualitative research and the developed CFD model. 96

4.6 Agreement between measured and simulated (using four RANS turbulence models) air speed values. 99

5.1 Simulation scenarios. 118

5.2 Monitoring points near the manikins. 119

5.3 Discretization error calculation (Celik, 2008) 120

5.4 "Indian sari" clothing for the IESD-Fiala model. 121

5.5 Clothing insulation values of the ensembles tested by Indraganti et al. (2014b) (highlighted in green the ensemble used in this research to develop the "Indian sari" option). 122
5.6 Air speed [m/s] recorded in each of the 12 monitoring points placed next to the virtual manikins - scenarios 1 to 8 (see Table 5.1 at page 118). 123
5.7 Duration of the simulations 137

6.1 Dynamic cooling set-point 144
6.2 Characteristics of construction elements 146
6.3 Population of the 10 most populated cities in India and their respective climatic zones (Census, 2011). 151
6.4 Dynamic cooling set-point - Mumbai. 152
6.5 Dynamic cooling set-point - Delhi. 152
6.6 Dynamic cooling set-point - Bangalore. 153
6.7 Energy saving (without including energy used by the fan). 155
6.8 Energy saving (including the energy used by the fan). 159
6.9 Energy saving including the energy used by two fans. 161
6.10 Energy saving (without including energy used by the fan) - Mumbai. . 163
6.11 Energy saving (including the energy used by the fan) - Mumbai. . . . 163
6.12 Energy saving (without including energy used by the fan) - Delhi. . . 164
6.13 Energy saving (including the energy used by the fan) - Delhi. 164
6.14 Energy saving (without including energy used by the fan) - Bangalore. 165
6.15 Energy saving (including the energy used by the fan) - Bangalore. . . 165

List of Abbreviations

φ_{ext}^{21} Extrapolated value

φ_i Significant simulated variable

$AIRNET$ Airflow Network

$ASHRAE$ American Society of Heating, Refrigerating and Air-Conditioning Engineers

BSL Menter Baseline

CCL CFX Command Language

CEL CFX Expression Language

CFD Computational Fluid Dynamics

clo Clothing insulation

CTM Computational Thermal Manikins

DES Detached Eddy Simulation

DNS Direct Numerical Simulation

DTM Dynamic Thermal Modelling

DTS Dynamic Thermal Sensation

e_a^{21} Approximate relative error

e_{ext}^{21} Extrapolated relative error

E_{AC} Air conditioning energy consumption

E_{fan} Fan energy consumption

E_{nofan} Energy demand for space cooling when no fan is used

$E_{savings}$ Energy savings

$E_{withfan}$ Energy demand for space cooling when fans are used

EMS Energy Management System

Erl EnergyPlus Runtime Language

fcl Local Clothing area Factor

GCI_{fine}^{21} fine Grid Convergence Index

GWP Global Warming Potential

h_c Convective heat transfer coefficient

h_e Evaporative heat transfer coefficient

h_i Representative cell size

IAQ Indoor Air Quality

IEQ Indoor Environmental Quality

$IESD$ Institute of Energy and Sustainable Development

$IMAC$ Indian Model of Adaptive Comfort

$ISHRAE$ Indian Society of Heating, Refrigerating and Air-Conditioning Engineers

LES Large Eddy Simulation

met Metabolic rate

MRT Mean Radiant Temperature

N_i Number of mesh elements

$NURBS$ Non-Uniform Rational Basis Spline

p Apparent order

p_a Water vapour pressure in the ambient environment

$p_{sk,s}$ Water vapour pressure at the skin

PIV Particle Image Velocimetry

PMV Predicted Mean Vote

PPD Predicted Percentage Dissatisfied

$preExp$ Pre exposure time

$r_{coarseFine}$ Grid refinement factor

$R_{e,cl}$ Evaporative heat transfer resistance of clothing layer

$RANS$ Reynolds-Averaged Navier-Stokes

RH Relative Humidity

RMS Root Mean Square

RNG Re-Normalisation Group

RSM Reynolds Stress Model

S_{air} Air speed

SET^* Standard Effective Temperature

SSG Speziale-Sarkar-Gatski

SST Shear Stress Transport

STL STereoLithography

T_m Monthly arithmetic mean of the daily average outdoor dry bulb temperatures

T_O Operative Temperature

T_{air} Air temperature

T_{cl} Mean temperature of the outer surface of the clothed body

T_{comf} Comfort temperature

$T_{max(90\%)}$ 90 percent temperature upper limit

$TMY2$ Typical Meteorological Year 2

TSV Thermal Sensation Vote

UCB University of California, Berkeley

$UR-UVGI$ Upper-Room UltraViolet Germicidal Irradiation

$URANS$ Unsteady Reynolds Averaged Navier-Stokes

Chapter 1

INTRODUCTION

1.1 Background and context

Buildings contribute more greenhouse gas emissions than either the industrial or transportation sectors, primarily due to space cooling and heating energy use, driven by the basic human need for thermal comfort and good indoor air quality. Statistical data show that the residential sector represents more than 25% of the entire energy consumption in the EU (Eurostat, 2013).

In recent years, there has been a proliferation of air conditioning in both residential and commercial buildings, and, due to the warming climate and the growing disposable income in several densely populated developing countries such as India, the energy demand for space cooling is dramatically increasing. The additional electricity demand generated by new in-room air conditioners purchased between 2010 and 2020 is projected to grow to more than 600 billion kilowatt-hours globally by 2020, and four countries, namely China, India, Brazil, Japan, together with the EU, are expected to represent 90% of this market in 2014 (Shah et al., 2013).

Due to a growing economy, the rising percentage of population which can afford to purchase and operate air conditioners, and a greater desire for thermal comfort, India is experiencing a rise in sales of air conditioners of approximately 30% per year

(Aarti et al., 2014). In cities such as Delhi, Mumbai and Kolkata, having annual cooling degree day totals in the range of 3000 to 3500, fans are being replaced with air conditioners despite the possibility of using a fan during certain times of the year to maintain thermal comfort. It is important to note that most air conditioners have low efficiency and use high-Global Warming Potential(GWP) refrigerants (Shah et al., 2013). The electricity demand for space cooling comprises up to 60% of summer peak load in large cities such as Delhi (DSLDC, 2012). Unless the use of energy-intensive air conditioning is limited only to periods of extremely hot weather, then overall Indian energy consumption and related CO_2 emissions will significantly increase, leading to severe implications for the global climate and also challenging the reliability of the Indian electricity grid.

In the UK, drier summers by up to 20% by the 2020s and up to 40% by the 2050s and warming of up to 1.5°C for some regions and scenarios by the 2020s and up to 3.0°C by the 2050s are forecast (Chris and Megan, 2005). Longer term projections go in the same direction (CIBSE, 2005). Moreover, overheating is already a problem in many UK houses (Beizaee et al., 2013). For these reasons, the use of air conditioning is likely to increase also in the UK, and, similarly, in other northern European countries.

Although several previous studies were focused on thermal comfort (de Dear et al., 2013; Djongyang et al., 2010; Mishra and Ramgopal, 2013; Parsons, 2014), there are only a few studies on asymmetrical environments or transient conditions, such as those expected when mixed mode ventilation or other low energy techniques such as elevated air movement generated by ceiling fans are adopted in the residential sector. Moreover, even fewer studies addressed the capability for prediction of human thermal comfort in non-uniform environmental conditions.

Traditional thermal comfort models such as the predicted mean vote (PMV) – predicted percentage dissatisfied (PPD) model initially developed by Fanger (Fanger, 1970) and the more recent adaptive approach (de Dear and Brager, 1998) have limited

use for complex transient and asymmetrical conditions. The former is applicable only to uniform steady-state conditions, while the adaptive model uses only the outdoor temperature as an input parameter, and therefore it cannot be used to study the effect of a specific device such as a fan on thermal comfort.

However, focusing on non-uniform thermal environments is important because the space conditioning systems that generate them are often likely to be less energy consuming than those which provide more homogeneous conditions. In these complex non-uniform thermal environmental conditions, more advanced models of human thermal comfort, such as the Institute of Energy and Sustainable Development (IESD)-Fiala model (Fiala et al., 1999, 2001) coupled with computational fluid dynamics (CFD), may provide more accurate predictions than traditional models.

1.2 Research hypothesis, aim and objectives

This research investigated human thermal comfort in non-uniform transient environmental conditions, focusing in particular on the capability of prediction of human thermal comfort in such conditions in residential buildings using a model that couples in real-time a CFD software and a human thermal-regulation model. Furthermore, this research estimated, by means of dynamic thermal simulations, the energy savings that can be achieved in residential buildings when the same level of thermal comfort is delivered using less conventional approaches that are more energy efficient, but lead to non-uniform environmental conditions.

In this research, a combination of computer based modelling, experimental work in controlled environments, and data from field studies was used. Computer modelling comprised CFD (stand alone), CFD coupled with a human thermal regulation and thermal comfort model, and dynamic thermal modelling. In the experimental work, environmental chambers were used to collect data to validate the CFD models. The data from field studies on real domestic buildings in India and in the UK was used to

identify the most relevant configurations to be modelled with the coupled system.

This research examined one main research hypothesis: thermal comfort in residential buildings characterised by asymmetrical environments or transient conditions is more effectively predicted using a coupled CFD and human thermal regulation model than using the traditional thermal comfort models.

The criteria to evaluate whether the research hypothesis is true, or, in other words, to be able to say if and when the coupled model is superior to the traditional models, are linked to both inputs and outputs of the models. Regarding the inputs, a model is considered to be superior when it enables to better represent the actual scenario and therefore to minimise the number of questonable assumptions. The output of a model is superior when it is closer to the actual answer or solution, or when it is more detailed and therefore it enables to draw more accurate conclusions. For the output of the coupled model related to thermal comfort, this is evaluated by comparing the output of the model with the actual thermal sensation votes of people or by comparing the type of output that the coupled model generate with the type provided by traditional models. In general, these criteria will be reiterated in the discussion of the results of each experimental chapter.

The aim of this research was to develop a better understanding of human thermal comfort in domestic buildings and to improve the capability of prediction of human thermal comfort in domestic buildings by using CFD and human thermal regulation models. However, since the coupled system can be used in a wider range of buildings, but also be applied to other environments such as aeroplane and train cabins, developing a better understanding of human thermal comfort in domestic buildings means investigating what are the most likely non-uniform scenarios in the domestic sector and how they are generated (for instance, using a ceiling fan).

The aim was achieved through the following objectives:

1. Literature review: extensive analysis of the previous work on thermal comfort in non-uniform conditions (field studies, experiments, and modelling) in order

to define the starting point of this research, and to demonstrate the gap in knowledge, and the most appropriate methods to achieve the aim

2. Initial development of the CFD and human thermal regulation model in order to predict thermal comfort in non-uniform scenarios

3. Testing of the coupled system and validation of the results using data from in-house experiments

4. Evaluation of possible real residential indoor scenarios in the UK and in India characterised by asymmetric and transient conditions

5. Implementation and experimental validation of a transient three-dimensional CFD model of a typical Indian ceiling fan to be used within the coupled system to model realistic residential indoor scenarios

6. Application of the coupled system to real residential indoor scenarios in India identified in objective 4, and using the ceiling fan model developed in objective 5

7. Estimate of the likely energy savings in a typical Indian apartment when the air conditioning use is reduced due to the usage of ceiling fans

1.3 Structure of the thesis

The structure of the thesis is as follows.

Chapter 2 presents the literature review which comprises international standards of thermal comfort, field studies based research, and physical and numerical models.

The following four chapters are the experimental chapters, which explain the methodology, describe in detail the methods chosen to conduct this research and the reasons behind each choice, and present and discuss the results of this research.

Chapter 3 presents the initial testing and validation (with data collected in an environmental chamber) of the coupled system. Chapter 4 illustrates the developed CFD model of a typical Indian ceiling fan, its accuracy, and its limitations. Chapter 5 presents the application of the coupled system to investigate how the use of ceiling fans affects human thermal comfort in real residential buildings in India. Chapter 6 focuses on the likely energy savings that can be achieved in a typical Indian apartment if ceiling fans are used to increase the set-point temperature of the air conditioning system while maintaining the same level of thermal comfort.

Chapter 7 presents the conclusions. This chapter summarises the key findings of the research, clearly highlighting the contribution to knowledge made by this work, describing the impact of this research on academia, industry and policy, and stating the key limitations of this work.

At the end of each chapter (chapters 2 to 6), in order to guide the reader, there is a section that summarises the key points presented and discussed in that chapter, and highlights the link with the previous and following chapters. This section is usually called "Summary". Only in chapter 2, it is called "Justification for the research" to better highlight its scope and importance.

Chapter 2

LITERATURE REVIEW

The literature review is the first essential step in order to gain the knowledge of the state of-the-art in this specific topic and to locate the contribution to knowledge made by this thesis within the current evidence base. Past and present research and work in this area have been examined. The aim has been to define the gap to be filled by this project, to understand all the aspects of the problem, and also to analyse the methods that previous research adopted.

The literature review has been organised into four main sections: in the first section, the topic and the relevant international standards are introduced. Sections two and three then respectively address field studies and modelling. The last section clearly identifies the gap in knowledge that this research aimed to fill.

2.1 Introduction and international standards

2.1.1 Thermal comfort

Thermal comfort in the built environment has been studied for decades (de Dear et al., 2013; Djongyang et al., 2010; Mishra and Ramgopal, 2013; Parsons, 2014). The overall aim of the research is to understand what thermal comfort is and which parameters mainly affect human thermal comfort in order to create models that de-

signers can use to compare the performance of different design solutions, and thus maximise the perceived thermal comfort. Moreover, policy makers can use the predictions of such models to support technologies that produce the same, or even higher, level of comfort while consuming less energy.

Thermal comfort is definied as "that condition of mind that expresses satisfaction with the thermal environment and it is assessed by subjective evaluation" (ASHRAE, 2013a). In other words, according to this definition, thermal comfort is the personal judgement that a person gives to say whether certain thermal conditions are comfortable or not. However, this definition does not explicitly include levels of satisfaction or de-satisfaction.

Although human comfort in the indoor environment is affected by at least four components, namely thermal, acoustic, indoor air quality (IAQ) and visual, a literature survey by Frontczak and Wargocki (2011) showed how thermal comfort is usually ranked as the most influencing factor, and therefore the overall satisfaction with the indoor environmental quality (IEQ) is likely to be heavily affected by it. However, the other components (acoustic, IAQ and visual) cannot be completely overlooked, especially while comparing environmental chamber and field-based research, because they could explain the discrepancy of the respective findings (Gossauer and Wagner, 2007; Peeters et al., 2009). In general, this discrepancy can be reduced by implementing more "real building characteristics" (for instance, windows to have a connection with the outdoor environment) in climate chambers (Gossauer and Wagner, 2007).

Two main theoretical approaches have been used to evaluate thermal comfort, namely the PMV-PPD method developed by Fanger (1970) and the more recent adaptive approach, which was conceived by De Dear and Brager (de Dear and Brager, 1998; Brager and de Dear, 2000), and by Nicol and Humphreys (2002). The former method is essentially a heat-transfer based approach in which the likely thermal sensation is predicted as a function of four environmental parameters (air temperature (T_{air}), mean radiant temperature (MRT), relative humidity (RH) and air speed (S_{air}))

and two human components (metabolic rate (met) and clothing insulation (clo)).

The thermal sensation is definied as "a conscious subjective expression of an occupant's thermal perception of the environment, commonly expressed using the categories cold, cool, slightly cool, neutral, slightly warm, warm, hot" (ASHRAE, 2013a). Thus, while the definition of thermal comfort includes the idea of satisfaction, the thermal sensation does not provide any explicit indication of the thermal satisfaction of an occupant. However, the PPD is defined as "an index that establishes a quantitative prediction of the percentage of thermally dissatisfied people determined from PMV" (ASHRAE, 2013a), and this enables to link the thermal sensation with the level of satisfaction. Indeed, for each PMV value, there is one and only one corresponding PPD value. A PPD of 10% corresponds to the PMV range of ± 0.5, and even with PMV $= 0$, about 5% of the people are dissatisfied. In other words, the largest proportion of the people should be satisfied in thermally neutral environments (that is when PMV $= 0$), and the level of satisfaction then decreases as the thermal sensation is shifted away from neutrality.

The PMV-PPD method does not include the outdoor air temperature or any possibility of adaptation, which are instead the basis of the latter method. In the PMV-PPD method, "lack of adaptation" does not mean that a person cannot change the status of the six input parameters (for instance, clothing or air speed) to achieve a higher level of thermal comfort, but it simply means that a given set of six input parameters will give as an output one single set of values (one PMV and one PPD value) to define the level of thermal comfort. In the adaptive approach, for a given value of the prevaling mean outdoor air temperature, an indoor environmet is considered to be thermally comfortable if the indoor operative temperatre (T_O) is within a certain range, and this range is calculated from the prevaling mean outdoor air temperature. The basic idea is that a person, within this operative temperature range, can adapt to achieve the desired level of comfort (for instance, by changing clothing or air speed). Within the "field studies" section, strengths and weaknesses of these two methods

will be discussed.

Research in this field includes several aspects, such as improved met and clo estimates (Havenith et al., 2002; Broday et al., 2014), smart comfort sensing (Kumar et al., 2014; Zhu et al., 2015a), mixed-mode buildings (Brager, 2006), the development of a new concept of alliesthesia (de Dear, 2011) which is connected to thermal delight (Brager et al., 2015) and the role of airflows in indoor environments (Arens et al., 2009; Zhu et al., 2015b). In particular, recent studies claim that transient and asymmetric conditions, such as those generated by elevated air movement in domestic and non-domestic buildings, lead to thermal pleasure, shifting away from a neutral design as optimum solution (Brager et al., 2015). However, predicting thermal comfort in such environments is by far more challenging than in steady state uniform environment for which the PMV was developed.

2.1.2 International standards on thermal comfort

Both methods have been included in the international standards. The PMV-PPD calculation is included in both ISO 7730-2005 (ISO, 2005) and ASHRAE 55-2013 (ASHRAE, 2013a). However, in the last two versions, namely 2010 (ASHRAE, 2010) and 2013 (ASHRAE, 2013a), the PMV calculation has been modified in the ASHRAE 55 to better take into account the effect of elevated air speed by integrating PMV calculation with the Standard Effective Temperature (SET*) (Schiavon et al., 2014b). This method was developed based on the idea that SET* contours represents the boundaries of an air movement comfort zone (Arens et al., 2009). The SET* is defined as "the equivalent air temperature of an isothermal environment at 50% relative humidity in which a subject, wearing clothing standardized for the activity concerned, has the same heat stress (skin temperature) and thermoregulatory strain (skin wettedness) as in the actual environment" (ASHRAE, 2013b). In the 2013 version of ASHRAE 55 (ASHRAE, 2013a), if air speed is equal or lower than 0.2 m/s, then the algorithm to determine the PMV is identical to the ISO 7730-2005 (ISO,

2005) procedure. On the other hand, for higher air speed values, the steps are as follows: calculation of the SET* with actual air speed, definition of the air temperature that gives the same SET* with air speed equal to 0.2 m/s, and finally calculating the PMV using this new (lower) air temperature and air speed equal to 0.2 m/s. In this PMV calculation, all other inputs do not vary.

More detailed information about met and clo are given in ASHRAE handbooks (ASHRAE, 2009, 2013b), and in ISO 8996-2004 (ISO, 2004) and ISO 9920-2007 (ISO, 2007), while ISO 7726-2001 (ISO, 2001) provides specifications for the monitoring equipment. On the other hand, the adaptive method is included in ASHRAE 55-2013 (ASHRAE, 2013a) (as an option) and EN 15251-2007 (EN, 2007; Nicol and Humphreys, 2010; Nicol and Wilson, 2011). However, these two standards treat the outdoor temperature in two different ways leading to different results (Borgeson and Brager, 2011).

2.2 Field studies based research

Field studies are a key method for understating human thermal comfort. Indeed they analyse the real world that is then replicated in a simplified way in environmental chambers and computer models. The better this understanding is, the more appropriate the simplification process is.

2.2.1 Non-domestic buildings

In the past, most of the field-based research focused on non-domestic buildings (Mishra and Ramgopal, 2013). Reviewing all these studies is out of the scope of this work, which is mainly focused on residential buildings. However, some particularly relevant studies have been included in the literature review, especially when related to air movement or other transient and asymmetrical conditions.

In the 1980s, the air flow characteristics in the occupied zone were studied by Han-

zawa et al. (1987), whose research focused on ventilated or air-conditioned spaces, and by Melikov et al. (1988), who considered heated spaces without mechanical ventilation. In both studies, there is always a certain heating system and the parameters such air velocity, turbulence intensity and energy spectrum are analysed. This research took place in furnished buildings in Denmark, using instruments which complied with ISO 7726, and its aim was to study the risk of draught, defined as an undesired local cooling of the human body caused by air movement (Melikov et al., 1988). In a cold climate, unwanted air movement may indeed lead to an increase of the set-point temperature, and therefore to an higher space heating energy consumption.

In 1995, a comparison between predicted and reported thermal sensation was carried out by Oseland (1995). The study included both thermal chamber studies and real buildings, namely offices and homes. In real buildings, no restrictions were placed upon participants' clothing and activity level, and the environmental conditions were monitored, but not controlled. Thus, a more realistic scenario was studied. Results showed that in this more realistic transient environments participants were able to achieve thermal comfort across a wider range of conditions compared with PMV (Fanger, 1970) predictions.

Research by Raja et al. (2001) also supported the idea that occupants who have greater access to control report less discomfort than those who have less access. Ten office buildings were analysed by using both longitudinal and transverse surveys. Results highlighted that in warm or hot weather, air movement was the best means of improving thermal comfort. Most windows were open when outdoor temperature exceeded 26°C, while the thresholds for the usage of fans were 20°C indoor and 15°C outdoor temperature, respectively. Moreover, solar shading control increased the level of thermal comfort, as pointed out by Barlow and Fiala (2007) as well.

Not only offices, but also educational buildings (Buratti and Ricciardi, 2009; Guedes Correia et al., 2009; Matias et al., 2009) and homes for the elderly (Guedes Correia et al., 2009; Matias et al., 2009) were studied. Classrooms of the University

of Perugia, in Italy, were analysed in autumn, winter and spring, concluding that the questionnaire data tend to accentuate discomfort perception (Buratti and Ricciardi, 2009). Aiming to define indoor thermal comfort requirements applicable to Portuguese buildings, researchers (Guedes Correia et al., 2009; Matias et al., 2009) found that, considering the ASHRAE 55-2004 adaptive temperature limits, most results were within the comfort range, but occupants also accepted higher temperatures in summer and lower temperatures in winter than the ASHRAE reference. Monitoring equipment complied with international standard requirements. However, in this study it is not clear which adaptive measures allowed participants to tolerate such temperatures.

While most of the studies focused on naturally ventilated or on air-conditioned buildings, Rijal et al. (2009) investigated mixed-mode office buildings, which are heated in winter, free running in mid-season, and have cooling available in summer as required. Based on data from the UK, Greece and Pakistan, it was noted that occupants reported to be satisfied with their thermal comfort, and their behaviour is similar to that observed in naturally ventilated buildings, including the usage of fans and windows, but except for the use of cooling when necessary for comfort.

Aiming to develop a Brazilian standard for naturally ventilated buildings, Cândido et al. (2010, 2011) focused on air movement acceptability. Both qualitative data, via questionnaires, and detailed measurements were collected at the same time. In particular, indoor conditions were measured by using a micro-climatic station (air temperature, globe temperature, air speed and humidity), a hot wire omnidirectional anemometer, and a surface temperature thermometer. The anemometer allowed measurement of air speed close to the participants, while smoke sticks provided the direction of the airflow. The outdoor mean annual temperature was 26°C while relative humidity was within 78-84% range. Results showed that in such a climate the notion of draught does not apply. Participants required a minimum air speed of 0.4 m/s for an operative temperature of 26°C, and up to 0.9 m/s with 30°C. Air

movement therefore improved the thermal sensation and participants demanded air speed higher than 0.8 m/s (Figure 2.1), which is the ASHRAE limit when there is no user control (ASHRAE, 2010).

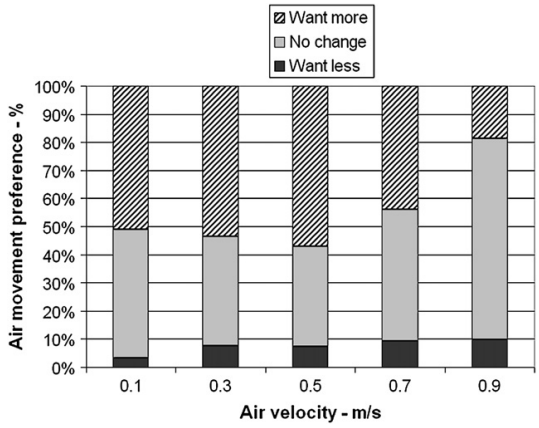

Figure 2.1: *Overall air movement preference and air velocity range (Cândido et al., 2010).*

Research carried out in India by Manu et al. (2014) also supports the idea that in a warm and hot climate air movement enhances thermal sensation, rather than causing discomfort. By using ceiling fans and windows, air speed as high as 2.0 m/s was recorded in Indian naturally ventilated offices.

Mixed-mode office buildings were studied also by Deuble and de Dear (2012), who analysed academic offices in Sydney, Australia, by using a longitudinal field study which provided with 1359 thermal comfort questionnaires. This building switched to air-conditioning when indoor temperature exceeded 25°C. Results demonstrated that participants' thermal sensation were affected by how the building was operating. Indeed the PMV (Fanger, 1970) and the actual votes are in agreement when in air-conditioning mode, but not when in naturally ventilated mode. In the latter case, better predictions were given by EN 15251 (EN, 2007). Thus, in a certain measure this study supports the idea promoted by Rijal et al. (2009), that mixed-mode buildings have many points in common with naturally ventilated buildings. Since, as reported also by Karava et al. (2012), mixed-mode buildings may lead to significant energy savings, understanding thermal comfort, which is a main driver of

energy consumption, is the key to develop realistic design solutions. For instance, automatic control algorithms may be quite difficult to be implemented (Ackerly and Brager, 2013).

Although these studies were mainly focused on CFD modelling, Hajdukiewicz et al. (2013a,b) gave a complete and detailed description of the equipment used to measure the physical parameters required to replicate an environment in a model in order to predict thermal comfort and IEQ (Table 2.1).

Table 2.1: *Measurements taken to replicate an environment in a model in order to predict IEQ using CFD (Hajdukiewicz et al., 2013a,b).*

Outdoor measurements	Indoor measurements
dry-bulb air temperature	air temperature*
relative humidity	air speed
barometric pressure	relative humidity
wind speed	CO_2 concentration
wind direction	ambient lighting levels
global solar irradiance	sensor movement
diffuse solar irradiance	noise
rainfall	air speed at openings
	surface temperature
	(walls, floor and ceiling)

2.2.2 Domestic buildings

Field studies in residential buildings have been recently conducted both in European and extra-European countries, including Denmark (Frontczak et al., 2012), Finland (Karjalainen, 2009), China (Huang et al., 2013; Lai et al., 2009; Lai and Yik, 2009; Wang et al., 2010, 2011), Israel (Becker and Paciuk, 2009), Portugal (Matias et al., 2009), the UK (Oseland, 1995; Hong et al., 2009; Limbachiya et al., 2012; Lomas and Kane, 2013; Pathan et al., 2008), France (Derbez et al., 2014) and India (Indraganti and Rao, 2010; Indraganti, 2010a,b,c, 2011). Some of them focus directly on thermal comfort, others on IEQ (Frontczak et al., 2012; Lai et al., 2009; Lai and Yik, 2009) or on the use of devices such as air-conditioners (Pathan et al., 2008).

Huang et al. (2013) report their study about the demand for air movement in warm environments in China. There are two main parts in their work. Firstly, an online survey was used "*to study electric fan use at home [...] in order to investigates people's real demand for air movement*"(Huang et al., 2013). The survey had a total of 1583 respondents and only 2% reported zero use of fan. Moreover, fans were used even with air-conditioners. The top reasons for using a fan were that it is an economical and environmental friendly solution, that it prevents the potential risk of over-cooling, and that users feel fresh. Then, a thermal chamber was used to identify the lower limit of air speed at 28°C, 30°C, 32°C and 34°C. Results show that these values are respectively 0 m/s, 1 m/s, 2 m/s, while none of the tested air speeds could keep the thermal sensation below the value 0.5 at 34°C. Thus, this study provides evidence that thermal neutrality could be achieved using only air movement in domestic buildings at temperatures up to 32°C. However, there are no tests or measurements done in real houses.

Indraganti (2010a,c) illustrates a study which was "*aimed at obtaining the occupants' thermal comfort responses within the apartment buildings* [in India] *along with the diverse adaptation mechanisms and practices. Therefore it was necessary to record the indoor environment every time the subject answered the questionnaire*". This research shows how also in Indian dwellings air movement is used to provide thermal comfort. However, it could lead to discomfort as well. Indeed when in May the temperatures were extremely high (33.5°C or more) and the relative humidity was low (20.0 - 34.0%) people reported dryness of the mouth and eyes irritation. Thermal discomfort was basically due to the fact that the air being moved using fans or cross ventilation was too hot. On the other hand, in cooler and more humid conditions air movement improved thermal comfort. In this studies measurements were taken in real houses in Hyderabad and a class-II protocol, as defined by de Dear (1998), was used. Results show that "*the comfort band (voting within -1 and +1) based on the regression analysis was found to be 26.0 – 32.5°C with the neutral temperature at*

29.2°C", well above the limits (23 – 26°C) set by Indian standards. In addition, the PMV was always found to be higher than the actual sensation vote.

Indraganti and Rao (2010) investigated also the effect of age, gender, economic group and tenure on thermal comfort in Indian residential buildings. Although statistically significant, a weak link between actual thermal sensation and both age and gender was noticed. On the other hand, economic group and tenure play a relevant role: thermal acceptance was higher in lower economic classes, while the thermal acceptance reported by house owners is higher in all the economic groups. The same study also confirmed that the majority of participants in warm and hot conditions prefer elevated air movement. Indraganti (2010b) reported that ceiling fans were available in almost all the surveyed spaces, while air coolers and air conditioners were less common. In particular, air conditioners were used by participants from the higher income groups. Moreover, the use of all these cooling systems depends on the indoor temperature, the outdoor temperature and the thermal sensation of the user.

There are also other studies conducted in China (Wang et al., 2010, 2011) which show that air movement in residential buildings has a positive effect on the thermal sensation. 257 families were involved and 423 sets of physical data and subjective questionnaires were collected. It has also been noted that often windows are opened just to improve IAQ. Instruments used in this study met the ASHRAE 113 (ASHRAE, 2013c) and ISO 7726 (ISO, 2001) standards requirements for accuracy. The questionnaire included an air movement sensation survey (ASHRAE 7 point scale: - 3 much too still, -2 too still, -1 slightly still, 0 comfortable and no breeze, +1 comfortable and slightly breeze, +2 too breezy, +3 much too breezy) and an air movement preference survey (-1 lower, 0 no change, +1 higher). It is interesting that the results of this study reveal that among the votes at which the indoor air temperature was higher than 28°C, more than half (53%) voted no change in air movement, with the air speed range of 0.05 – 0.30 m/s. Moreover, 80% of the occupants can accept an air temperature range of 21.5 – 31.0°C, which is 1.0 – 1.5 °C wider than the summer comfort

temperature limits set by the adaptive model (EN 15251 (EN, 2007) and ASHRAE 55-2004). Basically, air movement is due mainly to natural ventilation, therefore the speed is low, but thermal comfort is still achieved without fans or air-conditioners.

There is then a number of field studies which supports the idea, suggested for instance by Peeters et al. (2009), that within domestic buildings a wider range of situations can be considered comfortable compared to the range defined by the adaptive comfort model (such as ASHRAE 55 (ASHRAE, 2013a), EN 15251 (EN, 2007)). Indeed the available degree of adaptation is in general wider than in offices, and models included in the standards are based on offices' studies. This seems to be a common characteristic in different countries, as field studies in Portugal (Matias et al., 2009), the UK (Oseland, 1995; Lomas and Kane, 2013), Israel (Becker and Paciuk, 2009) and China (Wang et al., 2010, 2011) show. In this context, the use of air movement can be one possible solution used to achieve thermal comfort.

Adaptation cannot only expand the range of acceptable conditions, but it can also lead to higher thermal comfort when conditions are within the "*traditional*" adaptive comfort model boundaries. Although it does not focus on air motion, a study (Karjalainen, 2009) conducted in Finland with over 3000 participants reveals that indeed thermal comfort in offices is lower than in homes due to the greater adaptive opportunities that the domestic environment provides.

Other interesting information reported by Karjalainen (2009) are about summer temperatures, cooling systems and level of energy efficiency of Finnish houses. Indeed temperatures (mean temperature 14 - 18 °C and daily maximum temperature up to 30°C in July) are fairly similar to those experienced now in England, but typical wall U-values (0.3 W/m^2K or less) are lower than current UK average values. Only 1% of Finnish dwellings has a cooling system of any kind. In well-insulated residential buildings in Finland, similar to those the UK might have in the next decades, thermal comfort in summer is guaranteed simply by opening a window.

2.3 Physical and numerical models

2.3.1 Environmental chamber studies

Thermal chambers have been used in thermal comfort studies since the early stages of the research in this area. They can be considered as full-scale experimental models (Chen, 2009) because essentially a simplified reality is recreated in a laboratory, rather than in software.

Fanger developed the PMV model (Fanger, 1970) and the draught risk model (Fanger and Christensen, 1986; Fanger et al., 1988) by using a thermal chamber without windows. To develop the PMV model, experiments were carried out on students in a controlled environmental room at Kansas State University (USA) (Nevins et al., 1966) and similar tests were performed at the Technical University of Copenhagen (Denmark) (Fanger, 1970). No significant difference was found in the comfort conditions between American and Danish students, between students and elderly people or between males and females (Fanger, 1970). Some years later (Fanger and Christensen, 1986; Fanger et al., 1988), testing temperature between 20°C and 26°C and air speed up to 0.4 m/s, a draught chart was developed (Figure 2.2). The head resulted in being the most sensitive region of the body (Fanger and Christensen, 1986) and higher turbulence accentuated discomfort (Fanger et al., 1988). However, despite the application of rigorous methods, results obtained in such an artificial environment may differ significantly from real world results, as reported by Oseland (1995). Moreover, while air movement created a negative effect with that range of temperatures, in 1998 research by Arens et al. (1998) highlighted that participants were thermally comfortable at temperatures up to 31°C by using air speed up to 1.4 m/s.

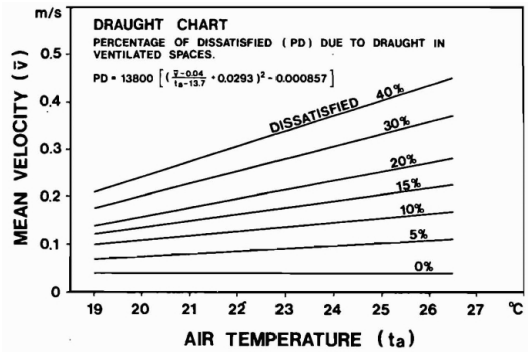

Figure 2.2: *Draught chart developed by Fanger and Christensen (1986).*

In other studies, thermal manikins were used in thermal chambers. Gao and Niu (2004, 2005) used manikins to provide data for the validation of CFD models. From their research, it can be noted that an accurate representation of the human body is essential while studying the micro-environment around a person and that the respiration process and radiative heat transfer cannot often be overlooked.

One of the most complete studies about thermal sensation and comfort in non-uniform and transient environments was carried out by Zhang and presented in three papers. The first describes a local thermal sensation model which includes 19 body parts (Zhang et al., 2010c), the second one deals with local comfort of individual body parts (Zhang et al., 2010b) and the last one with the whole body sensation and comfort (Zhang et al., 2010a). The authors stated that overall thermal comfort was previously quantified using thermal sensation, but this approach does not apply to local body parts, or to asymmetrical or transient thermal environments. Their hypothesis is plausible since the traditional approach (Fanger, 1970) was developed in uniform steady state conditions, and other studies (Schellen et al., 2013a,b) also highlighted the complexity of the prediction of thermal comfort in non-uniform environments due to the significant impact of local effects.

To develop the local thermal sensation model based on skin and core temperatures (Zhang et al., 2010c), several human participants were recruited for environmental chamber studies in which air was used to cool or heat each body part. The input required by this model can also be calculated by using a physiological computer

software. The scale used to collect the actual thermal sensation was an extended ASHRAE 7-point scale, from very cold to very hot (Figure 2.4). Conversely to other studies, there were windows in this thermal chamber. The adopted thermal comfort scale is also different from previous studies (Figure 2.3), and many participants used the positive part of the scale (Figure 2.4). Local thermal comfort is derived from local and whole-body thermal sensation (Zhang et al., 2010b). Finally, the overall thermal sensation and comfort are both estimated from local values (Zhang et al., 2010a).

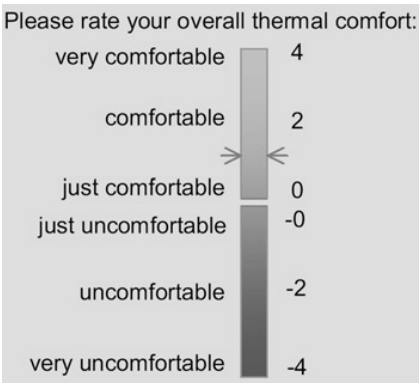

Figure 2.3: *Bidirectional comfort scale (Zhang et al., 2010b), which has been adopted in most recent research at University of California, Berkeley (UCB).*

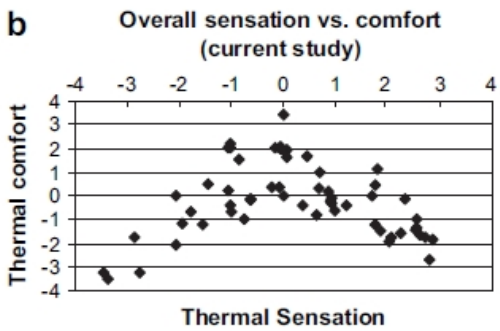

Figure 2.4: *Overall thermal sensation vs. comfort (Zhang et al., 2010b).*

Zhang's models (Zhang et al., 2010a,b,c) were then improved four years later by Zhao et al. (2014) by addressing two main issues: creating accurate segment set-point temperature for specific clothing and activity levels, and minimising unrealistic differences in output at the transition between body parts. More empirical data could lead to further enhancements of the smoothing function created to cope with the latter problem. Moreover, although undeniably accurate and indeed one of the most comprehensive works published up to date, this research was conducted in thermal chambers. Even if there were windows in this chambers, it might be possible that people would express different votes in real (thus, non artificial) environments.

There are then a number of recent chamber studies about thermal comfort and IAQ, and air movement. Most of them involved human participants (Arens et al.,

2011; Huang et al., 2013, 2014; Melikov and Kaczmarczyk, 2012; Pasut et al., 2014; Schiavon et al., 2014b; Zhai et al., 2013, 2015) and aimed to understand human preferences, while others (Yang et al., 2015) used manikins to developed indices such as the cooling fan efficiency. Thus, both recent and past research used either human participants or manikins according to the issue to be addressed.

Air movement improves the perceived IAQ (Melikov and Kaczmarczyk, 2012) despite the air temperature. However, at low temperatures such as 20°C, this movement may generate thermal discomfort even greater than what was expected by using the international standards (Schiavon et al., 2014b).

Within the Chinese warm context, research (Huang et al., 2013) showed that airflows can help to maintain thermal sensation below 0.5 between 28°C and 32°C, while this was not possible at 34°C despite the air speed used (Figure 2.5). However, participants were all college students, who were not likely to be a representative sample of society.

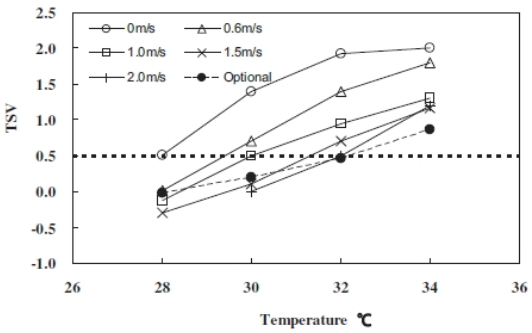

Figure 2.5: *Thermal sensation votes for optional (user selected) air speed (Huang et al., 2013).*

Research conducted at UC Berkeley extensively analysed the effect of air movement on thermal comfort. Recent studies found that with personalised air movement, thermal comfort can be maintained up to 30°C and 60% RH, and perceived IAQ up to 80% RH. Although less pronounced, these results are reasonably in agreement with Huang et al. (2013). A sample with the similar young age group may explain that. Moreover, in further studies (Zhai et al., 2015), over 80% of Chinese participants

perceived the environment acceptable at 30°C and 80% RH due to air movement up to 1.8 m/s.

Pasut et al. (2014) showed that at 28°C and 51% RH thermal comfort can be achieved by using fans with airspeed between 0.8 and 0.9 m/s without causing dry-eyes discomfort. Both fixed and oscillating ceiling fans were used. The concept of alliesthesia (de Dear, 2011) would suggest that oscillating fans should produce higher comfort, but the 15 s fluctuation interval was probably too long and indeed no statistically significant difference was found between no fan and oscillating fan.

Another study by Huang et al. (2014) demonstrated that the indices derived from Gagge 2-Node model (Gagge et al., 1971) and included in the PMV calculation in ASHRAE 55 (ASHRAE, 2010, 2013a) such as SET* can effectively predict thermal sensation under most non-uniform air movement conditions (Figure 2.6), while traditional PMV (ISO, 2005) underestimates cooling effect in warm environments.

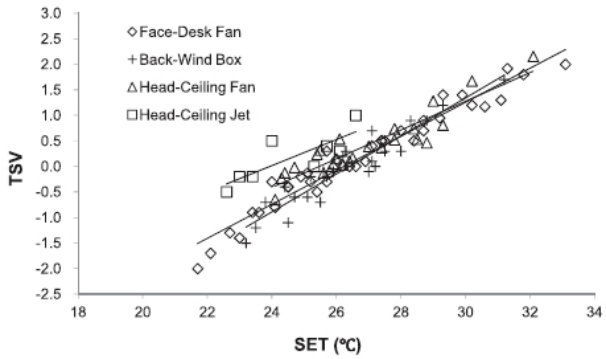

Figure 2.6: *Relationship between TSV and SET* in different experiments (Huang et al., 2014).*

2.3.2 Biophysical principles of fan use

In the previous sections on field based research and on environmental chamber studies, it has been highlighted the role of air movement on thermal comfort. In warm and hot environments, air movement usually has a positive effect on thermal comfort. On the other hand, it is a cause of discomfort in cool and cold conditions, where the concept of draught applies. This section aims to analyse how the heat is exchanged between

a human body and the surrounding thermal environment, and to explain therefore the biophysical principles of fan use and its impact on the users.

The heat exchange between a human body and the surrounding thermal environment has been extensively investigated (Fanger, 1970; Gagge et al., 1967; ASHRAE, 2013b). It occurs through four mechanisms, namely conduction, convection, radiation, and evaporation (Figure 2.7). Conduction refers only to solids, and therefore this mechanism is not affected by the use of a fan, or in general by variation of the air speed. A human body may exchange heat with its surroundings by conduction only when there is a direct contact with a surface at different temperature. Similarly, radiation heat exchanges occurs due to the temperature difference between the surface of the human body and the surrounding surfaces, and they are therefore not affected by air speed variations on the human body.

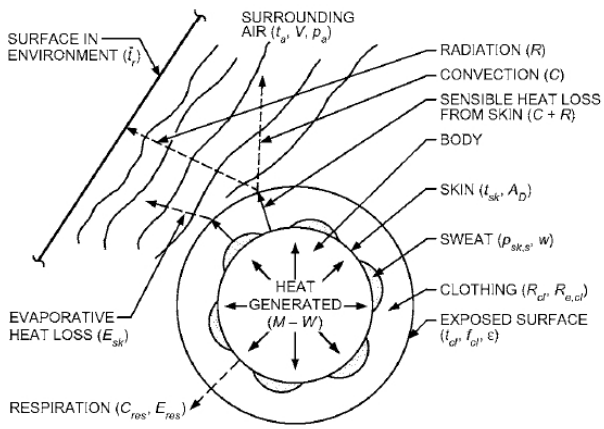

Figure 2.7: *Thermal Interaction of Human Body and Environment (ASHRAE, 2013b).*

Air movement affects the convective and evaporative heat loss from the skin. The convective heat losses from the outer surface of a clothed body can be expressed as a function of the clothing area factor (f_{cl}), a convective heat transfer coefficient (h_c) evaluated at the clothing surface, and the difference between the mean temperature of the outer surface of the clothed body (T_{cl}) and the air temperature (ASHRAE,

2013b):

$$C = f_{cl} h_c (T_{cl} - T_a) \tag{2.1}$$

When a fan is used to increase the air speed on the outer layer (this might be the skin or clothed areas) of a human body, the convective heat transfer coefficient varies. In particular, the more elevated the air speed is, the higher this coefficient becomes. Thus, providing that the temperature difference in equation 2.1 does not change and it is positive (meaning that air temperature is lower than t_{cl}), then convective heat losses increases, too. On the other hand, if this temperature difference was negative, then the direction of the heat flow would be the opposite. In hot conditions, this may set a temperature limit for the usability of air movement to provide cooling, and the thresholds discussed in the previous sections support this idea. The highest air temperature limit, 34°C at 50% relative humidity, was reported by Huang et al. (2013). On the other hands, convection is not the only heat loss mechanism affected by air movement, and therefore those limits might depend also on other things.

Evaporative heat losses from skin depend on the amount of moisture on the skin (expressed by the skin wettedness w), the difference between the water vapour pressure at the skin ($p_{sk,s}$) and in the ambient environment (p_a), evaporative heat transfer resistance of clothing layer ($R_{e,cl}$), and the evaporative heat transfer coefficient (h_e) (ASHRAE, 2013b):

$$E_{sk} = \frac{w(p_{sk,s} - p_a)}{R_{e,cl} + 1/(f_{cl} h_e)} \tag{2.2}$$

Skin wettedness is defined as "the fraction of the skin that is covered with water to account for the observed total evaporation rate" Gagge (1937). Thus, the highest achievable rate of evaporation occurs when skin wettedness is equal to one. Evaporative heat loss is a combination of two components: the evaporation of sweat due to thermoregulatory control responses, and natural diffusion of water through the skin.

Without sweating, skin wettedness caused by diffusion is approximately 0.06 for normal conditions, but this figure may decrease down to 0.02 in very dry environments (ASHRAE, 2013b). With sweating, the human body regulates the sweat rate, and the skin wettedness then varies accordingly.

When a fan is used to increase the air speed on the outer layer of a human body, air at certain relative humidity, and therefore water vapour pressure, replaces the air near this outer layer. Evaporation would occur also without this air movement, providing that water vapour pressure difference in equation 2.2 is positive, but at a lower rate. The forced convection generated by the fan increases the rate of evaporation, and this has a noticeable importance in presence of sweat. The sweat production remains the same, but the sweat evaporate faster, and thus the skin wettedness is lower. This is important since skin wettedness is strongly correlated with warm discomfort and is also a good measure of thermal stress ASHRAE (2013b). In very humid environments, the effect of air speed on evaporative heat losses is lower as the air moved by the fan on the outer layer is already close to saturation.

Considering both convective and evaporative heat exchanges, it is therefore possible to say that, in general, the cooling effect of a fan is higher in dry conditions and when the air temperature is lower, and then it decreases as ambient relative humidity and air temperature decreases. Furthermore, there are other factors that may affect the air speed preferences of people since the human perception of air movement involves also non-thermal sensory perception of air motion through mechanoreceptors in the skin, particularly near hair follicles de Dear et al. (2013). Taking into account all these elements, plus the fact that there might be significant difference between different human bodies, it appears important to highlight that limits (temperature and relative humidity) for the use of air movement as a cooling means may vary according to the group of people considered. Nevertheless, the biophysical principles discusses in this section remain valid.

2.3.3 Human thermal regulation models

Numerical models of human thermal regulation have been widely studied over the last 50 years (Cheng et al., 2012; Foda et al., 2011; de Dear et al., 2013; Teixeira et al., 2014). These models essentially predict the physiological reaction of a human body to a given surrounding thermal environment by calculating parameters such as skin and core body temperature. While analysing the existing most established models, there are two primary aspects to be taken into account: the capabilities and robustness of the model itself, and its ease of connection with other models such as a CFD model.

However, before discussing the latest and most advanced numerical models of human thermal regulation, it is useful to start with the analysis of the most relevant older models. Although these have limited capabilities compared with more recent models, their analysis enables a better understanding of the purpose, logic and mechanisms used in this type of models.

Wissler (1964) described the elements to be included into a model of human thermal regulation: (1) the manner in which heat generated by metabolic reactions is distributed throughout the body, (2) conduction of heat due to thermal gradients, (3) convection of heat by circulating blood, (4) the geometry of the body, (5) the relatively low thermal conductivity of the superficial layer of fat and skin, (6) countereurrent heat exchange between large arteries and veins, (7) heat loss through the respiratory tract, (8) sweating, (9) shivering, (10) the storage of heat, and (11) the condition of the environment, including its temperature, motion relative to the body, and relative humidity. At that time, the available computational power was significantly limited, and the main issue was the solution of the transient state heat conduction equation. Thus, Wisser focused on the usability of finite difference techniques to solve the equations that describe his model in which the human body is divided into 15 cylinders (Figure 2.8), and therefore to predict the temperature distribution across the body. Although limited due its pioneering nature, this work showed the potential of this type of numerical models, but, as note by Wissler, also highlighted the need for accurate

validation and for experimental procedures to be used to evaluate those parameters that cannot be measured directly.

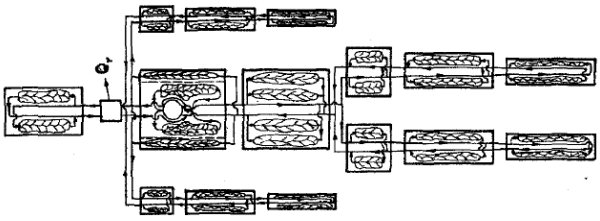

Figure 2.8: *Schematic diagram of the model developed by Wissler (1964)*

One of the first and simplest human thermal regulation model is the Pierce two-nodal model originally developed by Gagge et al. (1971) and currently used in the SET* calculation in the ASHRAE 55-2013 standard (ASHRAE, 2013a). In this model, the human body is represented by a sphere divided into two nodes, namely core and shell, and there are two subsystems: a controlled and a control system. Although this is a basic model, conceived for nearly sedentary activities and not extremely accurate in non-uniform spatial conditions, it has improved the PMV calculation for elevated air speed (see also section 2.1.2) and its algorithm is simple enough to be included in an on-line tool that every one can use to estimate thermal comfort (Schiavon et al., 2014a).

Another relatively simple model was developed by Stolwijk and Hardy (1966). In this model, the human body is represented by 3 cylinders: the head, the extremities, and the trunk (Figure 2.9). Head and extremities are then subdivided into two nodes, namely core and skin, while the truck comprises three nodes: core, muscle, and skin. A passive system models the heat transfer phenomena within and around the body. Inside the body, conduction occurs between adjacent layers, and there is a convective heat exchange between all nodes and a central blood element. The heat exchange between the body and the surrounding environment happens through the three skin nodes, and it comprises four components: conduction, convection, radiation, and evaporation. An active system models the response of the body to different thermal stimuli by causing, depending on the stimulus, heat loss by evaporation, heat produc-

tion by shivering, or changes in the blood flow. Although this model is simpler (for instance, there are fewer nodes and a less complex active system), its logic is similar to more advanced models such as the IESD - Fiala model (Fiala et al., 1999, 2001). Thus, it eases the understanding and use of such more recent models. Another point in common with many other models (including newer ones) is the difficulty of usability, intended as the possibility of being used by other researchers. As note also by Stolwijk and Hardy (1966), their model is useful primary to its developers.

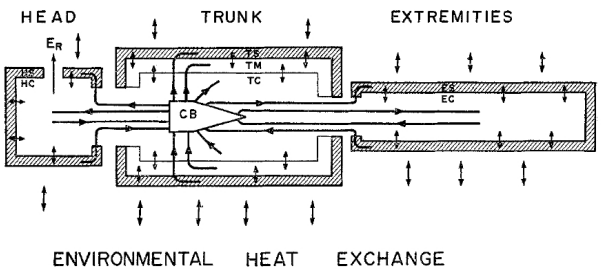

Figure 2.9: *Diagram of the model developed by Stolwijk and Hardy (1966)*

When more complex environments are studied, a more detailed model may provide better results. The multi-node model developed by Stolwijk for aerospace applications (Stolwijk, 1970, 1971) was limited to constant surrounding conditions, but its more accurate precision and improved flexibility compared with previous models, allowed for the use of this model as the basis for the two most advanced and currently used models: the IESD - Fiala model (Fiala et al., 1999, 2001, 2012) and the UCB model (Huizenga et al., 2001).

In this model (Stolwijk, 1970, 1971), the human body is divided into six parts, namely head, trunk, arms, hands, legs, and feet, and each part is subdivided into four nodes: core, muscle, fat, and skin. Thus, in total there are 24 nodes, plus an additional node that represents the central blood. Similarly to Stolwijk and Hardy (1966), in this model there are also two interacting systems, namely a passive (controlled) and an active (controlling) system. The heat exchange between the body and the surrounding environment happens through the skin nodes, but, in this case, it does not include conduction, but only convection, radiation, and evaporation. The possible reactions to

different thermal stimuli are sweating, vasodilatation, shivering and vasoconstriction. These represent natural, but short-term, means of thermal protection (Gagge et al., 1967). Long-term means are behavioural activities such as changing clothing, and are not considered by this type of models.

Sweating occurs at elevated internal temperature, and it is a control mechanisms that enables to cool the skin temperature and dissipate the heat from the core ASHRAE (2013b). Depending on the environmental conditions, the sweat may rapidly evaporate and let the skin dry, or it may have to spread on an area of the skin wide enough to be able to evaporate.

Shivering is his most effective physiological non-behavioural protection to the cold (Gagge et al., 1967), and it can increase the metabolic heat production from two to six times compared to resting levels ASHRAE (2013b). Shivering begins with an increase in muscle tension and by gooseflesh produced by muscle contraction in the skin, and it becomes violet at the highest levels.

Vasodilatation and vasoconstriction are mechanisms used to regulate the blood flow into the skin. Vasodilatation occurs when the internal temperatures rise above a set point, and it can increase skin blood flow by 15 times (from 1.7 mL/(s m^2) at resting comfort to 25 mL/(s m^2)) to ease the heat dissipation though the skin ASHRAE (2013b). Vasoconstriction is the opposite effect, and it happens when the internal temperature decreases below a set point. Its maximum effect is equivalent to the insulating effect of a heavy sweater ASHRAE (2013b).

The IESD - Fiala model (Fiala et al., 1999, 2001) is made by two complementary systems, namely the active (Fiala et al., 2001) and passive (Fiala et al., 1999) system. The former simulates the physiological phenomena by considering self-regulatory responses, that are vasoconstriction, vasodilatation, shivering and sweating. The latter estimates the heat exchange process inside the body and between the body and its surroundings. In this model, the human body is subdivided in 19 spherical and cylindrical elements (Figure 2.10) and there are 59 areas of the body surface.

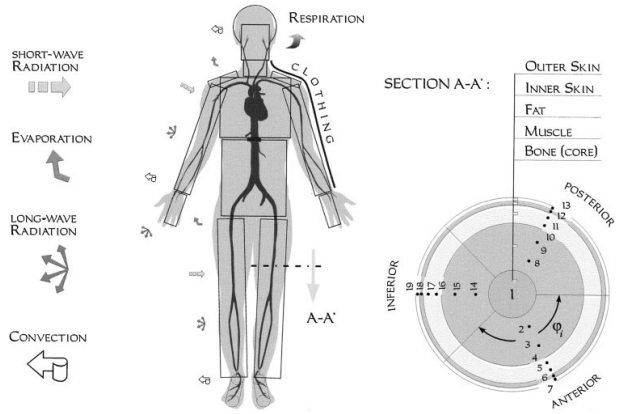

Figure 2.10: *A schematic diagram of the passive system (Fiala et al., 1999).*

Similarly to every other human thermal regulation model, the IESD - Fiala model requires some assumptions about the body: weight (73.5 kg), fat content (14 %), surface area (1.86 m^2), basal metabolism (87 W), basal evaporation from the skin (18 W) and basal cardiac output (4.9 l/min). While using this model to predict thermal sensation, these input assumptions must be remembered. Indeed experimental data may refer to real people or manikins that could have significantly different values.

The IESD - Fiala model has been well validated and is able to accurately predict thermal sensation in dynamic conditions (Foda et al., 2011). Moreover, it has been successfully and entirely coupled with a CFD commercial code (Cropper et al., 2008, 2009, 2010). "Entirely" means that there is a real-time information exchange between the two models, and therefore transient complex situations can be studied. Despite the need for further validation and maybe optimisation, it is curious that more recent papers (Cheng et al., 2012) claim the need for a coupling between CFD and human themoregulation models, ignoring that a procedure has already been implemented.

The model developed at UCB (Huizenga et al., 2001) is based on a similar approach, it has 16 body elements, and it has been also extensively validated. Further studies investigated also the moisture transfer through clothing (Fu et al., 2014). The model itself could be slightly more accurate than the Fiala model (Cheng et al., 2012; Foda et al., 2011) and it has been used together with CFD software (Gao et al., 2006, 2007; Schellen et al., 2013a). However, in these studies there is no real

time coupling. Information are simply taken from one model to the other, and used as boundary conditions. The process is not automated, and ends when the desired convergence threshold is reached.

Overall, this type of models significantly evolved from basic two-node models to complex ones that include a much higher number of nodes, and sophisticated controlled and controlling systems. This has been possible due to the rapid growth of the computational resources available to researchers. However, this also makes more relevant the point made earlier in this section about the usability of these models. These models are usually translated into computer programs (often in FORTRAN) by the researchers who conceived them. Since they are often non-experienced programmers, the collaboration with professional programmers appears to be extremely important now that the models are large and complex. This would ensure that the code is readable, maintainable, and therefore editable to include enhancements (as new research is completed) or for coupling purposes.

2.3.4 Computational fluid dynamics modelling

The use of CFD simulations for estimating parameters required to calculate room air distribution, and thermal comfort and IEQ indices has grown constantly over the last 15 years mainly due to the dramatic increase of computers computational power alongside the fall of their costs (Nielsen, 2015). CFD requires skilled users in order to avoid meaningless results, but it is faster and cheaper than physical modelling. Reliability is a major issue (Chen, 2009), thus validation with actual data such as measurements in real buildings and experimental facilities is extremely important.

Recent research by Hajdukiewicz et al. (2013a,b) aimed indeed to propose a procedure (Figure 2.11) to calibrate CFD models of naturally ventilated indoor environments. Firstly, CFD experience is required to decide the level of geometrical detail, select mesh type (e.g. structured or unstructured) and grid resolution, choose the turbulence model, set the numerical techniques such as the discretization scheme,

and define criteria to test the validity of the results.

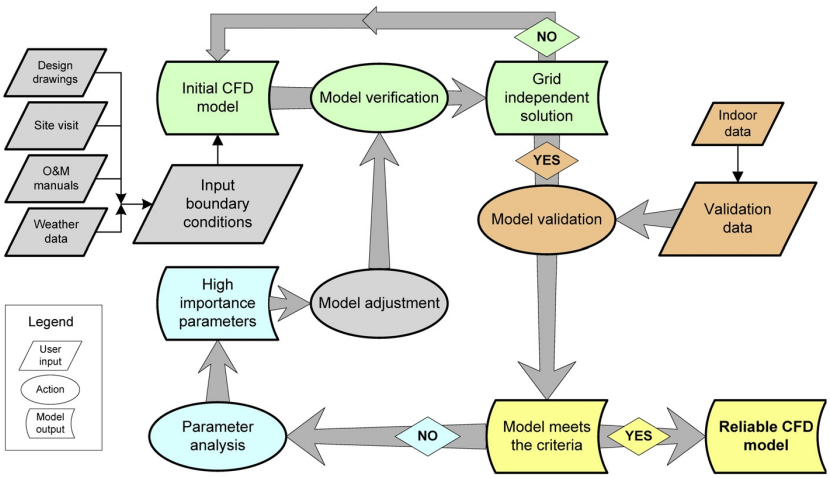

Figure 2.11: *Process of achieving a reliable CFD model of indoor environment (Hajdukiewicz et al., 2013a).*

As regards the grid generation, a mesh independence study should always be completed in order to ensure that a finer mesh did not lead to a significantly different solution. Hajdukiewicz et al. (2013b) evaluated that by using a grid convergence index for indoor air temperatures, but, in general, several methods are available in the literature. For instance, Celik (2008) proposed a procedure for calculating and reporting the discretization error estimates in CFD simulation. Using this methodology, the numerical uncertainty can be indicated by error bars on the results' graphs, enabling an accurate comparison with measured data and their respective errors. Moreover, a mesh independence or convergence study should be repeated if significant modifications are made to the model.

The formal procedure was illustrated by Hajdukiewicz with an example, namely a room in a library building (Hajdukiewicz et al., 2013b). Measurements were taken (see Table 2.1 on p. 15) and validation criteria defined: 0.1 m/s and 0.6°C absolute difference between measured and simulated air speed and temperature (Figure 2.12). If criteria were not met, a parametric analysis was completed to identify the effect of each boundary condition on the results. Steady state simulations were run with ANSYS CFX (2015). The full buoyancy model was applied, the standard k-ε was

chosen, convergence limit were 0.01 % of root mean square (RMS) residuals for mass and momentum equation, and 1.00 % of the energy conservation target. The importance of radiation model was tested by comparing two simulations: one without the model and one in which the discrete transfer radiation model was used. In the former case the convective heat flux from the person was 60 W/m^2, while in the latter there were a 18 W/m^2 convective and a 42 W/m^2 radiative heat flux. Results were similar and in agreement with experimental data, therefore the radiation model was not included in the final simulations. However, when a highly glazed space was tested by the same research team (Hajdukiewicz et al., 2013a), the radiance model became essential to get realistic results. Furthermore, single and double precision solutions were compared and no significant difference was noted. In these steady state conditions, the PMV model (Fanger, 1970) was used to evaluate thermal comfort.

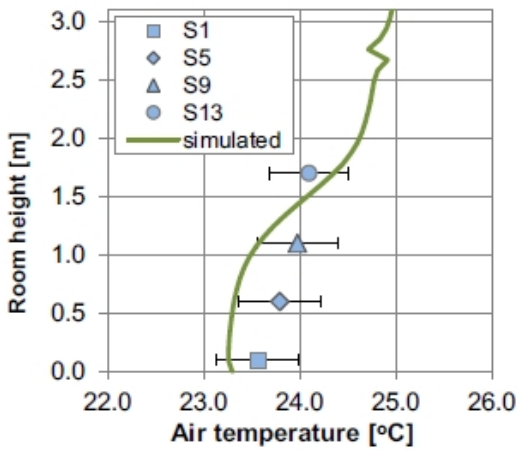

Figure 2.12: *Comparison between simulated and measured values (Hajdukiewicz et al., 2013b).*

While studying human thermal comfort, human bodies themselves play a central role. Indeed they are affected by the surrounding thermal environment, but they also modify it. Thus, research carried out at De Monfort and Loughborough University (Cropper et al., 2008, 2009, 2010; Cook et al., 2011) made a great step forward by coupling the IESD - Fiala model (Fiala et al., 1999, 2001) with a commercial CFD software, namely ANSYS CFX (2015).

The IESD - Fiala model was rewritten in Java programming language, therefore

it is platform independent, and ANSYS CFX (2015) was chosen for its ease to be customised. The Junction Box code was used to control the coupled simulation, to determine when information should be exchanged, to write heat flux valued to be used by IESD - Fiala model, to read new boundary condition from IESD - Fiala model and store them, which are then supplied to the solver by using the CFX expression language (CEL) (Cropper et al., 2010). There is no data exchange while the RMS residuals are below the chosen threshold. In detail (Figure 2.13), at the end of each time step of a transient CFD simulation, body surface temperatures, near-wall air temperatures, convective heat transfer coefficients, convective heat flux, radiative heat flux and near-wall relative humidity values are sent from the CFD software to the IESD - Fiala model for each of the 59 parts of the body surface. After the IESD - Fiala model reached a converged solution, the values of temperature, moisture mass fraction and emissivity for each of the 59 parts are sent back to the CFD program, and the CFD solver moves to the next time step.

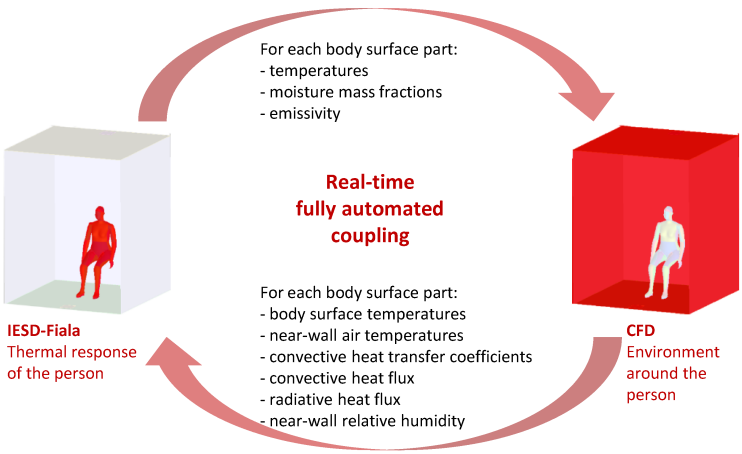

Figure 2.13: *A schematic diagram of the information exchange between the two models.*

This coupled system was used to model a person in a naturally ventilated environment (Cropper et al., 2010). The person was represented with a very high level of detail and two geometries were considered: a nude figure and a clothed one. ICEM CFD (2015) was used to optimise the geometry and therefore facilitate the mesh gen-

eration process. The chosen turbulence model is the Shear Stress Transport (SST) k-ω model due to its capability to resolve the boundary layer near the surfaces. Moreover, prism layers were used near the surface (Figure 2.14). In this study, the discrete transfer radiation model was also included to model the long-wave radiation heat exchange between the body and the surrounding surfaces. The Monte Carlo radiation model was not used because it requires a significantly greater computational time. Other studies (Cook et al., 2008) showed that this effort may not be compensate with higher quality results. The time required to complete this coupled simulation was 7.9 CPU hours using 16 processor cores (Cropper et al., 2010).

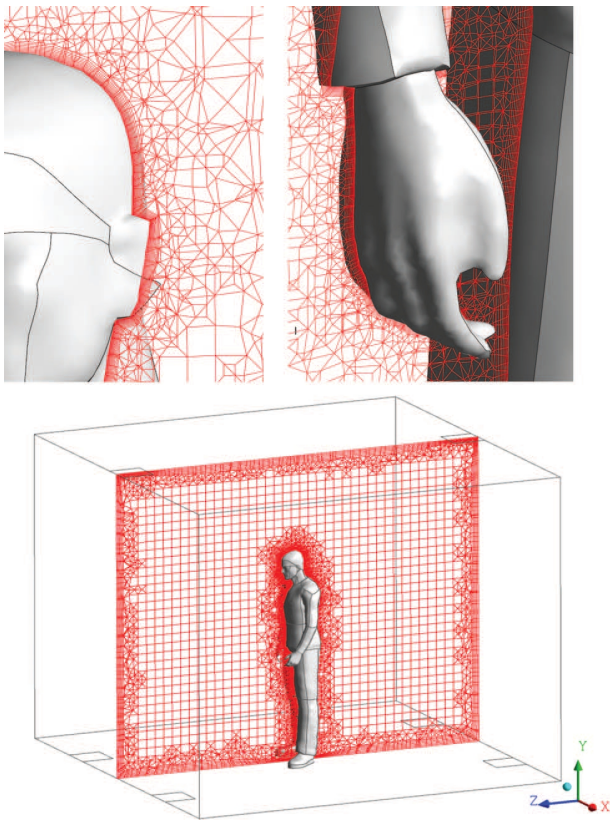

Figure 2.14: *The clothed body geometry within the CFD mesh (Cropper et al., 2010).*

The same coupled system was also applied to study buoyancy-driven natural ventilation in a school class room (Cook et al., 2011). In this case, one of the 31 occupants was modelled in detail as described above and coupled with the IESD - Fiala model, the others were represented by using rectangular blocks. While maintaining constant

the other parameters, two simulations were performed for each case: one without and one with the fully coupled model. Thermal sensation was estimated by using the PMV index in the former case and the dynamic thermal sensation in the coupled model. In the latter case, the body surface temperatures are lower due to the action of the active system. The difference between the two cases could be even higher in less uniform or in transient conditions because the uncoupled model would not capture the response of the human body. Moreover, the PMV model would not be accurate in such non-uniform conditions.

Although a real time coupling was never reached, other researchers also focused on this topic, highlighting the importance of moving from uncoupled systems (Gao and Niu, 2004, 2005) to manually coupled system (Gao et al., 2006, 2007). In this case the human thermal regulation model adopted is the UCB model (Huizenga et al., 2001). While studying thermal comfort in 2005, Gao and Niu (2005) also stated that the k-ε model was the best choice among the turbulence model, suggesting that a low Reynolds number k-ε model is more accurate for the prediction of heat loss from human body, and the standard k-ε and the Re-Normalisation Group (RNG) k-ε model are sufficient to predict airflow fields.

The k-ε turbulence model and the Reynolds Stress Model (RSM) were compared in 2004 by Nielsen (2004), while analysing air movement in a room in which a manikin was placed. The RSM predictions with wall reflection terms were closer to measurements, showing a higher growth rate of the wall jet parallel to ceiling than the growth rate perpendicular to the ceiling. Moreover, the use of a detailed human shape provided with a more accurate solution.

A study by Sevilgen and Kilic (2011) also analysed the air flow, heat transfer, moisture transport and thermal comfort in a heated room. A manikin with surfaces at constant temperature was used to simulate a human body, and good validation was completed in steady state conditions. Thermal comfort was predicted by using the PMV (ISO, 2005), but results were not compared with actual votes. A surface-

to-surface radiation model was used to account for the radiation exchange between the surfaces in the room. The RNG k-ε turbulence model was chosen.

Research by Martinho et al. (2012) investigated the sources of potential errors when the air flow and heat transfer around a human body are studied by using CFD. Two group of errors were identified, namely physical approximation and spacial discretization errors. As regards the former group, best fit with experimental data was achieved by the SST k-ω turbulence model and the Monte Carlo radiation model.

The effect of human body shape and the grid dependency for indoor thermal comfort were studied by Seo et al. (2013), who compared detailed and simpler computer simulated person, and natural and forced convection. The RNG k-ε model was chosen and combined with the enhanced wall treatment. Thermal comfort was estimated by using the PMV (ISO, 2005) and the equivalent homogeneous temperature, which evaluates the thermal comfort in different parts of the body. In the latter case, the use of a detailed human shape and prism layers is recommended since this leads to more realistic results.

CFD can be also used to predict thermal comfort in outdoor environments. Although in this case the concepts of comfort and discomfort would require different considerations that are out of the scope to this literature review, there are elements in common while using CFD simulations. Hamza et al. (2014) indeed discussed the advantages and disadvantages of CFD for this purpose, and compared Reynolds-Averaged Navier-Stokes (RANS) turbulence models with more sophisticated models, namely Large Eddy Simulation (LES), Detached Eddy Simulation (DES) and Direct Numerical Simulation (DNS). It was concluded that in general RANS models are a good compromise between quality of the results and computational power required, including the case in which thermal comfort depends on air movement, namely wind.

The acronyms RANS, LES, DES and DNS mentioned in previous paragraph are related to how the turbulence is treated. Turbulence occurs when the inertia forces in the fluid become significant compared to the viscous forces. The Reynolds number is

defined as the ratio between inertia and viscous forces, and therefore the higher the Reynolds number, the more turbulent the fluid flow becomes. Navier-Stokes equations could be used to describe any fluid flow, regardless of its turbulence level, but the required computational power to fully solve a given problem significantly exceeds the power that is currently available. For this reason, several turbulence models have been developed which simplify the original unsteady Navier-Stokes equations by the introduction of time-averaged quantities and a turbulent viscosity to produce the RANS equations. In these time-averaged equations, the fluctuating quantities, called Reynolds turbulent stresses, are taken into account by adding some extra terms in order to achieve closure. Additional equations are then required to balance the added unknowns. The equations used to close the system and their numerical coefficients define the type of turbulence model (Versteeg and Malalasekera, 2007).

Compared with RANS models, LES, DES and DNS are more advanced methods to treat the turbulence. LES is based on the idea that larger turbulent structures are anisotropic, problem-dependant, and represent the most significant energy-containing eddies, being therefore responsible for the majority of the effects such as transport, mixing and heat exchange. On the other hand, smaller eddies are dissipative, isotropic and do not depend on the specific problem. Thus, using LES, large eddies are directly simulated, while small eddies are modelled by means of a sub-grid scale model. However, this procedure increases the computational power required to solve a given problem as a finer mesh is need. DES is a method that combines LES and RANS using LES in those regions where the grid is sufficiently fine, and RANS elsewhere. DES was developed for the Spalart-Allmaras model (Spalart et al., 1997), and its use is still limited. DNS are the most advanced method as, in this case, Navier-Stokes equations are solved numerically without any model. However, the computational power is very high, and therefore DNS are not usable to investigate typical engineering problems.

Focusing again on CFD and thermal comfort,only one study (Prakash and Ravikumar, 2015) has been found about the analysis of thermal comfort in residential build-

ing by using CFD, while another fairly limited research was about indoor air quality (Yang et al., 2014). Prakash and Ravikumar (2015) focused on the effect of window opening position at the adjacent walls, starting from the fact that thermal comfort in ventilated buildings mainly depends on the size and orientation of windows. The PMV index was used to predict thermal comfort. Although dealing with residential environments, no measurements were taken in real houses. The model indeed was validated only by using results from wind tunnel and with a network model. Thus, there is no direct connection with a real domestic environment. Moreover, also in this study the PMV calculation was done according to ISO 7730 (ISO, 2005), which does not take into account the elevated air speed effect (ASHRAE, 2013a). This seems a significant limitation for a research that analyses thermal comfort in relationship to window openings, and therefore to air movement.

Horikiri et al. (2015) studied the flow and heat transfer characteristics, and analysed thermal comfort in rooms considering different flow complexities and geometrical features varying the type and location of furniture and heat sources. Thermal comfort was assessed using the traditional PMV and PPD indices (Fanger, 1970), which were calculated by an FORTRAN code developed by the authors, while a commercial CFD package was used to predict the flow field using steady-state simulations. Thus, in this study there is no real-time connection between thermal comfort model and CFD.

There is then a significant amount of published research which does not deal with thermal comfort or IEQ, but with the use of CFD to predict other things such as natural ventilation in buildings, or with methods such as uncertainties analysis in CFD.

A report by Faragher (2004) focused on probabilistic methods for quantification of uncertainty and error in CFD. Four sources of errors were identified: physical modelling, discretization, programming and computer round-off errors. In the first group, potential sources of error for an indoor environment analysis are forcing steady solution for unsteady flows, using RANS instead of LES or DNS, using wall functions

instead of a fine mesh near the wall, using an inappropriate radiation model and using Bossinesq approximation. Discretization errors can be evaluated by grid refinement and time step refinement studies. Moreover, second order scheme should be used, if possible. Uncertainty can be divided into two types: the former is about how well the mathematical model represents reality (e.g. a turbulence model) and it is difficult to evaluate in terms of probability density function, the latter is often called "*parametric analysis*" and is due to the lack of precise data for the analysis (e.g. a variable not measured). Several techniques such as the Monte Carlo method are available, but the choice depends on the case to be analysed.

Turbulence models have always a significant impact on the results, and there is no perfect model that can be used in every situation, but the most suitable model should be identified each time. In a study about buoyancy driven natural ventilation, Cook et al. (2005) used the RNG k-ε model. Zhai et al. (2007) studied various turbulence models for the prediction of air flow in enclosed environments, identifying the prevalent models. It was concluded that the k-ω SST turbulence model is superior to the standard k-ε and the RNG k-ε models. However, comparison with measured data suggested that the RNG k-ε model is usually more suitable without modifications (Zhang et al., 2007). Other studies (Ito, 2014; Pasut and De Carli, 2012) also successfully used k-ε models in indoor environments. When more details are needed, LES can be used (Choi and Edwards, 2012). It was also noted that in transient simulations a Lagrangian approach with LES or DNS is more accurate (Wang et al., 2012), but the computational power and time required increase significantly.

Field studies (Indraganti and Rao, 2010; Indraganti, 2010a,b,c, 2011) showed that ceiling fans are often the main means used by people in warm and hot environments in fast growing countries such as India to improve their thermal comfort, but therefore they are also a major source of non-uniform conditions in indoor occupied spaces. A study by Jain et al. (2004) provided with very useful qualitative information about the flow field generated by a ceiling fan. Using smoke from thick incense sticks, the

flow field created by the ceiling fan was visualised, identifying the main regions of the flow and its key behaviours such as the swirling movement. However, too little information is available in the literature in order to build detailed three dimensional CFD models of ceiling fans.

Adeeb et al. (2015) focused on the effect of the number of blades on the performance of ceiling fans, but the study is limited to steady state simulations and used a first order upwind scheme. In a model that explicitly represents the blades, if transient simulations and higher order schemes were used, the computational power and the complexity of the solution would increase significantly. Another work by Afaq et al. (2014) aimed to improve the flow field generated by a ceiling fan and its efficiency comparing different blades' geometry. Similarly to Adeeb et al. (2015), this research was carried out in collaboration with the Fan Development Institute Gujrat (Pakistan), and primarily focused on the geometrical features of the ceiling fan.

Momoi et al. (2004, 2007) proposed a model for predicting the air flow generated by a ceiling fan in large air-conditioned room, achieving in general a good agreement between simulation results and measurements, but overestimating the air velocity near the rotational centre of the ceiling fan. Moreover, there is a significant limitation in the applicability of the methods used in this research. The ceiling fan was not explicitly created in the model, but only its effect was modelled as boundary conditions of air velocity data measured near the ceiling fan. This required a very elevated number of measurements of air velocity, which means measuring the three components of the vector and not only air speed. Furthermore, more work is required to evaluate the effect of different turbulence models.

The features of air flow induced by a room ceiling-fan were studied also by Bassiouny and Korah (2011). However, although the authors highlight that this problem should be analysed in 3D, only two 2D domains were considered, namely a the fan plane, and a vertical mid-plane passing through the fan rotation axis. Thus, the truly three-dimensional behaviour of air flow generated by a ceiling fan is not cap-

tured, and their modelling approach cannot be therefore applied to three-dimensional models.

Another study on effect of ceiling fans on air mixing and Upper-Room UltraViolet Germicidal Irradiation (UR-UVGI) disinfection efficacy (Zhu et al., 2014) modelled the fan explicitly and used a moving mesh. However this does not guarantee better results, and indeed the authors stated that "*large differences were generated between the experimental and simulated results*". This shows how the larger computational effort required when the blades are modelled in detail and a moving mesh is used is not compensated by more accurate predictions, and this is due to the higher number of potential sources of uncertainty and error introduced within a model. In other words, minimizing the number of input parameters and assumption is likely to be the key for a reliable model.

Computer simulation results can be compared with measurements such as temperature and air speed to identify the most suitable turbulence model. However, there are also other methods to study air distribution. One of these is the Particle Image Velocimetry (PIV) (Cao et al., 2014a), which is the most popular and versatile optical anemometry for measuring velocity and related properties in fluids (Liu et al., 2012), and it has been used in several previous studies including research on airliner cabins (Cao et al., 2014b), exhaled flow from breathing thermal manikin (Feng et al., 2015), and human convective boundary layer and its interaction with room ventilation flow (Licina et al., 2014, 2015). Velocities are determined by the movement of a group of particles seeded into the flow. Thus, it is essential to clear the optical path during the experiment, which means that the considerable geometries are limited. Moreover, due the use of high power laser, a very accurate analysis of the potential risks for researchers must be carried out and then appropriate safety measures put in place before starting any experimental work with this powerful, but highly dangerous and expensive tool.

2.3.5 Dynamic thermal modelling

Dynamic Thermal Modelling (DTM) is a technique often used to study the performance of buildings and that can be combined with CFD, as they provide complementary information (Chen, 2009). A large variety of simulation software is available and used (Gandhi et al., 2014). As shown by Lomas et al. (2007), DTM can be used to predict the performance of a building over a period of time such as one year by comparing ventilation strategies or the impact of variable heat gains, and estimating likely energy consumption. However, DTM predicts overall space temperature, being not able to cope with spatially varying temperatures. This limitation may be partially overcome using some virtual partitions to split a space such a room into smaller portions. However, even with this method, DTM cannot reach the same level of spatial resolution of a CFD model. For instance, this approach can be useful to simply separate the south- and north-facing parts of a large room. Similarly, also Zhang et al. (2013) coupled DTM and CFD to predict the performance of natural ventilation. However, air flow network models, which are used in DTM, underestimated air flow rates.

Schiavon and Melikov (2008) investigated the potential savings of energy needed for cooling by means of DTM. In their research, air movement was used to avoid the high use of air conditioning while maintaining the same level of comfort. Thus, DTM was used to compare the energy consumption of fans and air conditioning. As reported by the authors, the power input of the fan is a critical factor. More recently, also Hoyt et al. (2014) estimated the energy savings that can be achieved by using air movement devices. In both studies, the cooling set-point temperature was chosen based on the available air-speed, but it did not vary across the year, and only office buildings were analysed.

While studying thermal comfort, the way in which this is measured plays a critical part. This is relevant when DTM is used since commercial computer programs give a variety of metrics related to thermal comfort, and the right index should be consid-

ered when comparing different design options. Peeters et al. (2009) noted that, for residential buildings, conditions are not comparable with those used to define PMV and PPD algorithms. This is due to the fact that residential environments are often characterised by transient thermal conditions due to fluctuating internal gain and rapid variations of activity level, and therefore of the metabolic rate. Moreover, the wider possibility of adaptation and the fact that the occupant is the person who pays for the energy usually lead to the acceptance of a wider range of conditions. Thus, a new zonal approach was proposed, which distinguished between bathroom, bedrooms and other rooms.

When mixed mode buildings are analysed, the level of complexity increases as the model needs to be able to cope with the contemporary use of mechanical and natural ventilation. Spindler and Norford (2009) proposed an approach to optimise mixed mode cooling performance prediction, but stated that this model cannot be used in domestic buildings because the occupants have direct control over the system.

Borgeson and Brager (2011) also investigated thermal comfort metrics and mixed mode buildings, and noted that the choice of the comfort criteria such as PMV or adaptive model significantly affects the results and thus the acceptability of a solution. Therefore, these metrics should not be taken too seriously and the authors said that better quantitative models to predict thermal comfort are required.

Personal characteristics also affect thermal comfort prediction, especially when the PMV method is used as it requires met and clo values as an input. Based on a field campaign in Switzerland, Haldi and Robinson (2011) found that clo is strongly correlated with the outdoor temperature, thus a logistic model was developed which gives a probability of distribution. Met are instead affected by drinks. Cold drinks assumption is linked with the indoor conditions, and the indoor temperature was found to be the best predictor for their consumption. Hot drinks assumption varies with seasons, and can be predicted using a running mean of the outdoor temperature as predictor. Thus, binary logistic model was implemented. However, despite the

applicability of this approach to offices or schools, its use in domestic buildings, where clo and met are more varied, could not be so easy.

Weather data are then another crucial elements, especially when future scenarios are analysed (de Wilde and Tian, 2010; Shikder et al., 2012; McLeod et al., 2013). Occupants of more energy efficient buildings such as passive houses are likely to experience overheating if appropriate solutions are not put in place (McLeod et al., 2013). Therefore, both reliable thermal comfort metrics and weather data are essential to compare different alternatives, including the use of air movement.

2.4 Justification for the research

Based on the arguments presented and discussed in the introduction and literature review, it clearly appears that, in recent years, there has been a proliferation of air-conditioning in both residential and commercial buildings, and, due the growing disposable income in several densely populated developing countries such as India, the energy demand for space cooling is dramatically increasing. Moreover, in a warming climate and with a building stock that is becoming more energy efficient for the cold season, the need for appropriate cooling systems is likely to become essential to avoid overheating also in cooler north-European countries. However, mechanical systems, such as built-in air conditioning, consume a lot of energy because they cool down quite evenly the entire space, rather than the occupants.

Several field studies, mainly in extra-European countries, support the idea that air movement in warm environments improves thermal comfort, rather than causing the so-called draught sensation. This idea would lead to a lower use of air-conditioners, but also to transient and asymmetrical environments. Recent research claims that these conditions generate more pleasant environments, but the extent to which this will happen cannot be easily predicted by using the traditional PMV model in the design stages.

The adaptive thermal comfort model can be used to evaluate the acceptability of certain temperature conditions when adaptation can take place such as in residential buildings. However, such a model does not allow for a direct comparison between the effect of different cooling design solutions, but simply shows that a certain temperature range is acceptable in relationship to the outdoor temperature.

Designers need to be able to accurately predict the performance of different solutions to use them, and cannot rely on a generic possibility of adaptation. If from an energy point of view a solution is preferable, then designers should make use of this solution the easiest choice for the occupants. But to do so, a robust method to evaluate its performance is required.

CFD alone has been used to predict thermal comfort for years, and recently manual coupling with human thermal regulation models has been done. However, almost all studies focused on steady state conditions and the manual coupling was quite complicated. Moreover, there is almost no research which used data measured in actual residential buildings to evaluate CFD predictions.

In the literature it has been found that there is only one existing fully coupled model, which is based on the IESD - Fiala model (Fiala et al., 1999, 2001) and ANSYS CFX (2015). The coupled model can be used in a variety of transient and asymmetrical conditions, but it has never been tested in such a real environment. Therefore further research is needed to understand the applicability of this coupled model in order to produce reliable results, and hence to be able to promote low energy space cooling solutions such as increased air movement while not jeopardising the occupants' thermal comfort. Challenges include the identification of realistic scenarios, the collection of reliable data in real buildings or in realistic simplified experimental facilities, and the need to balance model quality results and computational power required. However, such a model will be widely usable not only in residential and non-residential buildings, but also in several other non-uniform environments such as air plane cabins and train coaches.

Chapter 3

INITIAL TESTING OF THE COUPLED SYSTEM: ENVIRONMENTAL CHAMBER STUDY

3.1 Overview of the experimental chapters

This chapter is the first of four experimental chapters. In general, their aim is to describe in detail the methods chosen to conduct this research and the reasons behind each choice, and to clearly illustrate the results of the different parts of this research highlighting the most relevant ones.

In this research, computer simulations and laboratory-based experiments were used extensively to fully address the aim and objectives of this project, and therefore to answer the research question. Moreover, this research benefited from the close link to a wider international project which included field work in residential buildings in the UK and in India. Although this field study was not designed as part of the PhD research, some of the data collected and the information obtained during this field

study were used for this PhD research.

In this research, CFD coupled in real time with a human thermal physiology and comfort model, the IESD-Fiala model (Fiala et al., 1999, 2001), was used to investigate thermal comfort in non-uniform thermal environments. The most relevant features of this coupled system are summarised in the following section 3.1.1.

In this study, this coupled system was initially applied to environmental chamber studies, and then to model more complex, but also more relevant, actual domestic buildings. Laboratory-based experiments were used to provide high-quality data to validate the CFD models. DTM was then used to estimate the likely energy saving that can be achieved in residential buildings by using air movement to increase the cooling set-point temperature without jeopardizing occupants' thermal comfort in such non-uniform conditions.

The structure of these four experimental chapters is as follows. Chapter 3 illustrates the first application of the coupled system, which comprises measurements and computer modelling. Chapter 4 describes the work done to create and validate a detailed CFD model of a typical Indian ceiling fan, whose crucial importance will be introduced in section 4.1 in the same chapter. This section explains the connection with the wider international project, what real buildings were considered in this PhD research and why, within this sample, certain scenarios were chosen to be studied using the coupled system. Chepter 5 is about the application of the coupled system to real domestic buildings, which brings together the work undertaken in the previous experimental chapters. Lastly, Chapter 6 illustrates how DTM was used in this project for estimating energy savings due to air movement in mixed mode buildings in India.

3.1.1 CFD and IESD-Fiala coupled model: key features

The main characteristics of the IESD-Fiala model have been presented and discussed in section 2.3.3, while the whole coupled system has also been previously described

in section 2.3.4. However, at this point, it is useful to highlight the most relevant features of the coupled system in relation to this research. Furthermore, it is worth noting that, in the context of this research, the expressions "coupled model" and "coupled system" mean the same thing and therefore used interchangeably.

Firstly, the coupling was done using ANSYS CFX version 14.5.7 (Cropper et al., 2008, 2009, 2010; ANSYS CFX, 2015) and therefore this version of this commercial CFD program had to be used for this research. Secondly, in CFD, a generic occupant is represented by a virtual manikin. To couple the two components of the system, the surface of this virtual manikin must be divided into 59 parts, whose names must match those used by the IESD-Fiala model. Thirdly, the coupling between CFD and ISED-Fiala model currently works only with one virtual manikin per CFD model. Thus, other occupants may be included in the CFD model, but modelled only as passive uncoupled elements (for instance, simple boxes with a fixed surface temperature).

The coupling required transient CFD simulations to reach a converged solution due to the truly transient behaviour of the modelled phenomenon (Cropper et al., 2008, 2009, 2010). At each time step of the CFD simulation, for each of the 59 surface parts, body surface temperatures, near-wall air temperatures, convective heat transfer, coefficients, convective heat flux, radiative heat flux, and near-wall relative humidity are sent from the CFD to the IESD-Fiala model. After IESD-Fiala model has reached a converged solution, temperatures, moisture mass fractions, and emissivity values are sent back to the CFD model. The total duration of this process depends on the length of the period simulated in CFD. For instance, if the time-step in CFD was 10 s and the simulated period 120 s, then the exchange process would end when total simulated time would be equal to 120 s.

Lastly, it is essential to highlight that the coupled system generates two metrics that are related to thermal comfort, namely the Dynamic Thermal Sensation (DTS) and the PPD. The former is a thermal sensation index, and it uses the 7-point ASHRAE scale (from 3 to -3: hot, warm, sprightly warm, neutral, slightly cool,

cool, cold). The latter predicts the percentage of occupants that will be dissatisfied with the thermal conditions. The minimum level of dissatisfaction corresponds to a neutral thermal sensation (the mathematical relationship DTS-PPD is the same as PMV-PPD). In other words, this means that the number of people that are satisfied with their surrounding thermal conditions is maximum when their thermal sensation is zero (that is neutral). Based on these consideration, although the DTS is a thermal sensation and not a thermal comfort metric, it is possible to use it as a means to evaluate thermal comfort. The closer the DTS is to zero, the lower the number of dissatisfied people is.

3.2 Initial testing of the coupled system: environmental chamber study

To test and validate the coupled model by comparing simulation results with measured data for a number of different realistic scenarios, two likely configurations were created in an environmental chamber. Typical furniture, a thermal manikin and devices such as portable fans were used to generate non-uniform controlled environments, and detailed measurements were taken. These included air temperature, mean radiant temperature, relative humidity and air speed at several points within the room. The same configurations have then been modelled using the coupled CFD and IESD-Fiala model, and simulations run. Actual values and computer-based predictions have been compared, and the reasons for any differences analysed. Since in this part of the research there are no actual thermal sensation votes available as no human participants were involved in the experiments, the thermal comfort realted outputs of the coupled model are discussed by comparing them with the type of output that would be generated by the PMV-PPD method.

3.2.1 Experimental set-up

Environmental chambers have been used in thermal comfort studies since the early stages of research in this field, and both human participants and thermal manikins have been used. The latter were especially used to provide accurate data for the validation of CFD models (Gao and Niu, 2005), highlighting the importance of an accurate representation of the human body shape when studying the micro-environment around a person, and that the radiative heat transfer cannot often be overlooked.

For this first application of the coupled system, a rectangular environmental chamber located at Loughborough University was used, together with a thermal manikin "Victoria" seated in the room (Figure 3.1). The manikin "breathing" capability was turned off during the experiment. Use of a manikin provides an objective and repeatable human-shaped heat source for comparative testing. Moreover, a common 320 mm diameter desk-fan with 3-step regulator has been placed on the floor inside the chamber to provide air movement.

Figure 3.1: *The experimental facilities.*

During the entire experiment, Victoria was wearing panties, a shirt, a thick sweater, trousers, socks and shoes. These are very common garments, and their thermal insulation values (that are clo values) were not measured in this experiment. Section 3.2.2 explains how they have been represented within the coupled model. The manikin is divided into 20 body parts, and they were all kept at a constant sur-

face temperature, 34°C. This is done by the software that controls Victoria, which increases or reduces the amount of power that is supplied to each body part. The power required to maintain a constant temperature provides a measure of the rate of heat loss to the surrounding environment. Thus, the higher the insulation provided by the clothing, the lower the power required to maintain the 34°C surface temperature. Focusing on the structure of the manikin (Pt-teknik, 2017), Victoria is made of glass fibre (thickness: 3 mm) with nickel wire embedded in a heat-conducting compound. The type of sensors used for measuring the surface temperatures is nickel all over the manikin 0 to 0.3 mm under paint with 2.2 mm spacing. The power (24 V) is supplied to each body part in pulses (40 Hz, 0 to 90% duty cycle).

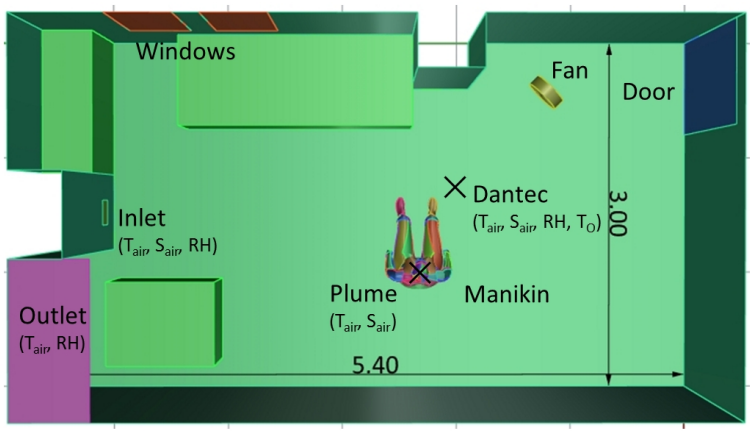

Figure 3.2: *The experimental facilities. In brackets, the measured quantities in each location (with Dantec, air temperature and air speed were measured at three heights, namely 0.1 m, 0.6 m, and 1.1 m from the floor).*

Air was supplied to the chamber via a low-level inlet, and could leave the space only through a roof-level opening (Figure 3.2). The door was closed while taking each set of measurements, and the windows of the chamber cannot be opened. Moreover, due to their multi-glazed well insulating structure, the internal surface temperature of the windows can be assumed equal to the temperature of the surrounding wall. Indeed these windows only provide a visual connection to the outside.

The environmental chamber has been warmed up using the walls, inside which there are pipes in which heated water circulates, and pre-heating the air entering

into the room. Having left the room warming up for 24 hours, due to the severe outdoor winter conditions at the time of the experiment, the maximum air temperature achievable was between 25°C and 26°C. For this preliminary measurements, U12 Hobo sensors (Onset, 2015) were used, and the temperature values reported in this paragraph are the average values of the temperature recorded (every 10 minutes) in the two hours before starting the main test. During this period of time, the fluctuations of the temperature values were significantly smaller than the accuracy of the sensors (Table 3.1). Nine sensors were placed near the walls and in the centre of the environmental chamber at 1.1 m above the floor (indicated as x_i in Figure 3.3). An additional sensor was placed on the floor in the centre of the room (indicated as x_{floor} in Figure 3.3), and a lower temperature value was recorded in this spot, namely 23°C. Although this type of sensors does not measure surface temperatures, but only the near-wall air temperatures, the information obtained from this preliminary set of measurements was used to assume that all walls of the chambers have the same temperature, while the floor has a lower value.

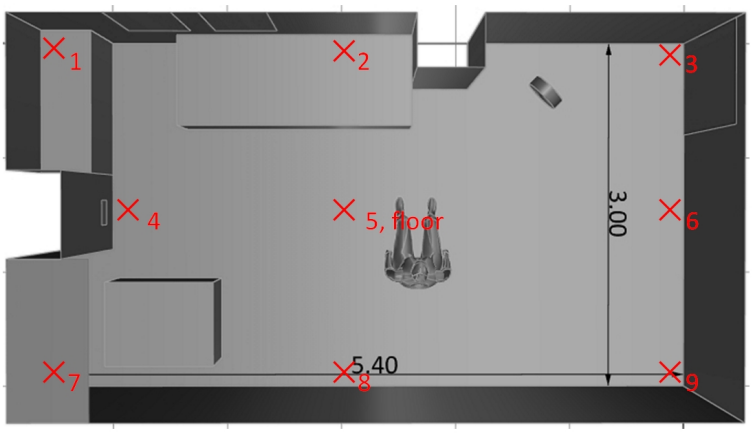

Figure 3.3: *Position of U12 Hobo sensors (Onset, 2015) during the preliminary measurements.*

In the main test, measurements have been taken with U12 Hobo sensors (Onset, 2015) and with Dantec ComfortSense kit (Dynamics Dantec, 2015), whose characteristics are summarised in Table 3.1. One U12 sensor has been placed in the inlet and one in the opening to measure the relative humidity and the temperature of the air

going into and out of the chamber. A complete Dantec kit has been placed close to Victoria, measuring air temperature and air speed at three heights (from the floor: 0.1 m, 0.6 m, and 1.1 m), operative temperature and relative humidity (Figures 3.1 and 3.2). The mean radiant temperature has not been measured directly, but it has been calculated at a later time using the Dantec ComfortSense software. This procedure was chosen due to the type of sensors and software provided with the Dantec ComfortSense kit (Dynamics Dantec, 2015). Another two Dantec ComfortSense probes have been placed respectively 50 cm above the head of the manikin and in front of the inlet. The former has been used to gain information about the thermal plume (air speed and air temperature), the latter to measure the air speed at the inlet.

Table 3.1: *Measurement equipment characteristics*

Feature	Hobo U12	Dantec	Hobo Pendant
Measurement range	T_{air}: -20 to 70°C RH: 5 to 95 %	T_{air}: -20 to 80°C RH: 0 to 100 % T_o: 0 to 45°C S_{air}: 0.1 to 30 m/s	T_{air}: -20 to 70°C
Accuracy	T_{air}: ± 0.35°C RH: ± 2.5 %	T_{air}: ± 0.50°C RH: ± 1.5 % T_o: ± 0.2°C S_{air}: ± 2 % of reading (OR) ± 0.02 m/s	T_{air}: ± 0.53°C
Response time	T_{air}: 6 minutes RH: 1 minute	T_{air}: 4-5 s RH: 10 minutes T_o: 2 minutes S_{air}: 2-3 s	T_{air}: 10 minutes

Two sets of measurements have been taken. In both cases the measurement equipment was identical, and data have been recorded for 50 minutes. However, during the first test, the fan was switched off, while during the second it was operating. Therefore, the effect of higher air speed on the predicted thermal sensation can be assessed.

Lastly, all sensors used in this study were previously calibrated. The Dantec ComfortSense kit (Dynamics Dantec, 2015) was delivered with its own calibration

data, which is loaded into its controlling software during the set-up of the experiment. All U12 Hobo sensors (Onset, 2015) were brand new sensors which came with their calibration certificate. In addition, they were tested in-house before the first use. This was done by placing them in the environmental chamber for one hour together with a Hobo Pendant data logger (Onset, 2015), and comparing the recorded temperature values (the sensors were grouped as close as possible). This reference sensor is waterproof, measures air temperature (Table 3.1), and was previously calibrated using a water bath. This procedure was chosen because the U12 Hobo sensors are not waterproof, and therefore the water bath cannot be used for the calibration of these devices. Although this procedure is not a formal calibration, it was still useful to further test these brand new sensors before their first usage.

3.2.2 Modelling approach and assumptions

A model of the environmental chamber as it was during the measurements was defined. Since the coupled model uses ANSYS CFX 14.5.7 (ANSYS CFX, 2015), the first steps have been generating a geometry and then a mesh that could be imported into this program.

Firstly, due to the complexity of the human shape, a STereoLithography (STL) file has been simplified using MeshLab (2016), and then imported into Rhino (2016), in which Non-Uniform Rational Basis Splines (NURBS) have been generated. The virtual manikin is then divided into parts, whose names must match those used by the IESD-Fiala model. In general, the remaining part of the geometry could be built either in Rhinoceros or in ICEM CFD.

Secondly, ICEM CFD has been used to generate an unstructured mesh. Since the fan was modelled in CFX as a momentum source, at this stage two sub-domains have been defined, namely the room itself and the fan. The shell mesh parameters have been set to "all triangle" and "patch independent". In order to generate a robust surface mesh, but also a smooth volume mesh, the mesh has been initially generated

using the Octree algorithm, then this volume mesh has been deleted and the quality of the surface mesh increased, and later the final volume mesh has been generated using the Delaunay algorithm. In the final mesh, 10 prism layers were also added to accurately model the boundary layer near surfaces. In the final mesh, the maximum mesh size on the manikin parts is 0.02 m, the maximum volume mesh size is 0.128 m, and the initial height of the prism layers is 0.002 m for the manikin and 0.004 m elsewhere. The surface mesh is shown is Figure 3.4, the volume mesh in Figure 3.5 and 3.6.

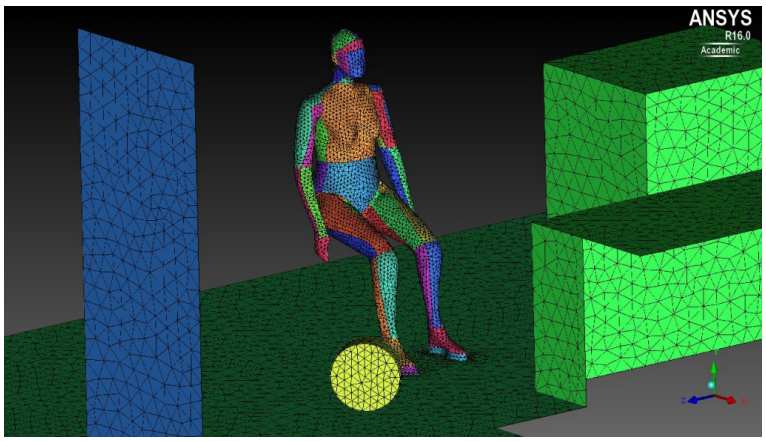

Figure 3.4: *Shell mesh.*

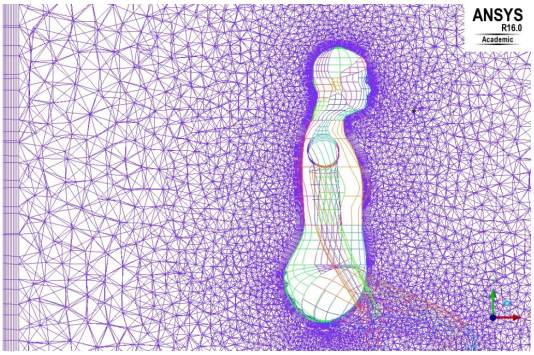

Figure 3.5: *Volume mesh.*

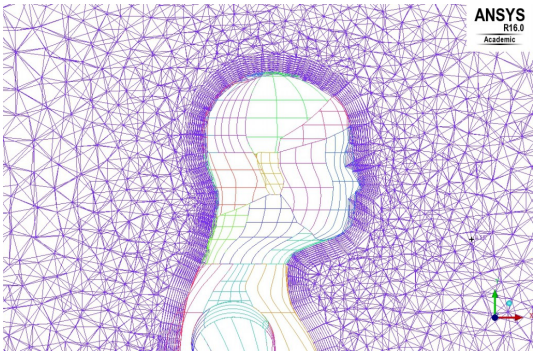

Figure 3.6: *Detailed volume mesh close to Victoria's head.*

The final mesh has then been imported into CFX. The boundary conditions for the manikin have always to match the requirements of the IESD-Fiala model, while the other surfaces have been modelled as fixed temperature surfaces. Based on

the considerations in the previous section, the same temperature (25.5°C) has been set on all walls and other internal surfaces (except from the manikin), but a lower temperature has been chosen for the floor (23.0°C). The boundary conditions for the manikin have not been directly typed into this CFX model, but imported using CFX Command Language (CCL) from a previous model developed by Cropper et al. (2010). Due to the length and complexity of these conditions (which includes the body surfaces' temperature and moisture mass fraction), this method ensured that there were no errors such as the misspelling of a variable or the forgetfulness of setting another one. This might be seen as a limitation of this study in terms of replicability. However, as it is now, the coupled system can be provided and installed only by its developers (Cropper et al., 2010), and therefore, for future tests conducted by other researchers, an existing model can be also provided at the same time. Air speed (S_{air} = 0.4 m/s), air temperature (T_{air} = 27.0°C) and relative humidity (RH = 34%, that means, in CFX, moisture mass fraction = 0.00826) at the inlet have been defined according to the measured values. Only air temperature (T_{air} = 25.8°C) and relative humidity (RH = 36%, that means, in CFX, moisture mass fraction = 0.00734) have been defined at the opening, plus a 2.69 loss coefficient, which is equivalent to a discharge coefficient of 0.61.

For the moist air inside the room, the initial mass fraction (0.00663) and buoyancy reference density (1.17801 kg/m^3) have been calculated based on the air temperature and relative humidity initial values using the following method (Cropper et al., 2010). The ideal gas law can be expressed as:

$$PV = nRT \tag{3.1}$$

where P is the pressure [Pa], V the volume [m^3], n is the amount of the substance [mol], R is the ideal gas constant [JK^{-1}mol^{-1}], and T the temperature [K]. Considering that M is the mass [kg] and m is the molar mass [kg/mol], and that n=m/M

by definition, then equation 3.1 becomes:

$$PV = \frac{m}{M}RT \tag{3.2}$$

The density of the gas ρ [kg/m^3] is defined as ρ=m/V, and therefore:

$$P = \rho\frac{R}{M}T \tag{3.3}$$

R$_{specific}$=R/M is called the the specific gas constant [Jkg^{-1}K^{-1}], and therefore:

$$P = \rho R_{specific}T \tag{3.4}$$

Equation 3.4 can be rearranged as follows:

$$\rho = \frac{P}{R_{specific}T} \tag{3.5}$$

At this point, it is assumed that the density of moist air is the density of dry air plus the density of water vapour. Thus, the buoyancy reference density is:

$$\rho = \frac{P_s}{R_{waterVapour}T} + \frac{P_d}{R_{dryAir}T} \tag{3.6}$$

Where R$_{waterVapour}$ is the specific gas constant of water vapour (461.495 Jkg^{-1}K^{-1}), R$_{dryAir}$ is the specific gas constant of dry air (287.058 Jkg^{-1}K^{-1}), P$_s$ is the partial vapour pressure of water vapour (expressed in Pa) and P$_d$ is the partial pressure of dry air (expressed in Pa). It is assumed that the partial pressure of dry air is the barometric pressure minus the partial vapour pressure of water vapour.

In CFX, the moist air has been modelled by creating a new material made by a mixture of "air ideal gas" (modelled using a constraint equation) and "water ideal gas" (modelled using a transport equation). The mass fraction calculated as explained above has been specified in the initial conditions for the latter component. The thermodynamic state of this new material was defined as gas. In CFX, as stated in

its modelling guide (ANSYS, 2015a), if the flow of a component is modelled using a constraint equation, its mass fraction is calculated to ensure that all the component mass fractions sum to unity, that is, the mass fraction of the component is set equal to the total mass fractions of the other components in the same fluid subtracted from unity. On the other hand, if the flow of a component is modelled using a transport equation, then it is transported with the fluid and may diffuse through the fluid, and its mass fraction is calculated accordingly (ANSYS, 2015a). Thus, this component has its' own equation for conservation of mass, and, after Reynolds-averaging, this equation can be expressed in tensor notation as (ANSYS, 2015b):

$$\frac{\partial \tilde{\rho}_i}{\partial t} + \frac{\partial \tilde{\rho}_i \tilde{\mathbf{U}}_j}{\partial x_j} = -\frac{\partial(\rho_i(\tilde{\mathbf{U}}_{ij} - \tilde{\mathbf{U}}_j) - \rho_i^{''}\bar{\mathbf{U}}_j^{''})}{\partial x_j} + S_i \tag{3.7}$$

Similarly to previous work by Cropper et al. (2010), the SST k-ω turbulence model has been chosen for its accuracy and robustness (turbulence models are extensively discussed in section 4.3.3), and a discrete transfer radiation model has been used to model the long-wave radiation heat exchange between the body and surrounding surfaces. Transient simulations have been performed to better model the real transient heat exchange process. A second order backward Euler scheme, and high resolution advection scheme and turbulence numerics have been used. The double precision option has also been selected.

In CFD, radiation models are not always used. However, when the coupled model is used to predict the thermal sensation, then it becomes essential to model the radiative heat exchange that happens between surfaces at different temperature since this heat exchange affects the thermal sensation. In general, radiation models are used to solve the radiation transport equation. In the discrete transfer radiation model, this equation is (ANSYS, 2015b):

$$\frac{dI_v(\mathbf{r,s})}{ds} = -(K_{av} + K_{sv})I_v(\mathbf{r,s}) + K_a I_b(\nu, T) + \frac{K_{sv}}{4\pi}\int_{4\pi} I_v(\mathbf{r,s'})d\Omega' + S \tag{3.8}$$

In this study, it is assumed that the medium, that is the moist air, is transparent to radiation, and therefore the radiation only affects the medium by heating or cooling the surfaces of the domain. Thus, in CFX, the transfer option "surface-to-surface" was selected within the discrete transfer radiation model. This radiation model is based on tracing the domain by multiple rays leaving from the bounding surfaces, and the path along a ray is discretized by using the sections formed from breaking the path at element boundaries (ANSYS, 2015a). Similarly to previous research (Cropper et al., 2010), in this CFX model, the chosen number of rays is 16. Furthermore, the chosen spectral model is gray, which means that quantities that do not have spectral dependency (such as from frequency, wavelength, or wavenumber) (ANSYS, 2015a).

Convergence criteria have been set equal to 1e-05 for the RMS residuals and 0.01 for the conservation target, which are the typical values used to achieve accurate solutions in engineering applications. Residuals are a measure of the local imbalance of each conservative control volume equation, and they are therefore a measure of the accuracy of the numerical solution. In CFD, the target is usually set to the RMS residuals, not to the maximum residual. Moreover, the RMS Courant number was monitored aiming for values smaller than five. Since it is an implicit code (ANSYS, 2015a,b), CFX does not require the Courant number to be small for stability, but this still leads to more accurate results. To reach this target, the chosen time step has been 0.5 s for the case without fan, and 0.2 s the case with fan. The total time simulated in both cases is 10 minutes.

For the configuration with the active fan, four simulations have been completed, each of which has a different value for the momentum source. Although perfectly matching the actual speed profile is a very complex task, using this approach it has been possible to assess how sensitive the DTS is to small variations of the air speed. At a later time, a fifth simulation was completed using the momentum source value that led to the best agreement between CFD results and measurements. However, in this fifth case, the fan was activated after 5 minutes to assess how the DTS reacted

to a rapid change of the air speed. In this fifth case, an adaptive time step was used to ensure that the RMS Courant number was always not greater than five without the need for any manual changes of the time step.

As mentioned before, in this study, the fan has been modelled as a momentum source, and therefore only the effect produced by the fan (increasing the air speed) has been modelled, but not its detailed geometry with the blades. In CFX, a momentum source can be applied to a sub-domain in cartesian or radial components. In this case, the former option was chosen. For the two horizontal components, the same value has been used (due to the fact that angle between fan and horizontal axes was 45°), while a different and significantly smaller value has been used for the vertical component. An iterative process has been followed to identify the most appropriate values. Due to the elevated computational cost of these CFD simulations and the fact that this parametric study could not be automated, it was possible to run only a limited number of simulations. The values used in the simulations described in the previous paragraph are summarised in Table 3.2. In preliminary tests, also lower and higher horizontal values were tested. All transient simulations started with the fan not in operation. For this reason, the air speed values of initial 5 s of each simulation have non been included in the calculation of the mean values used to compare simulated and measured figures.

Table 3.2: *Momentum source values used in this study*

Simulation	Horizontal components [kg m^{-2} s^{-2}]	Vertical component [kg m^{-2} s^{-2}]
1	25	2
2	15	2
3	20	0
4	20	2

As shown in Figure 3.1, the manikin was seated on a typical armchair, but this has not been included in the CFD model (Figure 3.2). The reason is that the coupled system cannot model the direct contact between parts of the surface of manikin and other objects such as an armchair. This is a limitation of the coupled system that

could be overcome only by rewriting the whole coupling system, and this might be done as future research. Creating a geometry near (but not in direct contact) the manikin to represent elements such as the armchair is also not feasible as this would compromise the stability of the CFD simulations. Indeed this approach would create a thin layer of air between the two surfaces (namely armchair and manikin), and this would lead to a very fine and complex mesh. In general, in CFD, this type of things are avoided to ensure the stability of the solution (otherwise, a simulation may not converge at all). Moreover, this would still not replicate the actual configuration (that is direct contact). For this reason, the armchair was not included in the CFD model, and the fan was placed in a position such that air was blowing directly on the legs of the manikin. Since the armchair has not been included in all simulations (with and without operating fan), it is still possible to compare the outputs of the model related to thermal comfort in the two configurations (with and without operating fan). Similarly, the Dantec ComfortSense air speed probes have been placed in the free-stream air region, before that the armchair affected the air flow generated by the fan.

Finally, the parameters within the thermal comfort and human regulation model are set. The environmental initial conditions have been matched with those set in CFX, the chosen activity level has been 1.2 met, and the clothing has also been defined in order to represent what Victoria was wearing. In particular, the coupled model allows to select a clothing option from a pre defined list which includes several typical Western combinations of garments. Options can be added only by its developers (Cropper et al., 2010) since this requires the modification of the source Java code of the coupling program which must then be recompiled.

Alongside the main simulations, a mesh sensitivity analysis was carried out, with the aim of estimating the discretization error and calculating the numerical uncertainty in the fine-grid solution, which is the grid then used for the main simulations. To do so using the accurate method proposed by Celik (2008), three increasingly coarse meshes

were used (see number of elements N_i in Table 3.3), a representative dimension h_i to be calculate, and a significant simulated value φ_i has to be used quantify this uncertainty. In this research, the air temperature at 1.1 m above the floor (position of the highest Dantec probe – complete kit) has been chosen since it is close to the manikin and in a central location. The process has been repeated twice and results are reported in Table 3.3. In the second analysis, a finer mesh was tested.

The mesh chosen for the main simulations is "mesh 1" of the first analysis, which has 1,297,150 elements and a numerical uncertainty equal to 1.76 %. The finest mesh of the second analysis has not been used as the CPU time required to solve it would approximately 10 times higher, but the numerical uncertainty would have been reduced by only 1.64 %.

Table 3.3: *Discretization error calculation (Celik, 2008)*

	Analysis 1	Analysis 2
N_1	1,297,150	5,685,417
N_2	691,817	1,297,150
N_3	377,870	691,817
h_1	0.03	0.02
h_2	0.04	0.03
h_3	0.05	0.04
r_{21}	1.23	1.64
r_{32}	1.22	1.23
φ_1	25.71	25.7
φ_2	25.72	25.71
φ_3	25.74	25.72
ε_{21}	0.01	0.01
ε_{32}	0.02	0.01
p	0.7347874	1.0050768
φ_{ext}^{21}	25.6	25.7
e_a^{21}	0.000389	0.0003891
e_{ext}^{21}	0.0023423	0.0006078
GCI_{fine}^{21}	1.76%	0.12%

3.3 Results and discussion

In this section, the results of the initial testing and validation of the coupled system are presented. Firstly, the simulated values are compared with measurements in order to validate the CFD model. Secondly, the computational power required to solve these models is discussed. The last part presents the thermal comfort results.

3.3.1 CFD models validation

The key parameters used to validate the models are air temperature and air speed, due to their significant impact on the human thermal sensation and to the fact that they have been measured at several points within the environmental chamber. Although the numerical uncertainty of the CFD simulations has been quantified, 1.76 %, in all images there are error bars only for the measured values, in order to keep the images clearer. In principle, simulated results are in agreement with measured values whenever their respective error bars overlap. However, in this application, the discretisation error is negligible compared with the measurement errors. Thus, omitting its relative error bars in the graphs does not overlook any important information.

Figure 3.7 presents the comparison between simulated and measured temperatures for the first configuration, in which the fan was switched off. Taking into account the uncertainties, there is an excellent agreement at all three measured heights. Moreover, the temperature measured 50 cm above the head is 26.3°C, and the simulated corresponding value is 26.8°C, which is within the uncertainty interval. Thus, in all these cases, the CFD discretisation error is irrelevant. As expected in a buoyancy-driven system, the temperature is stratified and the thermal plume is clearly visible above the head in Figure 3.8.

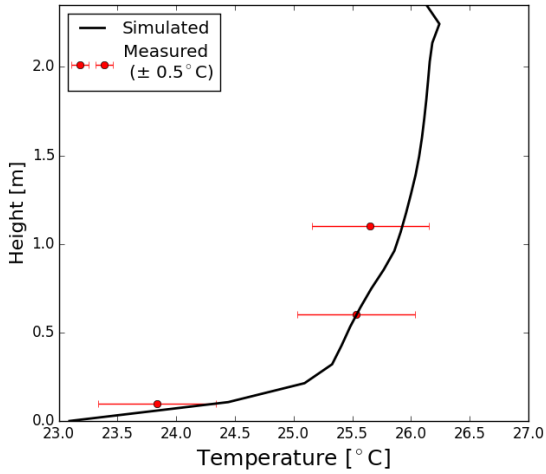

Figure 3.7: *Configuration without fan: simulated and measured air temperatures.*

In the first configuration, as expected in a mainly buoyancy-driven environment, the air speed is low, always below 0.5 m/s. The measured and simulated values within the thermal plume are respectively 0.14 m/s and 0.13 m/s. This agreement supports the choices made while defining the model. Previous studies have found slightly higher values, between 0.17 m/s to 0.5 m/s (Yousaf et al., 2011). This difference is likely to be due to the relatively high air temperature in the chamber in the present study: the difference between the mean density of the air within the room and the value of the warmer air in the plume is smaller, therefore the velocity in the plume is lower.

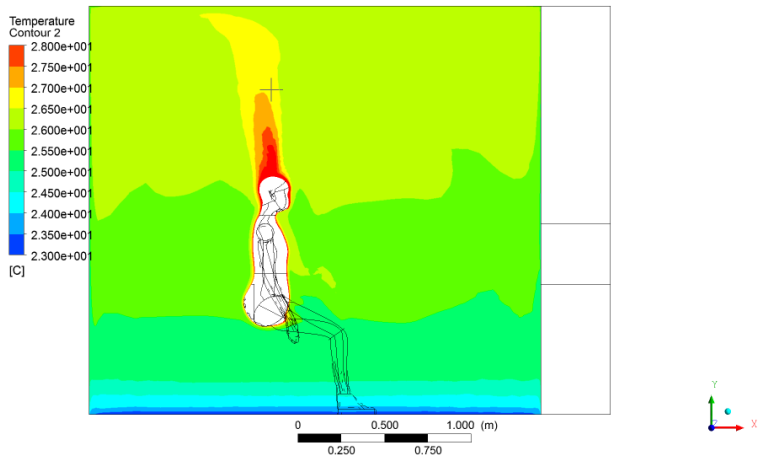

Figure 3.8: *Configuration without fan: air temperature field.*

For the second configuration, in which the fan was operating, achieving a reason-

ably good agreement between simulated and measured values was a more challenging task due to the complexity of modelling the effect of the fan. Therefore, the air speed at 0.1 m, 0.6 m, and 1.1 m above the floor was taken as the main data source for the validation. As shown in Figure 3.9, there is one case, namely "simulated 3", in which simulated values are within the error bars of the measured figures. Although there are only three points of comparison, this seems a good agreement given the small uncertainty in the measurement. In the other three simulations, at one or more heights there are differences that cannot be justified only by the uncertainties, neither in measurement nor in simulations. However, this difference is small, and its effect on the thermal comfort results is discussed later in this chapter.

It is arguable that more comparison points could have been used, but there are at least two reasons to avoid this option. Firstly, these are the three measurements used by the international standards to evaluate the human thermal comfort, therefore this enables a comparison with traditional models. The second reason is that an elevated number of probes placed within the air stream could affect the stream itself, and therefore the measurement equipment could alter the measured physical quantity. Future work might include more detailed and non-invasive measurement techniques such as PIV.

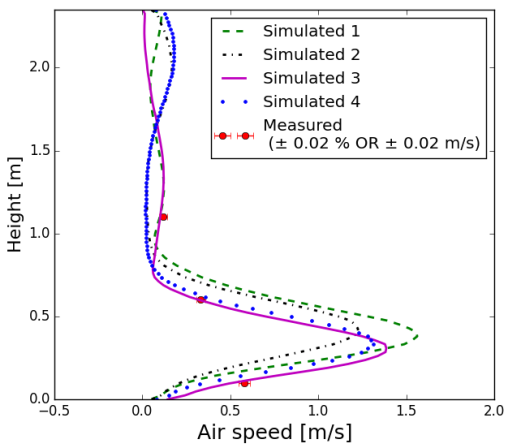

Figure 3.9: *Configuration with fan: simulated and measured air speeds.*

Due to the action of the fan shown in Figure 3.10, in this second configuration

the air in the room is well mixed and the system is primarily mechanically-driven. As highlighted in Figure 3.11, simulated and measured air temperature are in good agreement in each simulation, without any particular difference among the four CFD sets of results. The fact that at all points, including the lowest point (0.1 m), in both configurations the temperature and speed match the measured values suggests that the chosen turbulence model (SST k-ω model) and mesh (especially the use of prism layers near the surfaces - see section 3.2.2 for further details) are appropriate to model this experimental set-up. Moreover, Figure 3.12 shows that, due to the effect of the fan, the air inside the chamber is well mixed and the thermal plume above Victoria's head is significantly lower than in the configuration without fan (Figure 3.8).

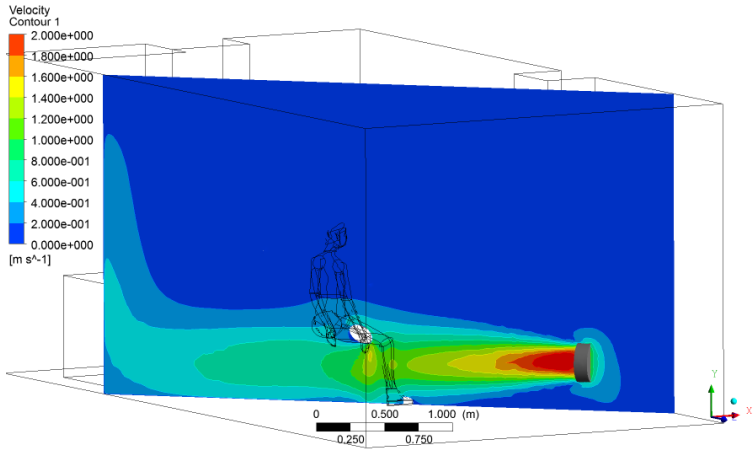

Figure 3.10: *Configuration with fan: air speed field.*

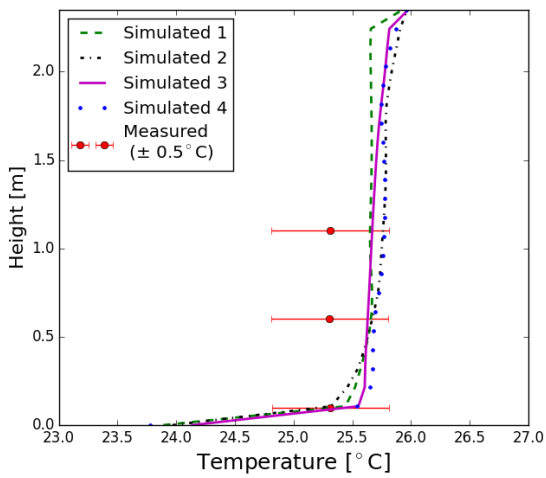

Figure 3.11: *Configuration with fan: simulated and measured air temperatures.*

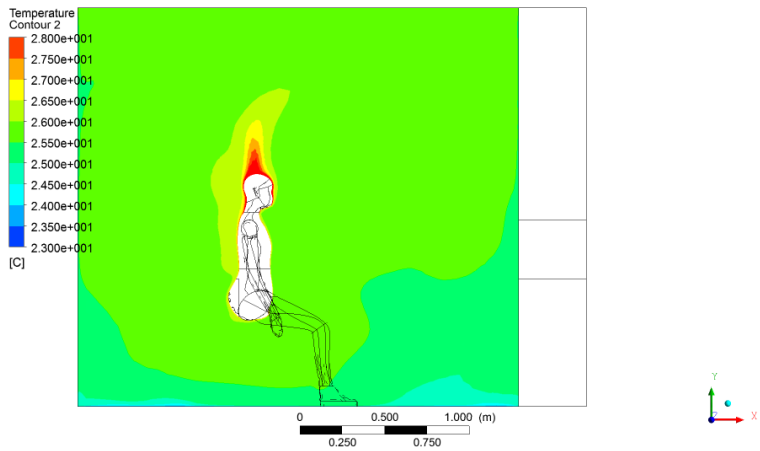

Figure 3.12: *Configuration with fan: air temperature field.*

Lastly, as reported in the methodology (section 3.2.2), a fifth simulation was completed. In this fifth case, the fan was activated after 5 minutes to assess how the DTS is affected by a rapid change of the air speed. The momentum source value used in this simulation is the same used in "simulated 3".

3.3.2 Required computational power

Simulations were run on the High Performance Computer System at Loughborough University, a 2460-core 64-bit Intel Xeon cluster. 12 cores were used in these simulations in order to make efficient use of the cluster architecture.

As reported in Table 3.4, the duration of the simulation without the fan is almost half of the others. This is due to the use of different time steps, respectively 0.5 s and 0.2 s, but the same total time, namely 10 minutes. In the first four cases with the fan, the CPU time is quite similar, and the small variations are likely to be due to the different values used for the momentum source which represented the effect of the fan. In general, the greater the total simulation time, the longer the simulation, but there is no clear linear relationship. Unless there is a significant change such as a different fan speed, a convergent solution for a single time step is reached faster after the initial time steps.

Table 3.4: *Duration of the simulations*

Simulation	Total CPU time
Without fan	18 h, 05 m
With fan - 1	1 d, 12 h, 08 m
With fan - 2	1 d, 11 h, 29 m
With fan - 3	1 d, 08 h, 18 m
With fan - 4	1 d, 10 h, 55 m
With fan - 5	1 d, 02 h, 45 m

The fifth simulation with the fan is slightly different. As explained in the methodology (section 3.2.2), in this case, the fan was activated only after 5 minutes of simulation. This means that for the first part a longer time step, such as 0.5 s, could have been used, but a smaller value, such as 0.2 s, would have been required for the

following 5 minutes. For this reason, an adaptive time step was used. This ensured that the RMS Courant number was always not greater than 5 without the need for any manual changes of the time step. Thus, the total CPU time of the fifth simulation (Table 3.4) is nearly half way between the case without fan and the third simulation with fan (the same momentum source was used in the fifth and third simulation).

In the pre-processing, the meshes were generated using a work station equipped with an Intel Xeon E5520 CPU and 24 GB of RAM. All the other pre- and post-processing activities were completed using a laptop with an i5-3320M CPU and 8 GB of RAM. The two coarser meshes could have also been generated with this laptop without exceeding its computational resources.

3.3.3 Thermal comfort results

As explained in the literature review (section 2.3.4), the coupled model provides two thermal comfort metrics: DTS and PPD (Figure 3.13). The former could be compared with the PMV as they both adopt the same 7-point ASHRAE thermal sensation scale, while the PPD calculated with this coupled model could be compared with the PPD included in the international standards as they both predict the percentage of occupants that will be dissatisfied with the thermal conditions.

However, due to the different structure and algorithm of the two approaches, DTS and PMV usually do not have the same value. Firstly, the thermal regulation model included in the coupled system is significantly more complex than the Gagge 2-node model (Gagge et al., 1971) that has been integrated into the PMV calculation in ASHRAE 55 (ASHRAE, 2013a). Secondly, the PMV algorithm uses only a unique value for the clothing and for the four environmental variables. For instance, this means that a subject wearing shorts, T-shirt and sweater, and another one wearing long trousers and T-shirt might have fairly similar clothing values in PMV calculation. If then there is a fan blowing air towards them at the same speed, and all the other four variables are the same, the PMV would be identical for two subjects. However,

the different direction of the air velocity, and the fact that the air hits the subject on body parts with different clothing resistance, may generate a different actual thermal sensation. The coupled model can accommodate this and correctly model the two different situations, while the traditional PMV cannot do so. Lastly, the PMV model assumes steady state conditions, while the coupled model requires only some initial and boundary conditions. For these reasons, a numerical comparison between DTS results and PMV should be done only when the actual thermal sensation reported by people is available in the same conditions (for instance, see chapter 5), as this would provide with the basis for a solid discussion.

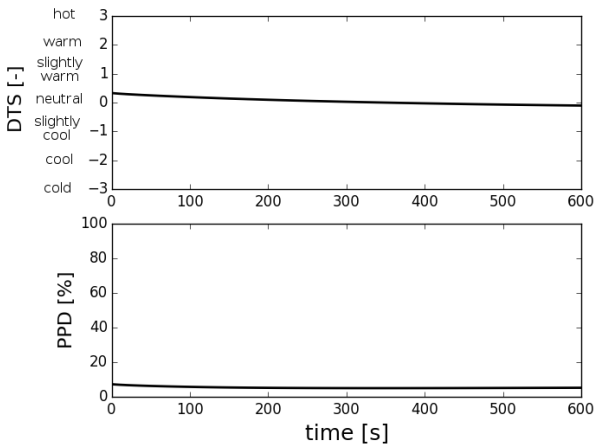

Figure 3.13: *Configuration without fan: DTS and PPD.*

In Figure 3.14, the DTS results highlight how the fan affects the thermal sensation, but slight variations of the air velocity do not have a significant impact on the DTS. In other words, the DTS does not seem to be very sensitive to a small inaccuracy in the choice of the momentum source. Indeed only in "simulation 3" the simulated and measured air speed match (Figure 3.9). Moreover, Figure 3.15 clearly shows how the coupled system can be used to assess transient conditions and why it has wider applicability than the traditional PMV model. In "simulation 5", the fan was activated after 300 s. The relative DTS is identical to the case without fan until that point, but it then decreases faster, and its value becomes closer to the DTS calculated with fan constantly on ("simulation 3"). The PVM method cannot be used to evaluate such

a rapid change in boundary conditions, since it requires the subjects to be in steady state conditions. In addition, even if this theoretical point was overlooked, then the PMV would assume only two values throughout the entire simulation. In the graph, there would be a horizontal line from time 0 to 300, and another lower horizontal line from time 300 to the end. On the other hand, the DTS is immediately affected by the new boundary conditions, but it also takes into account the effect of the duration of the exposition to certain boundary conditions on the thermal sensation.

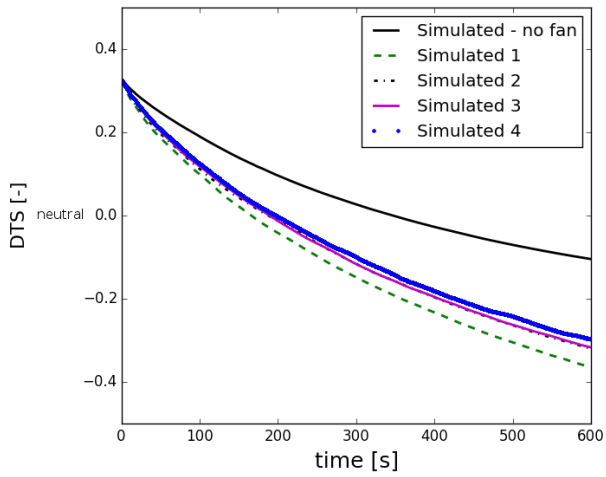

Figure 3.14: *DTS with and without the fan.*

Thus, this first complete application of the coupled model showed that this model is able to predict human thermal comfort in any given indoor configuration, as long as the environment around the human body is accurately modelled. In other words, the CFD model that represents the environment around the person must be accurate and validated. In particular, in relation to the research hypothesis, the DTS is superior to the traditional PMV calculation as both temporal and spatial variation and non-uniform conditions can be taken into account. Therefore, the higher required computational power is compensated by more accurate thermal sensation predictions.

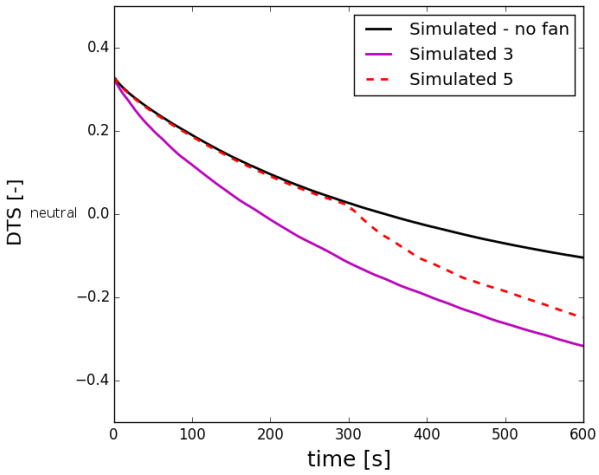

Figure 3.15: *DTS with different fan status: always off ("no fan"), always on ("simulation 3"), and on only in the second half of the simulation ("simulation 5").*

3.3.4 Heat transfer and air movement: how the coupled system models the variations of convective and evaporative heat transfer due to air speed changes

In the literature review, the heat transfer mechanisms between human body and surrounding thermal environment were discussed. In particular, the use of elevated air speed on the human body affects two of these mechanisms: the convective and the evaporative heat exchances.

The aim of this section is to show how this is captured by the coupled system. In theory, there should be a variation in the moisture mass fraction on the surface of the virtual manikin, and the convective heat transfer coefficient should be higher on those parts of the manikin surface on which air is blowing at higher speed.

Figure 3.16 clearly show the variation of the convective heat transfer coefficient due to the change of air speed. The data is from "simulation 5", in which the fan was activated after 300 s. The two lines represent the convective heat transfer coefficient calculated at each iteration of the simulation for two body parts, namely one on which no air was blowing when the fan was on (red line), and the part of surface of the manikin that was the closest to the fan (green dashed line). The former is part of

the neck, the latter is the lower part of the right leg of the virtual manikin (that is the right shin).

The convective heat transfer coefficients are close and stable on the two parts when the fan was not blowing air, from time 0 to 300, and the mean value, on the shin, is 3.2 W/m^2K, which is in similar to the figures reported in previous research (Cropper et al., 2010; de Dear et al., 1997). However, there is a significant difference between the two parts when the fan was turned on, and therefore the lower part of the leg was hit by air at elevated speed. The mean value on the shin rises at 7.2 W/m^2K (the initial 5 s, that are the time steps from immediately after time 300 to 305, have been excluded from this calculation as this is a transition time during which air starts to flow on the manikin), and therefore, as expected, the heat exchanged by convection became higher in the second part of the simulation.

However, it is important to say that extracting these values from the coupled system is not a simple process. This applies to all parameters that cannot be taken directly from CFX (such as air speed or air temperature) apart from DTS and PPD, and it is due to the current architecture of the coupling software and the IESD-Fiala model itself. As remarked in the conclusions of this thesis, in the future the coupled system should be rewritten to enable a better usability of the system. It is also important to note that the coupled system does not to model the effect of air gaps between the clothing and skin surface (Cropper et al., 2010), which means that this model does not include air movement between the skin and the cloths, ot between different layers of the cloths.

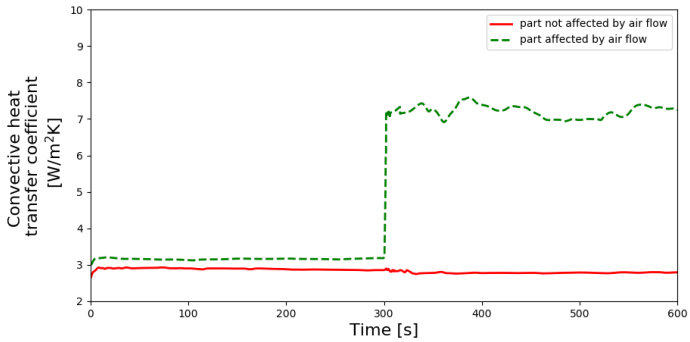

Figure 3.16: *Convective heat transfer coefficient with the fan switched off (time 0 to 300), and then on (time 301 to 600) (data from "simulation 5").*

The moisture mass fraction on the surface of the manikin is also affected by the elevated air movement. Within the coupled system, absorption of moisture by clothing is also not modelled, and it is assumed that all moisture excreted by parts of the body covered by cloths appears at the clothing surface. Figures 3.17 and 3.18 show the moisture mass fraction on the surface of the manikin (that is always the outermost layer - the skin on naked parts, cloths on the others) with and without the fan in operation, respectively. Both are taken from the final time step of "simulation 3" and "simulation - no fan", respectively. This was done to ensure that the only difference between the two conditions was the status of the fan, but not the duration of the exposure to the surrounding environment (this would have been the case if data had been taken from "simulation 5" at different time steps, such as time 300 and 600).

Although the thermal environment was relative mild and dry, figures 3.17 and 3.18 clearly show some differences. In the case without fan (Figure 3.18), the moisture mass fraction is overall higher and, most importantly, symmetrically distributed on the right- and left-hand sides of the virtual manikin. On the other hand, in the case with active fan (Figure 3.17), there is a difference between left- and right-hand sides, and this is clear looking at the front part of the legs (the shins).

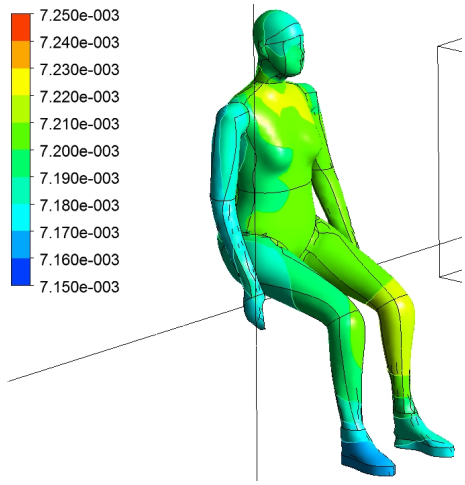

Figure 3.17: *Virtual manikin surface moisture mass fraction - with the fan (data from "simulation 3").*

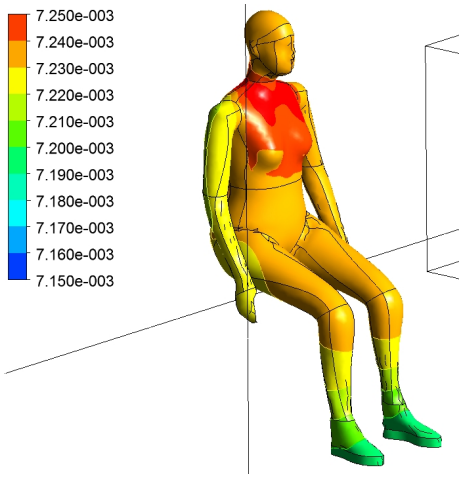

Figure 3.18: *Virtual manikin surface moisture mass fraction - without the fan (data from "simulation - no fan").*

It is possible to conclude that this lack of symmetry is due to the effect of the fan (which blew from the right-hand side of the manikin), and also, as expected, that the manikin is drier in the case with the active fan, but it is more difficult to say why the range of values is generally lower in the case with fan. It is likely that a combination of two things affects these values in presence of higher air speed: an higher convective heat exchange (thus, less moisture is produced as the body has another way to dissipate heat), but also a more elevated rate of evaporative heat exchange (the moisture produced evaporates faster). However, it is impossible to track what happens inside the IESD-Fiala model, and therefore it is impossible to make a detailed assessment of these two phenomena.

It is worth to remark that the PMV method cannot model these aspects, and therefore to highlight the higher capabilities of the coupled systems. Thus, in relation to the research hypothesis, this section showed how the coupled system operates in presence of elevated air speed, and therefore it supports what said in the previous section about the DTS and its being superior to the PMV.

3.4 Summary

This chapter begins with an overview of the entire experimental work conducted in this study, aiming to link the different steps followed by this research, and therefore to connect the different methods adopted to address aim and objectives of this work.

In this research, a combination of computer based modelling, experimental work in controlled environments, and data from field studies was used. Computer modelling comprised CFD (stand alone), CFD coupled with a human thermal regulation and thermal comfort model, and dynamic thermal modelling. In the experimental work, environmental chambers were used to collect data to validate the CFD models. The data from field studies on real domestic buildings in India and in the UK were used identify the most relevant configurations to be modelled with the coupled system.

The coupled system comprises two key components: a commercial CFD software, namely ANSYS CFX, and a human thermal regulation and thermal comfort model, namely the IESD-Fiala model. The former is a general purpose CFD software, it was chosen for its wide capability of customisation (which enabled the link with the IESD-Fiala model), and it was used to model the environmental conditions around the person. The latter is one of the most advanced models of human thermal comfort, and it comprises two parts: the passive system (which models the heat transfer phenomena within the human body) and the active system (which models the reaction of the person, such as shivering, to the given environmental conditions). It calculates two thermal comfort metrics, namely the dynamic thermal sensation and the percentage of people dissatisfied. The human body is represented in CFD by a virtual manikin whose surface is divided into 59 parts. These 59 parts are the link between the two components of the coupled system, and, in the transient coupled simulations, information are exchanged at the end of each time step between the two components.

This chapter presents the first step of this reseach, which was to test and validate the coupled model by comparing simulation results with measured data for a number of different realistic scenarios. These scenarios were created in an environmental

chamber at Loughborough University and then modelled using the coupled system. Two types of configurations were modelled: a buoyancy-driven system, and a forced convection system. In the latter, a common desktop fan was used to generate elevated air speed on the surface of the thermal manikin.

This chapter highlights the accuracy of the CFD results by comparing simulated and measured values (and including the respective errors in the analysis), describes the computational power required to model the chosen configurations, and shows the capabilities of the coupled system for predicting human thermal comfort in non-uniform environments generated by elevated air movement.

In both configurations (with and without the fan switched on), the simulated values of the air temperature were within the error bars of the relative measured values. In the first type of configuration, which was a buoyancy driven system, the simulated values of the air speed were also always within the error bars of the respective measured values. Moreover, as expected in a buoyancy driven environment, the air speed was low, always below 0.5 m/s. The measured and simulated values within the thermal plume generated by the manikin were similar to what previous studies found. In the second type of configuration, which was a forced convection system due to the action of the fan, four simulations were run, varying each time the value of the momentum source that was used to model the desktop fan. Only in one case, all the simulated air speed values are within the error bars of the respective measured values, but, as remarked later, this did not have a significant effect on the thermal comfort results. Overall, the positive agreement between measured and simulated values means that the chosen turbulence model (SST k-ω model) and mesh (especially the use of prism layers near the surfaces) were appropriate to model this experimental set-up.

All simulations were run on the High Performance Computer System at Loughborough University, and the total CPU time (that is the time required to achieve a converged solution) ranged between 18 and 36 hours. This total CPU time is significantly longer for the second type of configurations, in which the fan was active, since

the time step had to be reduced in order to ensure that the RMS Courant number was not greater than 5 also in these simulations. In general, the greater the complexity of the simulated configuration is, the longer the total CPU time becomes, providing that the simulated period (in this case, 10 minutes) is the same.

The thermal comfort results showed that the coupled system is capable to model the effect of elevated air movement on human thermal comfort. The dynamic thermal sensation in the two types of configuration is clearly different, being lower when the fan was active (with the same temperature and relative humidity). However, slight variations of the air speed did not have a significant impact on the dynamic thermal sensation. This is important because when more complex scenarios are modelled, it may not be possible to reach a perfect agreement between simulated and measured values using a simplified model of the fan (modelled as a momentum source - thus, without modelling the geometry in detail). Thus, using a simplified model of the fan enabled the reduction of the computational time and the uncertainties within the model without jeopardising the accuracy of the thermal comfort results. Furthermore, these results showed that the coupled system can also model rapid variations of the boundary conditions, with the dynamic thermal sensation that was immediately affected when the fan was activated half-way the simulation. The PMV model would not be able to account for such a rapid variation, as it requires the subject to be in steady state.

Chapter 4

CEILING FAN CFD MODEL

This chapter illustrates the developed three dimensional CFD model of a typical Indian ceiling fan, its degree of accuracy, and the reasons for which this model was needed. The chapter explains how this level of accuracy was achieved, and highlights the link between accuracy and computational power.

In this chapter the coupled system is not used, and therefore there is no direct test of the research hypothesis. However, this chapter offers insights into the type of real residential scenarios in which the coupled model is likely to be superior to the traditional thermal comfort models, and shows how a specific boundary condition for the coupled model is developed, including the required level of detail and computational power.

The structure of this chapter is as follows. Section 4.1 explains why, in this study, it was essential to develop a three-dimensional model of a typical Indian ceiling fan. The following section 4.2 describes the methods used in this study. The remaining sections present and discuss the results. In the first two of these result sections, qualitative and quantitative simulation results are presented. The former are compared with previous qualitative research on the air flow generated by ceiling fans, while the latter are compared with the measurements collected during this research. Section 4.3.3 presents the importance of the choice of the turbulence model, while section 4.3.4

deals with the required computational power. Lastly, the usability of the developed model is discussed.

4.1 Identification of suitable realistic residential indoor scenarios in the UK and in India

After the initial application of the coupled system to model an artificial environment such as an environmental chamber, the next step was the use of the coupled system to investigate thermal comfort in non-uniform thermal environments in real buildings. Thus, the aim of this section is to illustrate which real buildings were considered, and why, within this sample, certain configurations were chosen to be modelled. Details of the models, both CFD and dynamic thermal models will be accurately described in the subsequent sections.

This PhD research was closely linked to a wider international research project on thermal comfort and air movement in residential buildings (Loveday et al., 2016). The project involved Loughborough University and De Montfort University in the UK, CEPT University in India, and University of California Berkeley in the USA. Within this wider project, houses in the UK and India were selected to participate in a field study which comprised subjective and objective data collection. The former was done using an on-line survey that participants filled on average once a week, at a point in time that was convenient for them. The latter included long term monitoring of air temperature and relative humidity, and additional detailed measurements collected, in the UK, using a Dantec ComfortSense kit (Dynamics Dantec, 2015) (Figure 4.1). In total, 15 houses in the UK and 20 in India took part in this study.

Figure 4.1: *Detailed thermal comfort measurements using the Dantec ComfortSense kit (Dynamics Dantec, 2015) in one of the UK houses.*

The aim of this international project was to reduce the global energy use in buildings while improving occupant comfort and well-being by reversing the growing trend toward energy-intensive air-conditioning. The related field study aimed therefore to collect information about the current use of air movement and cooling devices in residential buildings in India and in the UK. The collected data and the information gathered during the on-site visits were used within this PhD research to identify suitable realistic indoor scenarios. Since the coupled system is meant to be used to investigate transient non-uniform thermal environmental conditions, the aim was to look for such scenarios in these 35 dwellings.

In the questionnaire, participants were asked to indicate whether there was any cooling equipment, such as fans and air conditioners, in the room and the status (on/off) of these devices while they were filling the questionnaire. Thus, it was possible to know whether, during the warm season, people relied only on natural ventilation to achieve thermally comfortable conditions, or whether some cooling equipment was used for this purpose.

Considering the UK participants and the responses collected from May to September 2015, it is clear that participants normally did not use any cooling device (Table

4.1). Fans and air conditioning were not available in the vast majority of the rooms, and, even if available, they were almost never in use. There might be several reasons behind these figures, such as personal habits, culture and mild outdoor temperatures, and a complete investigation would be out of the scope of this PhD research. However, whatever these reasons are, these data show that UK participants during the warm season relied almost exclusively on natural ventilation only to achieve thermally comfortable conditions in their houses. Thus, there were no common non-uniform scenarios that could be modelled using the coupled system.

Table 4.1: *Use of cooling devices in UK houses (15 houses).*

Cooling devices	Not available in the room	Available in the room	If available, ON
Hand held fan	99%	1%	0%
Desk top fan	96%	4%	2%
Pedestal fan	92%	8%	1%
Tower fan	99%	1%	0%
Ceiling fan	95%	5%	1%
Air multiplier fan	99%	1%	0%
Air cooler	99%	1%	0%
Air conditioner	91%	9%	2%

On the other hand, in the Indian houses, ceiling fans and air conditioners were widely available to participants (Table 4.2). Nearly 90 % of the participants reported to have at least one ceiling fan in the room where they were filling the questionnaire, and this is in good agreement with the information gathered during the initial visits of these houses, where the presence of at least one ceiling fan in most of the rooms was noted (Figure 4.2). Moreover, the ceiling fans were "on" in over 50 % of the cases, and usually set to higher speed settings. Air conditioners were available in around a third of the cases, but not used, being reported to be "on" in only 4 % of the cases. It is likely that this happened because air conditioners were located mainly in bedrooms and therefore likely to be used during the night to enhance sleep quality.

Table 4.2: *Use of cooling devices in Indian houses (20 houses).*

Cooling devices	Not available in the room	Available in the room	If available, ON
Hand held fan	99%	1%	1%
Desk top fan	99%	1%	1%
Pedestal fan	97%	3%	2%
Tower fan	98%	2%	2%
Ceiling fan	12%	88%	54%
Air multiplier fan	99%	1%	1%
Air cooler	98%	2%	1%
Air conditioner	64%	36%	4%

Figure 4.2: *Indian participants in their drawing room.*

Figure 4.3: *Drawing room with three ceiling fans.*

Ceiling fans are therefore by far the most used means to generate non-uniform thermal environmental conditions in these houses. Due to the nature of the air flow generated by a ceiling fan, the mutual position of fan and person is crucial while assessing thermal comfort. Thus, a typical Indian apartment offers the ideal scenario to apply the coupled system to a real building. Moreover, in some of the rooms, typically living/drawing rooms (Figure 4.3), there were two or more ceiling fans,

increasing the level of complexity of the indoor air flow, and therefore of the thermal conditions around people.

4.2 Indian ceiling fan CFD model: methodology

As highlighted in the previous section, ceiling fans are the most commonly used means to generate non-uniform thermal environments in Indian dwellings, and it is therefore essential to make an accurate representation of the ceiling fans within the CFD model for detailed thermal comfort studies. To date, as discussed in the literature review (section 2.3.4), there is no existing accurate CFD model of a typical Indian ceiling fan that can be used for this purpose.

Thus, the research presented in this section aimed to develop and validate a three-dimensional transient CFD model of a typical Indian ceiling fan by comparing simulation results and measured data. This model combines accuracy with efficient computation, and can be used for detailed thermal comfort studies.

Detailed measurements of the air movement generated by a typical Indian ceiling fan were collected in an environmental chamber, and the same experimental set-up was then modelled using a commercial CFD program, ANSYS CFX (2015). Having discussed on the aim of the experiment and established a detailed procedure to be followed, measurements were then taken by Indian researchers at CEPT University in India. In this model, the fan is modelled as a momentum source that is specified by radial components and applied to a sub-domain of the CFD model which has the same shape as the real fan. Measured values and computer-generated predictions have been compared, and the reasons for any differences analysed.

4.2.1 Experimental set-up

Environmental chambers have been extensively used to collect data for validating CFD models. Within an environmental chamber, most of the variables can be con-

trolled, and the state of the uncontrolled variables ought to be accurately determined. Thus, the number of required assumptions due to the lack of measurements or better information, and therefore the number of potential sources of uncertainties, are minimised.

For this research, a rectangular environmental chamber located at CEPT University, Ahmedabad, in India has been used (Figure 4.4). The external envelope is highly insulated using XPS insulation. There is one west facing window and two internal windows overlooking the adjoining indoor space to the east and internal circulation passage to the north. Their high performance (U-value 1.790 W/m^{2}K) fixed double glazed window maintains the chamber's thermal insulation from the surrounding environment. Furthermore, the external window is shaded from direct solar radiation throughout the entire year. The ventilation system comprises four supply ducts and two return ducts, which are located in the ceiling. The chamber ventilation system was never in use during any experiment, and the diffusers were sealed during both the second and third repetition of the measurements. This did not produce any significant difference in the measured values, but allowed to more accurately set the boundary conditions in CFD. A typical 1200 mm diameter Indian ceiling fan (BEE, 2016) with a 4-step regulator was installed on the ceiling of the chamber. Other than measuring equipment, no other objects were present in the room.

Figure 4.4: *Environmental chamber at CEPT University, Ahmedabad, India.*

Air speed measurements were recorded in three horizontal planes in the chamber: 0.1 m, 0.7 m and 1.3 m above the floor. In each plane, 12 measurements were recorded. These were located (Figure 4.5) below the centre of the fan ("*centre*"), below the perimeter of the fan ("*north*", "*east*", "*south*", "*west*"), and on a radius at increasing distance from the centre of the fan. For instance, "*r 800*" means 800 mm away from the fan centre. Thus, in total, measurements were taken at 36 points.

Measurements were recorded simultaneously at these three heights in each of the 12 horizontal locations using three air speed probes (Table 4.3). After the recording was completed in one location, the measurement equipment was moved to the next spot, but the new recording period always started a few minutes after having moved the equipment. The logging duration per location was 300 s and the logging period 1 s. It is important to point out that both types of probe used for measuring air speed are omnidirectional, which means that only air speed is recorded, rather than the three components of air velocity separately. Instantaneous measurements of room air temperature and relative humidity, room surface temperatures, and fan rotational speed have also been taken. In this study, the highest available fan rotational speed setting (level 4, rotational speed 290 RPM) has been chosen based on the considerations made previously (section 4.1) about the field study in India and in the UK on air movement in domestic buildings (Loveday et al., 2016).

A complete set of measurements was taken three times to ensure the quality of the data and repeatability of the experiment.

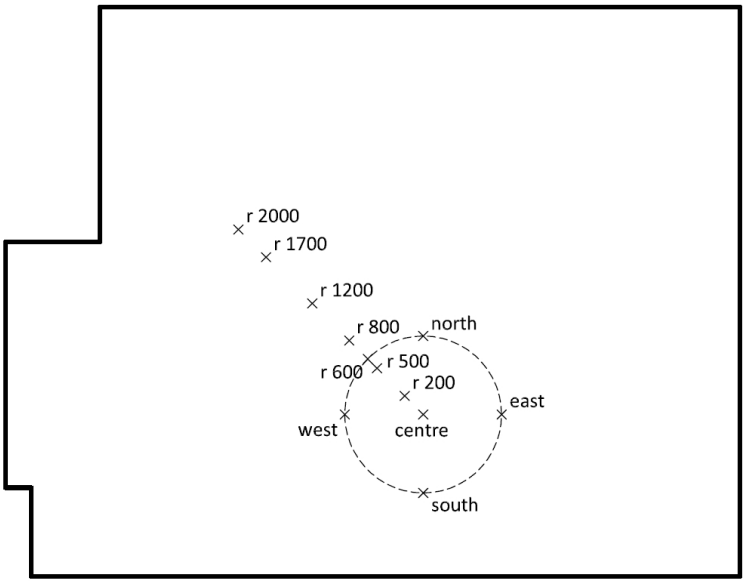

Figure 4.5: *Plan view of the environmental chamber with the measurement locations.*

Table 4.3: *Measurement equipment characteristics.*

Instrument	Parameter measured	Accuracy
Testo 480 Climate – Hot bulb anemometer	Air speed (at 0.1 m and 1.3 m height)	$\pm(0.03\,\mathrm{m/s} + 5\%$ of reading)
Testo 480 Climate – Turbulence Probe	Air speed (at 0.7 m height)	$\pm(0.03\,\mathrm{m/s} + 4\%$ of reading)
TSI Veloci-calc Multifunction Ventilation meter 9565	Dry-Bulb Temperature and RH	$\pm 0.3°$C, $\pm 3\%$ RH
Fluke-561 Infrared Thermometer	Surface temperature	$\pm 1\%$ or $\pm 1°$C whichever is greater
Lutron DT-2236 Digital contact tachometer	RPM	$\pm 0.05\%$ or 1 digit

4.2.2 Modelling approach and assumptions

The identical configuration used during the experiments was then recreated within the CFD program. In this study, the chosen software is ANSYS CFX (2015) primarily because the coupling between the IESD-Fiala model and CFD was completed using ANSYS CFX due to its customization features which facilitate the connection with other software (Cropper et al., 2010). Thus, this facilitated the use of this ceiling fan modelling approach in thermal comfort applications. However, the modelling approach presented here could be implemented in most CFD programs.

The geometry (Figure 4.6) was created in ICEM CFD (2015), a general purpose geometry and mesh generator for CFD. Air diffusers, windows and door were not included since they were all closed during the experimental work, and because only isothermal simulations were conducted to reduce the required computational power. This has been done because the surface temperatures and the air temperature were similar, being 31.8°C and 31.9°C, respectively. Thus, the magnitude of any buoyancy-driven air flow would have been negligible compared with the air speed generated by the fan.

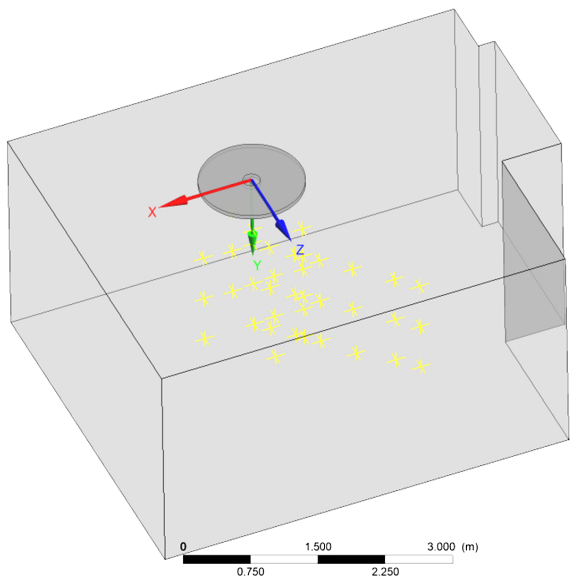

Figure 4.6: *CFD model of the environmental chamber (yellow marks represent the 36 monitoring points).*

The ceiling fan was modelled as a momentum source. Modelling the actual blades would require very detailed information about their geometry, and would lead to a much higher number of mesh elements and to the use of a moving mesh. Both these features would significantly increase the demand for computational power, and the possible sources of uncertainty, without guaranteeing better results, but limiting the usability and applicability of the model. Thus, the fan was modelled as a ring with the same diameter and distance from the ceiling as the actual fan (Figure 4.7), and with a central cylindrical solid element, since in a real ceiling fan no air emanates

from the centre. The momentum source has been applied to this ring.

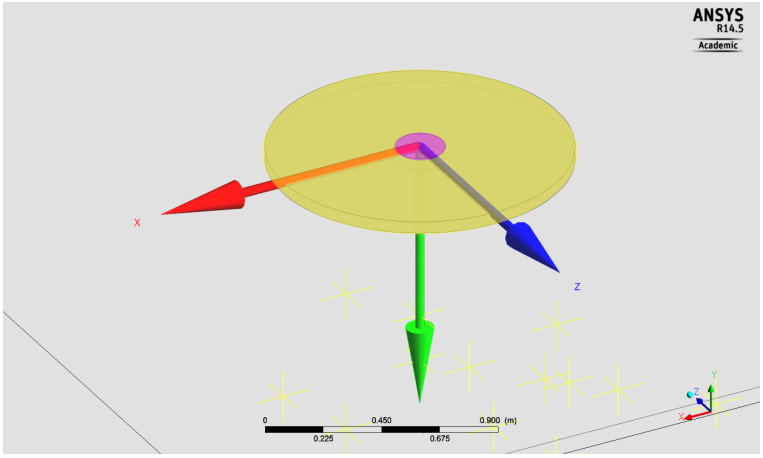

Figure 4.7: *Detail of the fan simplified geometry (ring highlighted in yellow, central element in purple).*

In this study, an unstructured mesh was used because it is more flexible and it can be used with any complex shape such as a human body, easing the wider applicability of the proposed modelling approach. Similarly to previous chamber-based work (section 3.2.2), both the surface and the volume mesh were initially generated in ICEM CFD using the Octree algorithm, then the volume mesh was deleted, and finally regenerated using the Delaunay algorithm (Figure 4.8). This procedure ensures the robustness of the mesh and a smoother transition from smaller elements to larger ones. Ten prism layers were added adjacent to the walls to accurately model the boundary layer near surfaces.

Transient simulations were performed to better model the real behaviour of the ceiling fan. A second order backward Euler scheme, and high resolution advection scheme and turbulence numerics were used. The double precision option was also used to enhance accuracy and robustness of the results. Convergence criteria were set equal to 1e-05 for the RMS residuals and 0.01 for the conservation target. Moreover, an adaptive time step as a function of RMS Courant number was chosen, with the limit for the RMS Courant number set equal to 1. Since it is an implicit code, CFX does not require the Courant number to be small for stability, but this still leads to more accurate results.

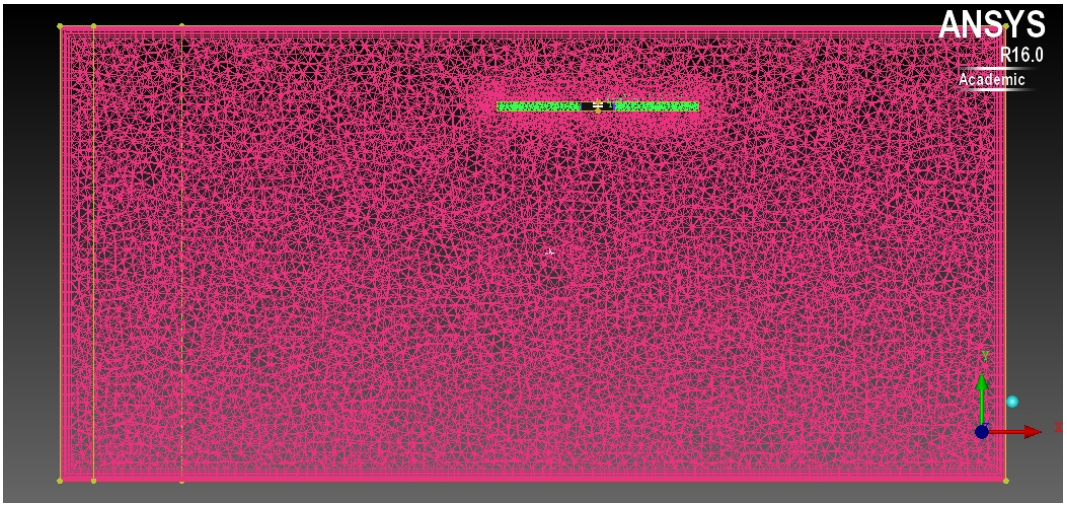

Figure 4.8: *Volume mesh generated using Delaunay algorithm.*

The momentum source that simulates the actual fan was applied to the subdomain using cylindrical components: axial component 55 kgm^{-2}s^{-2}, radial component 0 kgm^{-2}s^{-2} and theta component 8 kgm^{-2}s^{-2}. The sign of each component depends on the orientation of the defined local system of coordinates (Figure 4.7), while the absolute figures were defined with an iterative process by comparing simulation results with measured values and by comparing the qualitative features of the flow field with qualitative previous studies. As explained in the literature review, a study by Jain et al. (2004) provided with very useful qualitative information about the flow field generated by a ceiling fan. Using smoke from thick incense sticks, the flow field created by the ceiling fan was visualised, identifying the main regions of the flow and its key behaviours such as the swirling movement.

The chosen values for the axial, radial and theta components do not have a direct link to the actual rotational speed of the ceiling fan, and therefore the criteria used to arrive at these values are essentially the qualitative and quantitative comparisons described in the previous paragraph. The procedure used to identify the most appropriate set of values was as follows. The most sensitive parameter was the axial component since this has the largest effect on the numerical results, and therefore this was the first parameter to be tested. When the simulated air speeds (especially

below the centre of the fan) arrived in the range of the measured values, the theta component was tuned to address two purposes: matching the qualitative characteristics of the air flow generated by the fan (such as the swirling movement and the flow diverging with a certain angle), and enhancing the quantitative agreement.

For the axial component, the range of tested values goes from 40 $kgm^{-2}s^{-2}$ to 65 $kgm^{-2}s^{-2}$, and the step between two subsequent simulations was equal to 5 $kgm^{-2}s^{-2}$. For the theta component, the range of tested values goes from 6 $kgm^{-2}s^{-2}$ to 10 $kgm^{-2}s^{-2}$, and the step between two subsequent simulations was equal to 2 $kgm^{-2}s^{-2}$. Since the process could not be automated and the computational demand of these simulation is elevated, it was not possible to test a more combinations of values. In this case, the main limit of an automated process (assuming that this might be implemented by writing a piece of code within ANSYS or developing an external tool) is the fact that only air speed values were measured, not air velocity. Thus, both a quantitative and qualitative comparison was required. In addition to that, the use of an automated process would not have decreased the computational time, which is almost always a major constraint when performing CFD analysis.

Due to the intrinsic turbulent nature of the air flow generated by the fan, the correct choice of the turbulence model is fundamental. In this study, four of the most widely used Unsteady RANS (URANS) eddy-viscosity turbulence models were fully tested: the SST k-ω (Menter, 1992a,b, 1994, 1997; Menter et al., 2003), the RNG k-ε (Patel et al., 1985), the standard k-ε (Launder and Spalding, 1974) and the standard k-ω (Wilcox, 1988, 1993b,a, 1994). Two Reynolds-stress models were also considered, namely the Speziale-Sarkar-Gatski (SSG) (Wallin and Johansson, 2000) and the Menter Baseline (BSL) (Menter, 1993), for their potential higher accuracy for simulating swirling flows and boundary layers (ANSYS, 2015a). Only the SST k-ω model was used in the definition of the values for the axial, radial and theta components of the momentum source.

Before running the main simulations, a mesh sensitivity analysis was completed,

Table 4.4: *Discretization error calculation (Celik, 2008)*

	Analysis 1
N_1	1,996,278
N_2	678,834
N_3	76,539
h_1	0.03
h_2	0.05
h_3	0.09
r_{21}	1.43
r_{32}	2.07
φ_1	1.56
φ_2	1.53
φ_3	1.50
ε_{21}	-0.029834
ε_{32}	-0.029464
p	0.8947256
φ_{ext}^{21}	1.6
e_a^{21}	0.0191239
e_{ext}^{21}	0.0479778
GCI_{fine}^{21}	15.80%

with the purpose of estimating the discretization error and calculating the numerical uncertainty in the fine-grid solution, and thus identifying the most suitable mesh for the main simulations. To do so, three meshes of varying density were used (see number of elements n_i in Table 4.4), a representing dimension h_i to be calculated, and a significant simulated value φ_i has to be used to quantify this uncertainty (Celik, 2008). In this research, the air speed at a point below the centre of the fan at 1.5 m above the floor was chosen. The mesh chosen for the main simulations comprises 1,996,278 elements and a numerical uncertainty equal to 15.80 %.

4.2.3 Model validation - criteria for agreement

Measured and simulated air speed values were compared in 36 points (see the yellow markers in Figure 4.6) and considered to be in agreement when the respective error bars overlapped. For the simulated values, the upper and lower limits of the error bars are the mean over the simulated period plus and minus the discretization error,

respectively. Since the simulation started with no air movement (air speed was zero at time zero), the initial 10 s have been excluded in the means' calculation. For the measurements, since the experiment has been repeated three times, the upper limit of the error bars is the highest of the three measurements plus the measurement error, while the lower limit of the error bars is the lowest of the three measurements minus the measurement error.

Statistics such as root mean square error (RMSE) and the mean absolute error (MAE) have not been employed in this research for two key reasons. Firstly, using RMSE and MAE with n=36 might be misleading as they would spread the error across all points. However, in this study, it is more important to evaluate the accuracy of the model in the different regions (centre, perimeter, along a radius), separately. Secondly, all statistics are less useful when there are only a limited number of error samples (Willmott and Matsuura, 2005). Thus, in this research, presenting the values of the errors themselves (as error bars) is more appropriate.

4.3 Results and discussion

4.3.1 Qualitative analysis of the air flow generated by the ceiling fan

Previous research (Jain et al., 2004) investigated the key flow regions observed in a room with an operating ceiling fan, identifying eight regions (Figure 4.9). The comparison between previous research and the developed CFD model is summarised in Table 4.5. Region one is the area below the fan, and, in good agreement with previous research, in the CFD model presented in this paper air speed reaches the highest values in this region (Figure 4.10). The diameter of downward flow immediately below the fan is smaller than the diameter of the fan, the flow then starts to spread, and there is a significant swirling component (Figure 4.11). In the qualitative study (Jain et al., 2004), the half cone angle is about 10°, while in the CFD results this varies

depending on which time-step is analysed. This is due to the fact that in this region the flow is highly turbulent, and therefore the angle of the meandering plume and the characteristic of the local free shear layers vary over time (Figure 4.12).

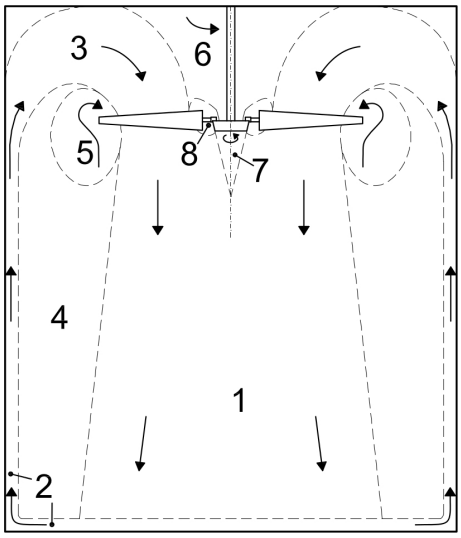

Figure 4.9: *Flow regions identified by Jain et al. (2004).*

Table 4.5: *Comparison between previous qualitative research and the developed CFD model.*

Region	Agreement	Key characteristics
1	Good	Highest higher speed, significant swirling component, divergent flow
2	Good	Very low air speed near walls (moving upward) and ceiling
3	Good	Increasing air speed and development of swirling component
4	Good	Very low air speed and negligible effectiveness of the fan
5	Weak	Local air recirculation underestimated by the CFD model
6	Good	Low air speed, recirculation area
7	Good	Air not driven downwards due to the blockage caused by the motor of the fan
8	Weak	Local air recirculation underestimated by the CFD model

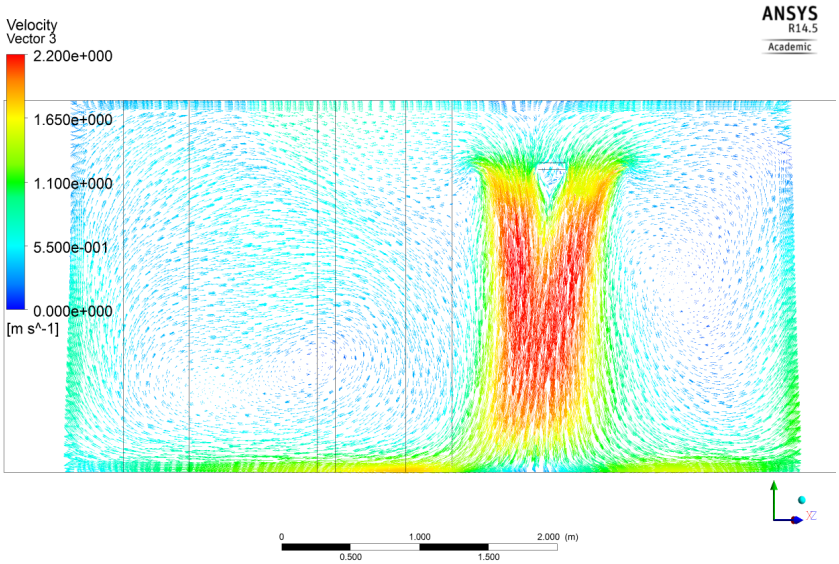

Figure 4.10: *Air flow generated by the ceiling fan (SST k-ω turbulence model) – side view.*

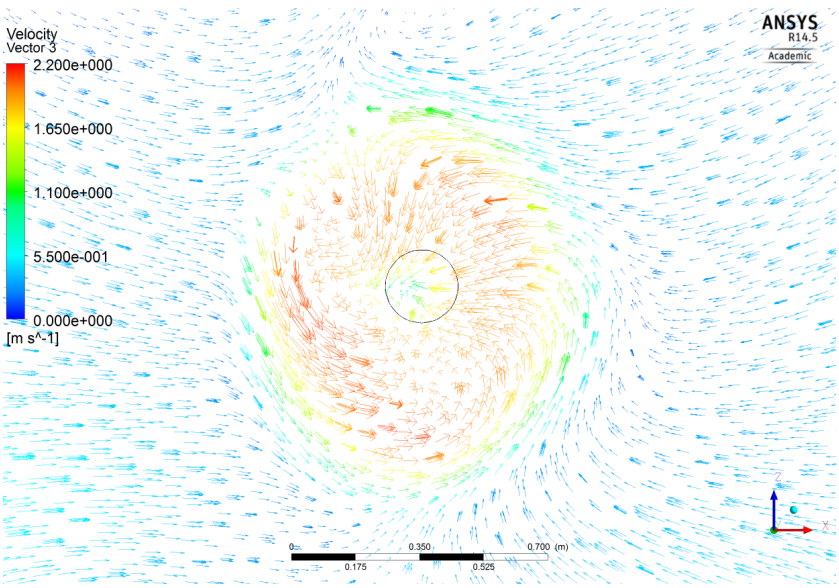

Figure 4.11: *The swirling air movement generated by the ceiling fan 10 cm below the blades (SST k-ω turbulence model) – plan view.*

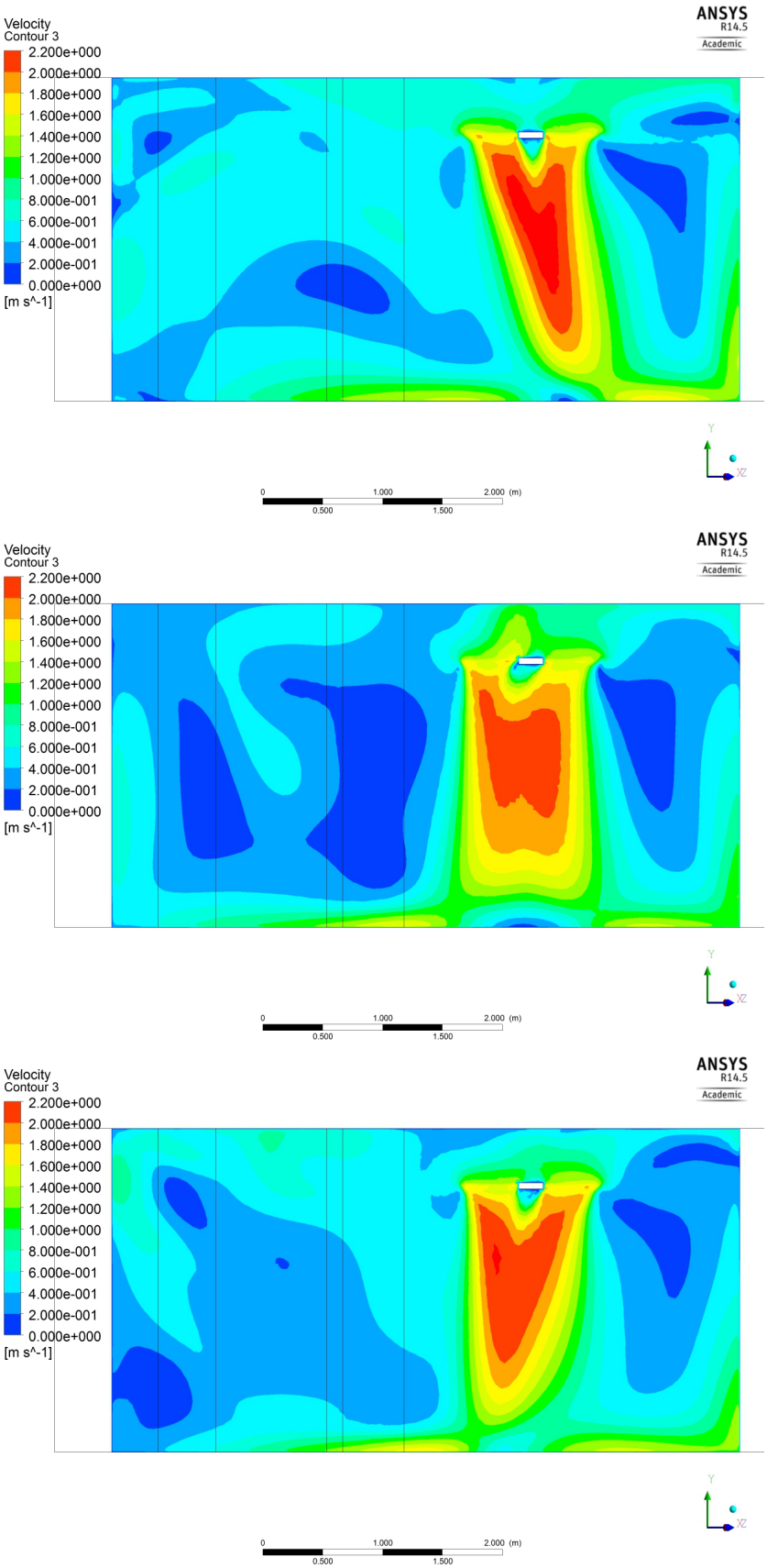

Figure 4.12: *Air flow field generated by the ceiling fan at different time steps (top, middle, bottom) (SST k-ω turbulence model).*

Similarly to previous research (Jain et al., 2004), in region two, the air speed near walls and ceiling is very low, air is moving upwards near the walls, and as soon as it is again in proximity of the fan, in region three, its speed increases and it starts to redevelop a swirling component. Moreover, the CFD model accurately predicts the small region below the ceiling fan where air is not driven downwards due to the blockage caused by the motor of the fan. In agreement with the qualitative study (Jain et al., 2004), the wide region (number four) between the surfaces of the room and region one is characterized by very low air speed and negligible effectiveness of the fan. Thus, the CFD model is able to accurately replicate qualitatively all the occupied regions of the room.

The major differences between the CFD results and previous qualitative studies are located in the two small regions near the ends of the blades, where the local air recirculation is underestimated by the CFD model. This is due to the fact that the actual blades are not modelled, but it is not a significant limitation of the model in this case since the aim is to model the air movement generated by the ceiling fan in the room with particular interest in the occupied zone.

4.3.2 Quantitative validation of the CFD model

In this study, four turbulence models have been fully tested and the results vary significantly depending on the model used (Table 4.6).

Table 4.6: *Agreement between measured and simulated (using four RANS turbulence models) air speed values.*

Location	Number of points	SST k-ω	RNG k-ε	k-ω	k-ε
Centre	3	100%	100%	100%	67%
Perimeter	12	50%	50%	42%	42%
Radius	21	100%	71%	48%	48%
Total	36	83%	67%	50%	47%
CPU time		6h 35m	6h 00m	3h 34m	2h 10m

Taking into account the uncertainties in measurement and the discretisation error in CFD, measured and simulated values are in excellent agreement when the SST

k-ω was used, with 83% of the simulated values being within the error bars of the respective measured value. There is an excellent agreement in the three points below the centre of the fan (Figure 4.13, three "centre" points) and in the 21 points located on a radius at increasing distance from the axis of the fan (Figure 4.13, points from "r200" rightwards). Only in six perimeter points (Figure 4.17), namely "Est 700" and "Est 1300", "North 700" and "North 1300", and "West 700" and "West 1300", the respective error bars do not overlap. In three of them, namely "North 700" and "North 1300", and "West 700", the difference between measured and simulated values is wide, while it is significantly smaller in the others. This is likely to be due to the fact that these six points are in the most turbulent and rapidly changing region of the flow, where air speed is characterised by rapid spatial and temporal variations (Figure 4.12).

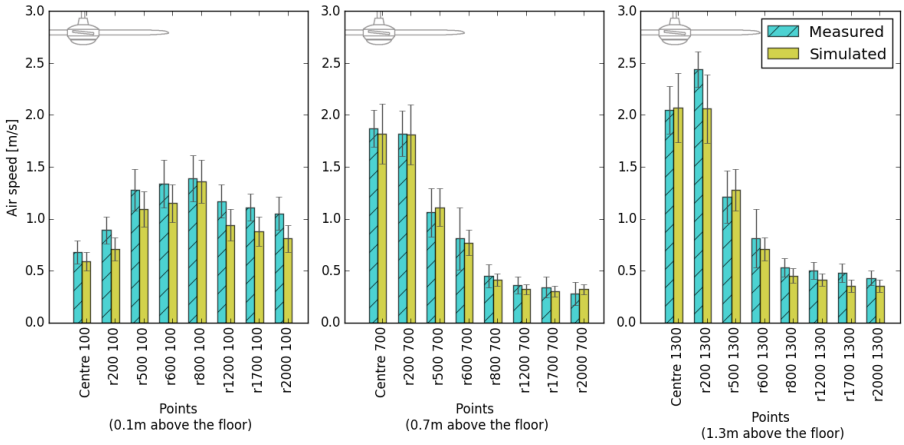

Figure 4.13: *Measurements and CFD results comparison at increasing distance from the axis of the ceiling fan (SST k-ω turbulence model).*

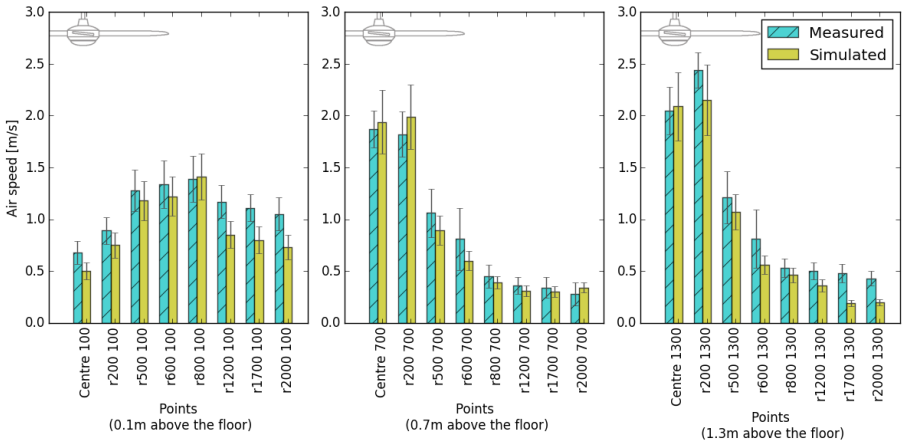

Figure 4.14: *Measurements and CFD results comparison at increasing distance from the axis of the ceiling fan (RNG k-ε turbulence model).*

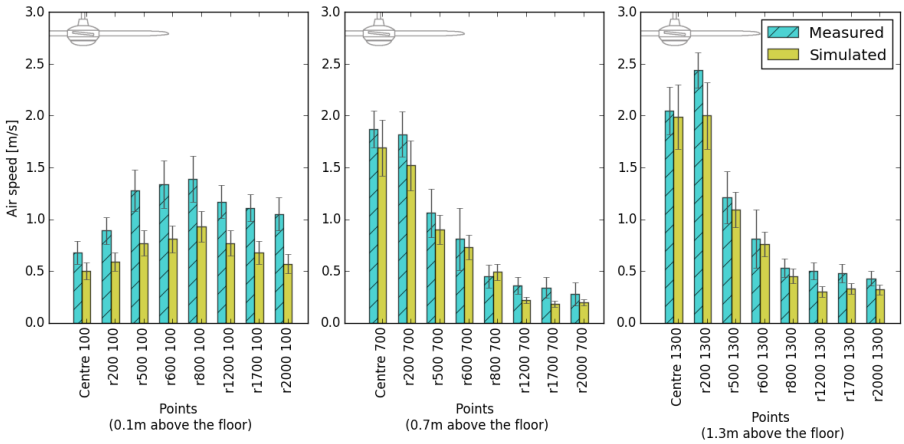

Figure 4.15: *Measurements and CFD results comparison at increasing distance from the axis of the ceiling fan (k-ω turbulence model).*

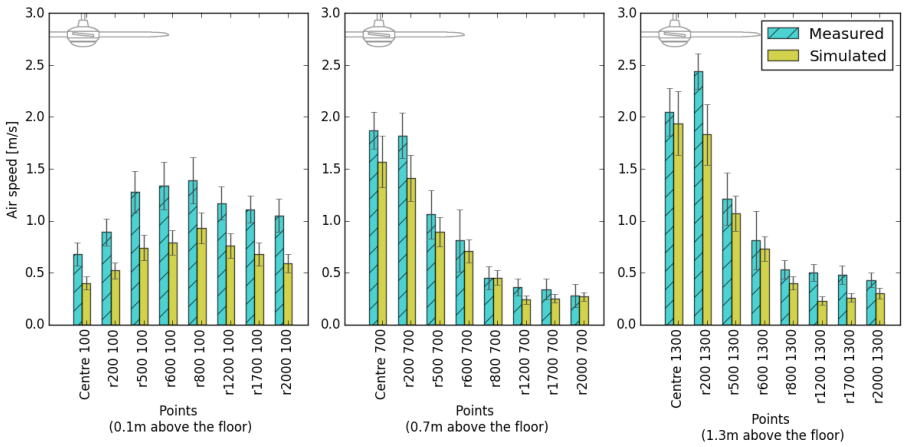

Figure 4.16: *Measurements and CFD results comparison at increasing distance from the axis of the ceiling fan (k-ε turbulence model).*

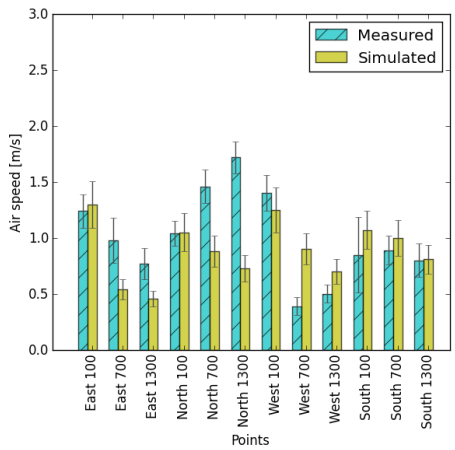

Figure 4.17: *Measurements and CFD results comparison – perimeter points (SST k-ω turbulence model).*

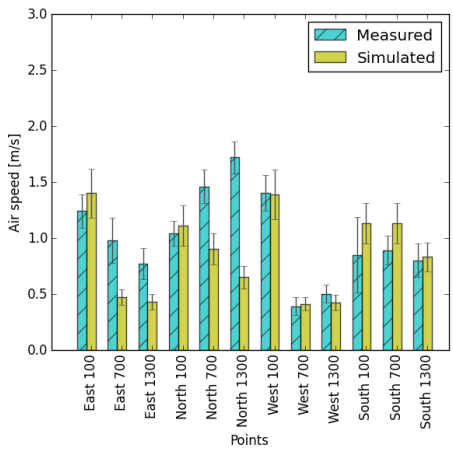

Figure 4.18: *Measurements and CFD results comparison – perimeter points (RNG k-ε turbulence model).*

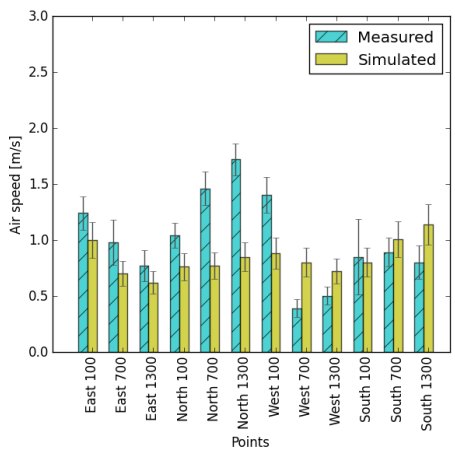

Figure 4.19: *Measurements and CFD results comparison – perimeter points (k-ω turbulence model).*

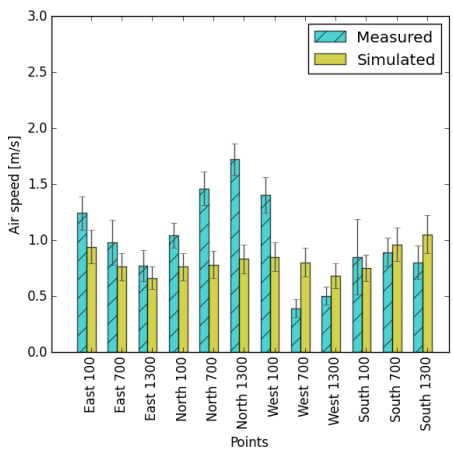

Figure 4.20: *Measurements and CFD results comparison – perimeter points (k-ε turbulence model).*

The other three turbulence models did not reach the same high level of agreement with the measured values (Table 4.6). In the three points below the centre of the fan, the RNG k-ε (Figure 4.14) and the k-ω (Figure 4.15) turbulence models are as good as the SST k-ω, while the k-ε fails to predict the air speed at 0.1 m above the floor, being 0.1 m/s the difference between the error bars (Figure 4.16). In the 12 perimeter points, 50% or less of the simulated values are within the error bars of the respective measured value (Table 4.6, and Figure 4.18 to 4.20). On the radial points, k-ω and k-ε models have limited capability of predicting the correct air speed, the percentage of agreement with the measurements being below 50%, and there is no clear pattern that can explain why, at certain points, the prediction is correct and in others it is not. When the RNG k-ε model is used, the agreement is excellent between "r200" and "r800" at any given height (Figure 4.14), while it weakens farther away from the fan, where air speed is lower.

4.3.3 The importance of the choice of the turbulence model

The air flow generated by a ceiling fan is highly turbulent. As shown in the previous section, it is characterised by elevated air speed variations, and therefore by significant Re variations. For this reason, choosing the most appropriate turbulence model is essential in order to obtain accurate results.

The SST k-ω turbulence model produced the most accurate and realistic results, being superior to the other three eddy-viscosity turbulence model considering both qualitative and quantitative results. This is in agreement with the results of the first application of the coupled system (see chapter 3) which used the IESD-Fiala model to investigate the effect of air movement generated by desktop fans on human thermal comfort. This can be explained by analysing the nature of the four eddy-viscosity turbulence models in relation to the application presented in this paper.

The four turbulence models tested in this research are two-equation eddy-viscosity models, which means that the Reynolds stresses are assumed to be proportional to

mean velocity gradients. In the k-ε models, the two additional transport equations are used to describe the kinetic energy k and the rate of dissipation of k per unit mass ε, respectively:

$$\frac{\partial(\rho k)}{\partial t} + div(\rho k\mathbf{U}) = div[\frac{\mu_t}{\sigma_k} grad(k)] + 2\mu_t S_{ij} \cdot S_{ij} - \rho\varepsilon \tag{4.1}$$

$$\frac{\partial(\rho \varepsilon)}{\partial t} + div(\rho \varepsilon\mathbf{U}) = div[\frac{\mu_t}{\sigma_\varepsilon} grad(\varepsilon)] + C_{1\varepsilon}\frac{\varepsilon}{k} 2\mu_t S_{ij} \cdot S_{ij} - C_{2\varepsilon}\rho\frac{\varepsilon^2}{k} \tag{4.2}$$

The equations contain five coefficients, whose value in the standard k-ε model are constant (Launder and Spalding, 1974): $C_\mu = 0.09$, $\sigma_k = 1.00$, $\sigma_\varepsilon = 1.30$, $C_{1\varepsilon} = 1.44$, $C_{2\varepsilon} = 1.92$. In the RNG k-ε model (Patel et al., 1985), the $C_{1\varepsilon}$ is not fixed, and it represent a strain-dependent correction term introduced to improve the performance at low Re. In the k-ω model developed by Wilcox (Wilcox, 1988, 1993a,b, 1994), the turbulence frequency $\omega = \varepsilon/$k is used as the second variable, and the two additional equations are:

$$\frac{\partial(\rho k)}{\partial t} + div(\rho k\mathbf{U}) = div[(\mu + \frac{\mu_t}{\sigma_k}) grad(k)] + P_k - \beta^* \rho k\omega \tag{4.3}$$

$$\begin{aligned} \frac{\partial(\rho \omega)}{\partial t} + div(\rho \omega\mathbf{U}) = \\ = div[(\mu + \frac{\mu_t}{\sigma_\omega}) grad(\omega)] + \gamma_1(2\rho S_{ij} \cdot S_{ij} - \frac{2}{3}\rho\omega\frac{\partial U_i}{\partial x_i}\delta_{ij}) - \beta_1\rho\omega^2 \end{aligned} \tag{4.4}$$

The model constants are: $\sigma_k = 2.00$, $\sigma_\omega = 2.00$, $\gamma_1 = 0.553$, $\beta_1 = 0.075$, $\beta^* = 0.09$. Subsequently, an improved k-ω model was suggested, namely the SST k-ω model [23–26], which is a combination of the standard k–ε model used in the fully turbulent region far from the wall where Re is likely to be higher, and a k–ω model in the near-wall region. In the SST k-ω model, the ω equation changes from equation

4.4 to:

$$\begin{aligned} \frac{\partial(\rho\omega)}{\partial t} + div(\rho\omega\mathbf{U}) = \\ = div[(\mu + \frac{\mu_t}{\sigma_{\omega,1}})grad(\omega)] + \gamma_2(2\rho S_{ij} \cdot S_{ij} - \frac{2}{3}\rho\omega\frac{\partial U_i}{\partial x_i}\delta_{ij}) - \beta_2\rho\omega^2 + \\ +2\frac{\rho}{\sigma_{\omega,2}\omega}\frac{\partial k}{\partial x_k}\frac{\partial \omega}{\partial x_k} \end{aligned} \tag{4.5}$$

There is an extra source term on the right hand side of the equation, and the numerical coefficients are (Menter et al., 2003): $\sigma_k = 1.00$, $\sigma_{\omega,1} = 2.00$, $\sigma_{\omega,2} = 1.17$, $\gamma_2 = 0.44$, $\beta_2 = 0.083$, $\beta^* = 0.09$. Moreover, blending functions are used to achieve a smooth transition between the two models, namely k-ε and k–ω.

Considering the three-dimensional transient ceiling fan model proposed in this paper, it is now easier to understand why the SST k-ω model produced the best results followed by the RNG k-ε model, while the other two turbulence models generated less accurate results. By combining the strengths of k-ε and k-ω models, the SST k-ω can deal with higher and lower Re, and it is able to accurately model the boundary layers and the flow separation under adverse pressure gradient conditions thanks to the extra cross-diffusion term on the right hand side of equation 4.5 (term in the third line). The CFD results indeed demonstrate that this turbulence model is more accurate in all considered locations, namely below the centre of the fan, on the perimeter, and on a radius at growing distance for any given height and therefore air speed. On the other hand, the RNG k-ε is as good as the SST k-ω in the central and perimeter points, where the flow is more turbulent and air speed is higher, while it shows its main limitations by failing to predict the air speed farther away from the fan.

In view of the fact that in none of these four turbulence models the agreement between measured and simulated values exceeded 50% in the 12 perimeter points, two more advanced turbulence models have been considered, namely the BSL (Menter, 1993) and SSG (Wallin and Johansson, 2000) Reynolds stress models. Theoretically,

these models are more suitable for complex flows, such as the swirling flow generated by a ceiling fan. Practically, their application proved to be fairly difficult. Without changing any other input data or element of the model, the simulation immediately stopped due to a "fatal overflow in linear solver" using both models. Within the context of this research, "fatal overflow in linear solver" means that the linear solver failed to reduce the residuals of the linearised equations because the solution was diverging. Two modifications were then tested: reducing the time step by setting a limit for the maximum, rather than the RMS, Courant number equal to 1, and using the best available results, namely those calculated with the SST k-ω model, as initial conditions. Even combining the two modifications, the simulation stopped due to the same overflow error after some iterations. Also a finer mesh was used, but unsuccessfully. Both using a finer mesh and reducing the time step would also have the disadvantage of exponentially increasing the time required to reach a converged solution. Thus, evidence suggests that more advanced turbulence models such as Reynolds stress models and LES require a complete explicit model of the fan, the use of a moving mesh, and therefore higher computational power. However, this would significantly limit the applicability of the model and increase the potential sources of uncertainties.

4.3.4 Required computational power

In this study, simulations have been run on the High Performance Computer System at Loughborough University, a 2460-core 64-bit Intel Xeon cluster. Two nodes and 20 cores per node, therefore 40 cores in total, have been used in these simulations in order to make efficient use of the cluster architecture, and reduce the computational time. In the pre-processing, the meshes have been generated using a work station equipped with an Intel Xeon E5520 CPU and 24 GB of RAM. All the other pre- and post- processing activities have been completed using a laptop with an i5-3320M CPU and 8 GB of RAM.

Due to extra terms in the two additional k and ε, or ω, equations, the CPU time required to achieve a converged solution using the SST k-ω and RNG k-ε models is twice the time required when the k-ω model is chosen, and three times higher than the time required when the standard k-ε model is selected (Table 4.6). In detail, the SST k-ω and RNG k-ε are both able to predict the meandering behaviour of the plume over time (Figure 4.12), which means that there are relevant differences between each time step and the following one, and therefore more iterations per time step are required to reach convergence. On the other hand, when the other two simpler models (standard k-ω and standard k- ε) are used, the differences between each time step and the following one become negligible after the initial time steps, and therefore only a few iterations per time step are required thereafter.

Although there is no direct linear relationship between the number of cores and the CPU time due to the time required to split, and then recombine, the results which increases with the number of cores, these total CPU times (Table 4.6) could be reduced if more cores were available. Considering the CPU time and the accuracy of the results, the SST k-ω model is still the best choice.

4.3.5 Usability of the developed model

Compared with the models previously developed (Bassiouny and Korah, 2011; Momoi et al., 2004, 2007; Adeeb et al., 2015), the model presented here is applicable to a wider range of fluid flow problems due to the small number of input parameters required, the reasonably low CPU time required, and the use of an unstructured mesh, which can accommodate complex geometries. This implicit model can therefore be used whenever a given piece of research requires a focus on the flow field generated by a ceiling fan, not on the actual design of the fan.

When assessing the effect of air movement on human thermal comfort using advanced thermal comfort models such as the IESD-Fiala model (Fiala et al., 1999, 2001), this CFD model is able to effectively predict the air flow generated by the

fan at any distance from the fan and therefore it reliably estimates the air flow on a person. The limited agreement between measurements and simulated values at the perimeter of the fan has little implication on the applicability of this model in thermal comfort studies, since this perimeter region is less than 10 cm wide, while any human body, regardless of age, gender, height, and weight, is significantly bigger. Moreover, it is almost always possible for a person to then move a short distance to increase or decrease the air movement on their body. Similarly, if the spread of pollutants (such as human bioeffluents, particulates, volatile organic compounds, and tobacco smoke) in a room is to be investigated, then any error in the perimeter region does not affect the overall distribution of the contaminants in the space, but only their concentration and movement in that narrow perimeter region.

From a practical point of view, this modelling approach can be used by other researchers to model other types of ceiling fans (with different features such diameter of the blades or rotational speed) by using the following procedure. Firstly, in this research, the fan was modelled as a ring with the same diameter as the actual fan, and with a central cylindrical solid element, since in a real ceiling fan no air emanates from the centre. Thus, the dimensions of these elements must be changed to match those of the fan to be modelled. Secondly, the values of the axial and theta components of the momentum source must be modified according to the air flow generated by the chosen fan. To do so, the same iterative process used in this research should be followed. However, based on the results of this study, it is possible to say that fewer points can be used to compare measured and simulated values. The key points are those placed in the axis of the fan, and those located along a radius at increasing distance from the axis of the fan (but only those near the floor, since the air speed values at higher locations are negligible). The total number of points used for the comparison will depend on the specific application. For instance, if the floor-to-fan distance is big (this might be the case of old buildings in which the internal height of the rooms is usually bigger), then more points would be required below the centre

of the fan (on its rotational axis). All other settings such as turbulence model and meshing strategy, can be used exactly as in this study.

4.4 Summary

This second experimental chapter begins with the identification of suitable realistic residential indoor scenarios in the UK and in India , since the analysis of these scenarios explains why the three-dimensional CFD model of a typical Indian ceiling fan was developed in this research. These two countries were chosen because this PhD research was linked to a wider research project that involved four partners: Loughborough University and De Montfort University in the UK, CEPT University in India, and University of California Berkeley in the USA. This project included detailed field studies in residential buildings in India and in the UK aiming to collect information about the current use of air movement and cooling devices in residential buildings in India and in the UK. Ceiling fans were found to be by far the most used means to generate non-uniform thermal environmental conditions in Indian houses.

This chapter presents the results of the detailed validation of the transient three-dimensional model of a typical Indian ceiling fan. The importance of this model within this research clearly emerged from the analysis of the scenarios in the UK and in India. However, this chapter contains information that could be used also in other future studies which do no use the coupled system or do not deal specifically with thermal comfort, but simply need to have an accurate and computationally efficient model of a ceiling fan.

The accuracy of the thermal comfort predictions of the coupled system depends on the quality of the CFD model since this defines the environmental conditions that affect the person. Due to the complexity of the air flow generated by a typical Indian ceiling fan, it was essential to develop and validate a three-dimensional transient CFD model of a typical Indian ceiling fan by comparing simulation results and mea-

sured data collected in an environmental chamber at CEPT University. Due to the highly turbulent nature of the air flow, several turbulence models were used and their respective performance evaluated.

The qualitative validation of the developed model was completed by comparing the flow regions identified in a previous qualitative study on ceiling fans with those generated by the model. The developed CFD model is able to accurately replicate qualitatively all the occupied regions of the room, including key behaviours such as the swirling and downward components of the flow. The major differences between the CFD results and the previous qualitative study are located in the two small regions near the ends of the blades, due to the use of the simplified modelling approach. However, this is not a significant issue as the focus is on the occupied zone of the room.

There is a perfect agreement in the points below the centre of the fan, and in those placed on a radius at increasing distance from the rotation axis of the fan. However, in the points located below the perimeter of the fan, only 50% of the simulated values fell within the error bars of the respective measured value (when the SST k-ω was used) due to the fact that these points are in the most turbulent and rapidly changing region of the flow. The other turbulence models provided less accurate results in all locations (below the centre of the fan, below the perimeter of the fan, and on a radius at growing distance from the rotation axis of the fan).

The choice of the most appropriate turbulence model proved to be essential in order to develop an accurate CFD model of the ceiling fan. The SST k-ω produced by far the most accurate results, and this is due to the fact that, by combining the strengths of k-ε and k-ω models, the SST k-ω can deal with higher and lower Re, and it is able to accurately model the boundary layers and the flow separation under adverse pressure gradient conditions thanks to the extra cross-diffusion term added to one of its equations. In simpler words, this turbulence model combines the straights of the other two models, and therefore can produce more accurate results when a

complex and highly turbulent flow, such as the one generated by a ceiling fan, is modelled.

All simulations were run on the High Performance Computer System at Loughborough University, and the total CPU time (that is the time required to achieve a converged solution) ranged between 2 and 6.5 hours. In general, the more a turbulence model produced accurate results, the longer the total CPU time became. All simulations were run with the same number of cores and nodes, which depended on the number of cores and licences available at the time of the simulation.

The limited agreement between measurements and simulated values at the perimeter of the fan has little implication on the applicability of this model in thermal comfort studies, since this perimeter region is less than 10 cm wide, while any human body, regardless of age, gender, height, and weight, is significantly bigger. Similarly, when a study addresses a different issue such as air pollutants distribution in a room in which a ceiling fan is operating, this limited accuracy in the perimeter region does not limit the use of this model. It is worth mentioning that a detailed model of the fan geometry would not guarantee to overcome this limitation, but would certainly increase the uncertainties in the model and the total CPU time.

Chapter 5

APPLICATION OF THE COUPLED SYSTEM TO REAL DOMESTIC BUILDINGS

This chapter illustrates the methods (section 5.1) used and the results section 5.2 obtained using the coupled system to investigate how the use of ceiling fans affects human thermal comfort in real residential buildings in India.

The focus is on the thermal comfort predictions generated by the IESD-Fiala model within the coupled system. Thus, in this chapter, the research hypothesis is tests by making a direct comparison between the actual thermal sensation votes of real participants and the thermal sensation calculated by both the coupled model and the PMV method. CFD results are illustrated only to show the boundary conditions, especially the air speed around the manikin, that led to these thermal comfort results. However, the complete validation of the CFD model of the ceiling fan typically available in Indian dwellings was presented in the previous chapter 4. Thus, in this chapter there is no direct comparison with measured values. Details of the required computational power are described in the final part of the chapter.

5.1 Methodology

The previous chapters described the first complete application of the coupled system to an artificial scenario, the process followed to identify suitable scenarios in real buildings, and the development of a CFD model of a typical Indian ceiling fan.

This section illustrates the approach and the methods used to apply the coupled system to real domestic buildings, which is basically the combination and synthesis of the work covered in the previous chapters. The expertise gained during the first application was used here to model more realistic, but also more complex, scenarios in which the number of uncertainties is higher compared to an environmental chamber. For this reason, the most critical boundary condition, the ceiling fan, was previously and extensively investigated.

Thus, in this part of the research, there is no direct comparison between simulated and measured values because the aim was to model likely Indian domestic scenarios using previously validated models, and, when appropriate, data from the literature.

5.1.1 Modelling approach and assumptions

For this application of the coupled system, a typical Indian drawing room was chosen (Figure 5.1). This is a domestic environment that was present in almost every house that participated in the field study (section 4.1) and it has the key characteristics that make it suitable and interesting for the use of the coupled system. Firstly, there is often more then one ceiling fan, and, secondly, this part of the house is mainly used when guests visit the household. This means that these people are exposed to complex non-uniform thermal conditions, but also that their possibility of adaptation is limited. Their posture, location, clothing, and activity level can be determined with confidence, minimizing the uncertainties.

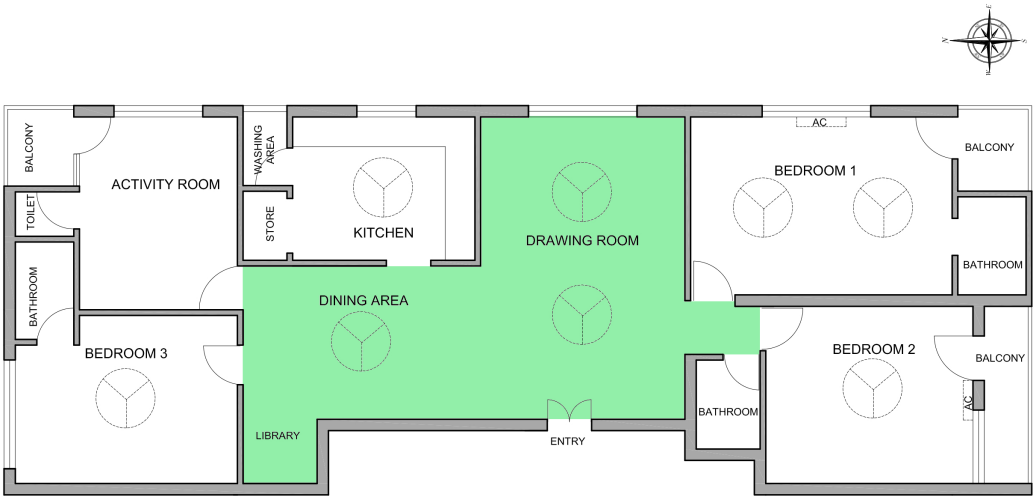

Figure 5.1: *Floor plan of the chosen Indian apartment (highlighted in green the part modelled in CFD).*

In this model, the geometry was created directly in ICEM CFD (Figure 5.2). Having already developed and tested a seated virtual manikin for the environmental chamber study, this can be imported later in any model built in ICEM CFD avoiding common import-related issues such as small gaps or wrong part names that occur when a geometry created with one software is imported into another software. Since the coupling between CFD and IESD-Fiala model currently works only with one virtual manikin per model, if thermal comfort has to be assessed in different locations within a room using the coupled system, the virtual manikin has to be relocated in the desired location each time.

Two manikin locations were investigated (Figure 5.3), namely "M1" and "M2". The coupled manikin can be clearly identified ("M2" in Figure 5.3) since its body surface is subdivided into multiple parts which are displayed in different colours. In this initial version model, the other occupants were modelled as a manikin with identical shape to the coupled manikin, but whose surface was not split into multiple parts (Figure 5.2 and 5.3, grey manikins).

However, using such a complicated shape for the other occupants did not add any relevant information to the model, but was unnecessarily and significantly increasing the number of mesh elements and therefore the computational time. Thus, the

model was simplified, replacing these three manikins with simple boxes (Figure 5.4) as used by previous researchers (Cook et al., 2011). Due to the simpler shape, the minimum shell mesh size of this element could be increased, and this led to a significant reduction of the number of mesh elements.

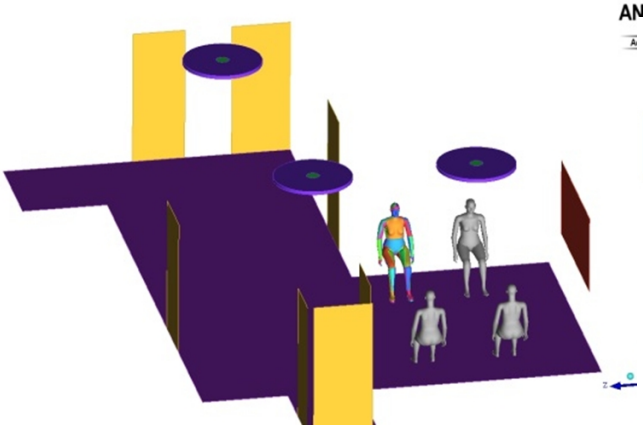

Figure 5.2: *Model of the drawing room with three ceiling fans - version 1.*

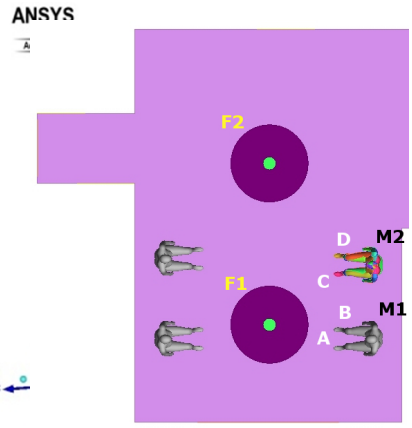

Figure 5.3: *Plan view of part of the model.*

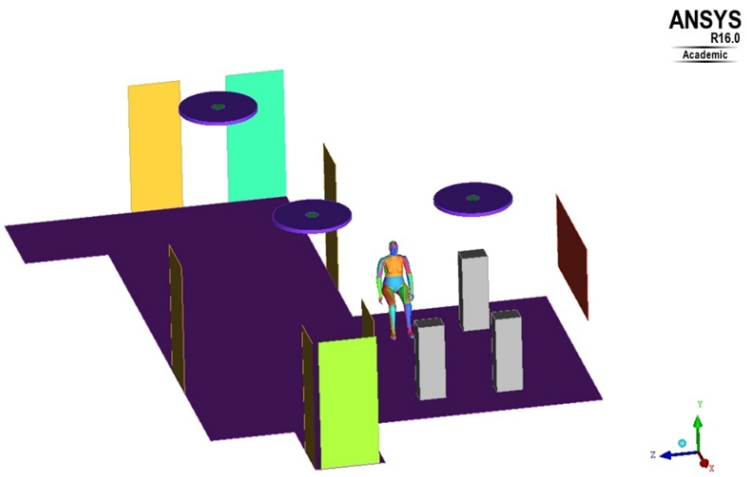

Figure 5.4: *Model of the drawing room with three ceiling fans - version 2.*

For both versions of the geometry, an unstructured mesh was generated using a combination of the settings adopted in the environmental chamber study and in the ceiling fan CFD model development. The settings and procedure used to create the surface and volume mesh are the same that were used in the environmental chamber model (section 3.2.2). The settings adopted here to model each ceiling fan are

identical to those used when the model of a typical Indian ceiling fan was developed (section 4.2.2).

Like in the previous application (section 3.2), within CFX, the boundary conditions for the coupled manikin were set according to the requirements of the IESD-Fiala model. As the geometry of the manikin can be imported from one model to another in ICEM CFD, so do the relative settings in CFX. This was done using a piece of CCL code exported from the environmental chamber model. Due to the high number of body parts, variables and expressions to be set, this automated procedure made the process quicker, but also drastically reduced the possibility of errors and the relative time required to debug the model.

All other surfaces were modelled as fixed temperature surfaces, whose values were equal to mean radiant temperature (Table 5.1). Mean radiant temperature, air temperature and relative humidity were defined according to previous studies on Indian apartments (Indraganti, 2010b) in the first group of scenarios (Table 5.1, scenarios 1 to 8), and then mean radiant temperature and air temperature were decreased, while relative humidity was increased to simulate increasingly milder conditions. For the moist air inside the room, the initial mass fraction and buoyancy reference density have been calculated based on the relative humidity and air temperature initial values using the procedure described in section 3.2.2.

In the first version of the model, there are no openings. Although in a real house a fan might be operating while a window or a door is open, the erratic nature of the wind would make the choice of any opening boundary condition that altered the air flow absolutely arbitrary and questionable. Moreover, in the occupied area in proximity to a ceiling fan, the magnitude of the air speed generated by the ceiling fan is significantly higher than the air flow that tiny and distant cracks might generate. In the second simpler version of the model, two doors were simulated as an opening, namely those facing the activity room and the second bedroom. This was done only because it made the simulation more stable. Air temperature and relative humidity

at the opening were set to be identical to the initial conditions within the room. A 2.69 loss coefficient, which is equivalent to a discharge coefficient of 0.61, was also used.

In total, 23 different scenarios were simulated (Table 5.1). In the first 20 cases, three variables that are defined only within the IESD-Fiala model, namely the metabolic rate, clothing and pre exposure time, did not vary. Using identical environmental conditions of scenario 10, the last 3 cases aimed to independently evaluate the effect on the thermal comfort results of metabolic rate, clothing and pre exposure time, respectively. The pre exposure time represents the amount of time during which the subject was exposed to the initial conditions in room before starting the simulation.

Transient simulations were performed using settings similar to those adopted in the environmental chamber study (section 3.2.2) and in the ceiling fan CFD model development (section 4.2.2). However, here only the SST k-ω (Menter, 1992a,b, 1994, 1997; Menter et al., 2003) was used as it provided with the best results with CFD ceiling fan model. Convergence criteria have been set equal to 1e-05 for the RMS residuals and 0.01 for the conservation target. An adaptive time step as a function of RMS Courant number was chosen, with the limit for the RMS Courant number set equal to 5. The total time simulated in all cases is 3 minutes. Similarly to the previous simulations, these simulations started with the fan not in operation (that means air speed was zero at time zero), and therefore the air speed values of the initial 10 s were excluded from the means' calculation.

Table 5.1: *Simulation scenarios.*

ID	T_{air} [°C]	MRT [°C]	RH [%]	Fan 1	Fan 2	Manikin position	Met [met]	Clothing	preExp [minutes]	Model
1	34.7	34.5	27	off	off	1	1.0	sari	30	1
2	34.7	34.5	27	off	off	2	1.0	sari	30	1
3	34.7	34.5	27	on	off	1	1.0	sari	30	1
4	34.7	34.5	27	on	off	2	1.0	sari	30	1
5	34.7	34.5	27	off	on	1	1.0	sari	30	1
6	34.7	34.5	27	off	on	2	1.0	sari	30	1
7	34.7	34.5	27	on	on	1	1.0	sari	30	1
8	34.7	34.5	27	on	on	2	1.0	sari	30	1
9	30	30	30	off	off	2	1.0	sari	30	2
10	30	30	30	on	off	2	1.0	sari	30	2
11	30	30	30	off	on	2	1.0	sari	30	2
12	30	30	30	on	on	2	1.0	sari	30	2
13	28	28	30	off	off	2	1.0	sari	30	2
14	28	28	30	on	off	2	1.0	sari	30	2
15	28	28	30	off	on	2	1.0	sari	30	2
16	28	28	30	on	on	2	1.0	sari	30	2
17	30	30	50	off	off	2	1.0	sari	30	2
18	30	30	50	on	off	2	1.0	sari	30	2
19	30	30	50	off	on	2	1.0	sari	30	2
20	30	30	50	on	on	2	1.0	sari	30	2
21	30	30	30	on	off	2	1.2	sari	30	2
22	30	30	30	on	off	2	1.0	summer	30	2
23	30	30	30	on	off	2	1.0	sari	1	2

In CFX, 12 monitoring points were placed near the manikins (Table 5.2; see also Figure 5.3 at p. 115) at three heights above the floor to record air temperature and air speed throughout the simulations. This facilitated the comparison between DTS, calculated by the IESD-Fiala model, and Fanger's PMV (Fanger, 1970), whose calculation requires as input accurate values of air temperature and air speed near the subject at these three heights.

Table 5.2: *Monitoring points near the manikins.*

Point	Height [m]	Description
A low	0.1	
A mid	0.6	Between F1 and M1
A high	1.1	
B low	0.1	
B mid	0.6	Between F2 and M1
B high	1.1	
C low	0.1	
C mid	0.6	Between F1 and M2
C high	1.1	
D low	0.1	
D mid	0.6	Between F2 and M2
D high	1.1	

Alongside the main simulations, a mesh sensitivity analysis was carried out using the method proposed by Celik (2008) as done for the environmental chamber model and the fan model. In this case, the process was repeated for both models (Table 5.3), namely the initial model and the subsequent simplified version in which the occupants not linked to the comfort model were represented with simpler shapes. In the former, the chosen critical variable φ_i was the air speed at a point below the axis of fan "F1" 0.7 m above the floor. In the latter, φ_i is the air speed at "C mid" (Table 5.2). The reason for changing point is that the second model was used only to investigate thermal comfort for a manikin in position "M2". Thus, using a point near that manikin position was considered to be more appropriate. The final meshes used in model 1 and 2 have 3,284,355 and 2,906,595 elements, respectively.

Table 5.3: *Discretization error calculation (Celik, 2008)*

	Model 1	Model 2
N_1	3,284,355	2,906,595
N_2	1,628,368	1,160,564
N_3	917,370	282,075
h_1	0.03	0.04
h_2	0.04	0.05
h_3	0.05	0.08
r_{21}	1.26	1.36
r_{32}	1.21	1.60
φ_1	0.84	0.296
φ_2	0.79	0.299
φ_3	0.80	0.313
ε_{21}	-0.046	0.003
ε_{32}	0.006	0.014
p	1.986	1.029
φ_{ext}^{21}	0.9	0.3
e_a^{21}	0.055	0.010
e_{ext}^{21}	0.085	0.028
GCI_{fine}^{21}	17.93 %	9.33 %

5.1.2 Development of an "Indian sari" clothing for the IESD-Fiala model

When the coupled model is used, metabolic rate, clothing and pre exposure time are set as input only in the IESD-Fiala model. The metabolic rate uses the usual international metric, the *met*, which is defined based on the activity level, and whose values can be taken from international standards such as ASHRAE 55-2013 (ASHRAE, 2013a). Similarly, the pre exposure time is simply defined in minutes. On the hand, the definition of the clothing is more complex.

In the IESD-Fiala model, the clothing is defined by specifying five variables for each of twelve macro-regions in which the manikin body surface is split (Table 5.4). These macro-regions are different from the 59 body surface parts, as more parts are grouped in each macro-region. The five variables are: local clothing thermal resistance, local clothing area factor, local clothing evaporative resistance, longwave emissivity, and shortwave absorbsion.

Table 5.4: *"Indian sari" clothing for the IESD-Fiala model.*

Body part	Thermal resistance [clo]	Area factor [-]	Evaporative resistance [m^2PaW^{-1}]	Longwave emissivity [-]	Shortwave absorbsion [-]
1. Head	0.00	0.00	0.00	0.00	0.00
2. Face	0.00	0.00	0.00	0.00	0.00
3. Neck	0.00	0.00	0.00	0.00	0.00
4. Shoulder	0.45	1.13	4.50	0.95	0.70
5. Thorax	0.98	1.27	4.50	0.95	0.70
6. Abdomen	1.80	1.50	4.50	0.95	0.70
7. Upper arm	0.00	0.00	0.00	0.00	0.00
8. Lower arm	0.00	0.00	0.00	0.00	0.00
9. Hand	0.00	0.00	0.00	0.00	0.00
10. Upper leg	1.91	1.53	4.50	0.95	0.70
11. Lower leg	1.12	1.31	4.50	0.95	0.70
12. Feet	0.41	1.11	4.50	0.95	0.70

The "Indian sari" option was specifically developed as part of this PhD research since the previously available clothing option covered only Western-like ensembles. The values used to define the "Indian sari" option were based on previous research by Indraganti et al. (2014b,a) on clothing insulation with different drapes of typical Indian sari ensembles. Within a range of nine possible ensembles, "En3" (Figure 5.5 and Table 5.5) was chosen since it is used in summer and it is quite symmetric. The latter aspect is important because the ISED-Fiala model does not allow to specify different clothing value for left and right arms and legs.

The values provided by Indraganti et al. (2014b) (Table 5.5) were translated into a set of values that can be used by the ISED-Fiala model (Table 5.4) making the following assumptions:

- Shoulder thermal resistance [clo] = mean of Shoulder_R and Shoulder_L
- Thorax thermal resistance [clo] = mean of Chest and Back
- Local area factor calculated according to ISO 9920 (ISO, 2007): $fcl = 1 + 0.28 * clo$
- Local clothing evaporative resistance is usually 0.004-0.005 m^2kPaW^{-1} for

mainly-cotton garments according to ISO 9920 (ISO, 2007). Thus, 0.0045 m^2kPaW^{-1}, that is 4.5 m^2PaW^{-1}, was used.

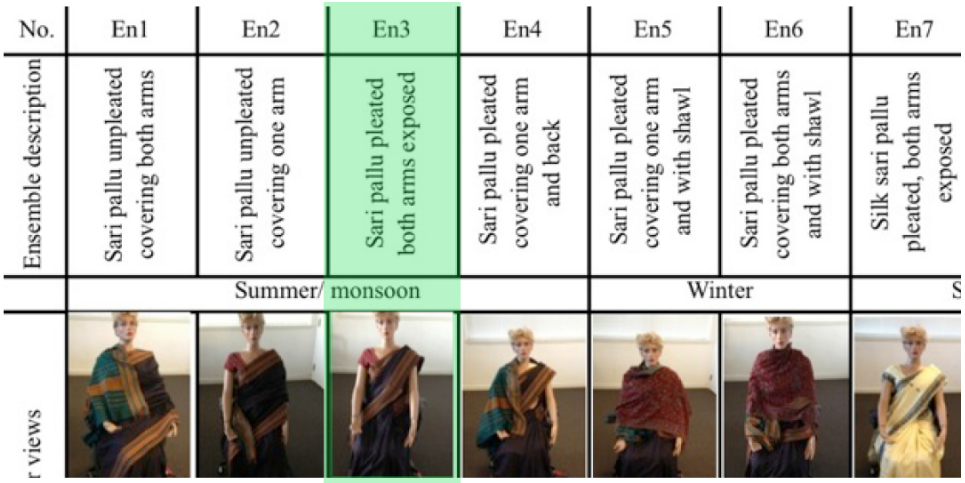

Figure 5.5: *Description of the ensembles tested by Indraganti et al. (2014b) (highlighted in green the ensemble used in this research to develop the "Indian sari" option).*

Table 5.5: *Clothing insulation values of the ensembles tested by Indraganti et al. (2014b) (highlighted in green the ensemble used in this research to develop the "Indian sari" option).*

Clothing ensemble	*BSAC (%)*	*Whole-body*	*Head*	*Chest*	*Back*	*Shoulder_L*	*Shoulder_R*	*Lower arm_L*	*Lower arm_R*	*Hand*	*Pelvis*	*Thigh*	*Lower leg*	*Foot*
Mesh Chair		0.03	0	0.05	0.14	0.01	0.03	0.01	0.03	0	0.02	0.11	0	0
BP	20	0.03	0	0.23	0	0	0	0.01	0.02	0	0.19	0.02	0	0
En1	81	0.96	0	1.9	1.23	1.58	1.07	0.56	0.4	0	2.01	0.75	0.98	0.33
En2	73	0.74	0	1.06	0.29	1.14	0.22	0.55	0.13	0	2.05	0.75	1.08	0.26
En3	65	0.65	0	1.5	0.45	0.73	0.17	0	0	0	1.8	1.91	1.12	0.41
En4	73	0.81	0	1.83	1.21	0.78	0.84	0	0.51	0	1.47	1.72	1.11	0.38
En5	81	1.11	0	2.71	1.94	1.75	1.29	0.84	0.69	0	1.99	1.92	1.09	0.38
En6	81	1.39	0	3.98	2.35	2.76	1.96	1.79	1.05	0	2.35	2.24	1.18	0.41
En7	65	0.62	0	1.32	0.51	0.85	0.25	0	0	0	1.58	1.62	0.95	0.25
En8	73	0.87	0	1.76	1.31	0.78	1.18	0	0.47	0	1.88	1.99	0.99	0.31
En9	81	0.94	0	1.58	1.35	1.15	1.08	0.57	0.49	0	1.83	1.84	0.97	0.27

5.2 Results and discussion

5.2.1 CFD results: air flow generated in the room by ceiling fans

The figures of the air speed recorded near the virtual manikins in the initial eight simulation scenarios are reported in Table 5.6. As explained in the methodology (section 5.1), in simulations 1 and 2 no fan was operating, thus, the air flow in the room was driven only by buoyancy. Due to the fact that the temperature of the surfaces and the air temperature were very similar, and close to the manikin average surface temperature, the air speed values recorded at all points are very low.

Table 5.6: *Air speed [m/s] recorded in each of the 12 monitoring points placed next to the virtual manikins - scenarios 1 to 8 (see Table 5.1 at page 118).*

Point	S1	S2	S3	S4	S5	S6	S7	S8
A low	0.01	0.02	1.28	1.27	0.81	0.79	0.90	0.88
A mid	0.02	0.01	0.33	0.30	0.21	0.22	0.48	0.43
A high	0.01	0.00	0.36	0.34	0.20	0.18	0.44	0.42
B low	0.02	0.02	1.25	1.19	0.67	0.66	0.75	0.81
B mid	0.01	0.01	0.31	0.31	0.20	0.20	0.46	0.44
B high	0.01	0.00	0.37	0.35	0.19	0.24	0.43	0.39
C low	0.02	0.02	1.26	1.21	0.92	0.91	1.00	1.00
C mid	0.01	0.01	0.45	0.43	0.22	0.22	0.59	0.57
C high	0.01	0.00	0.46	0.45	0.21	0.20	0.52	0.52
D low	0.02	0.01	1.07	1.02	1.06	1.03	1.12	1.11
D mid	0.01	0.01	0.28	0.28	0.18	0.19	0.41	0.42
D high	0.01	0.00	0.35	0.35	0.16	0.17	0.28	0.30

In simulations 3 and 4, only the fan (F1) (see Figure 5.3 at page 115) that is closer to both manikins was active. Firstly, the figures (Table 5.6) are almost identical regardless of which manikin (M1 or M2, see Figure 5.3 at page 115) was coupled with the ISED-Fiala model, and the small differences can be explained by the discretization error. Secondly, looking at the air speed figures, the highest values were recorded at low level (0.1 m above the floor) in each of the four locations (A, B, C and D), while the vales are significantly lower at mid and high level (0.6 and 1.1 m above the floor,

respectively). A direct comparison with the values measured in the environmental chamber at CEPT University and used to validate the CFD model of the ceiling fan is not possible due to the different locations of those measurement points in relation to the ceiling fan. However, the pattern is qualitatively similar, with higher values near the floor and lower speed at higher level. Moreover, since neither manikin is below the perimeter of the fan, the limited accuracy of the developed model in that narrow region (see Table 4.6 at page 99) does not affect this application of the developed model.

In simulations 5 and 6 (Table 5.6), only the other fan (F2) was active. The air speed pattern is again similar to what was measured in the full-scale experiment. At low level, the air speed is higher in location D (point "*D low*") since this is the closest to the active fan, while the lowest value was recorded at point "*B low*" due to the fact that air flow is hindered by one of the manikins. At higher levels, air speed was always low, around 0.2 m/s. In simulations 7 and 8 (Table 5.6), both ceiling fans were operating, increasing the complexity of the air flow. Compared with the other cases where only one fan (F1 or F2, but not both) was active, the most noticeable difference is a general increase in the air speed figures at mid and high level in all four locations.

As explained in the methodology (section 5.1), in the subsequent simulation scenarios from 9 to 23, the same four possible ceiling fan configurations were tested varying other parameters such as air temperature and relative humidity. In these 15 simulations, the coupled manikin was always M2. Figure 5.6 can be used as a reference to better understand the following Figures 5.7 to 5.12, which provide a visual representation of the air flow field around the manikin in the different ceiling fan configurations. Simulation 10 has the same ceiling fan configuration as simulations 3 and 4, and indeed air was blowing from the fan (F1) on the left-hand side of the manikin (Figure 5.8), while no air was blowing from the other fan (Figure 5.7). As in simulations 5 and 6, the opposite fan configuration was tested in simulation 11. Air

was flowing from F2 (Figure 5.9), but not from the other ceiling fan (Figure 5.10). Simulation 12 is then an example of a scenario in which both fans were active at the same time. As shown in Figures 5.11 and 5.12, air is blowing from both directions, and air speed at torso level is higher than in the other two cases in which only one fan was operating.

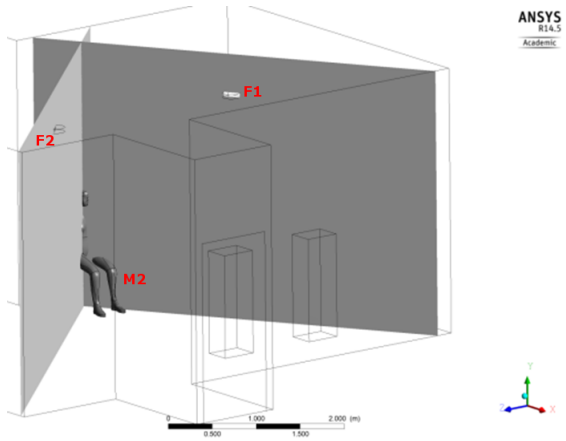

Figure 5.6: *Three-dimensional view of the model with the two planes used to show the air speed field in Figures 5.7 to 5.12.*

Although the thermal comfort results will be illustrated in the next section, these CFD results offer a first opportunity for reflection. According to international standards on thermal comfort (ASHRAE, 2013a; ISO, 2005), air speed should be measured at three levels near the person. However, in the PMV calculation, only one air speed value is supplied as an input to the model. When the three measured values are similar, using a simple average is likely to be the best solution. On the other hand, when there are significant differences, such as in the case of air movement generated by ceiling fans, the solution is less obvious. Using an average value might still be acceptable. However, the thermal sensation might be more influenced by the most elevated air speed value, or by the air hitting a naked and more sensitive part of the human body such as the back of the neck. This problem is an example of how the coupled system used in this research has advantages over the PMV model. Because 59 air speed values are supplied to IESD-Fiala model from the CFD model, there is no need for questionable assumptions to be made.

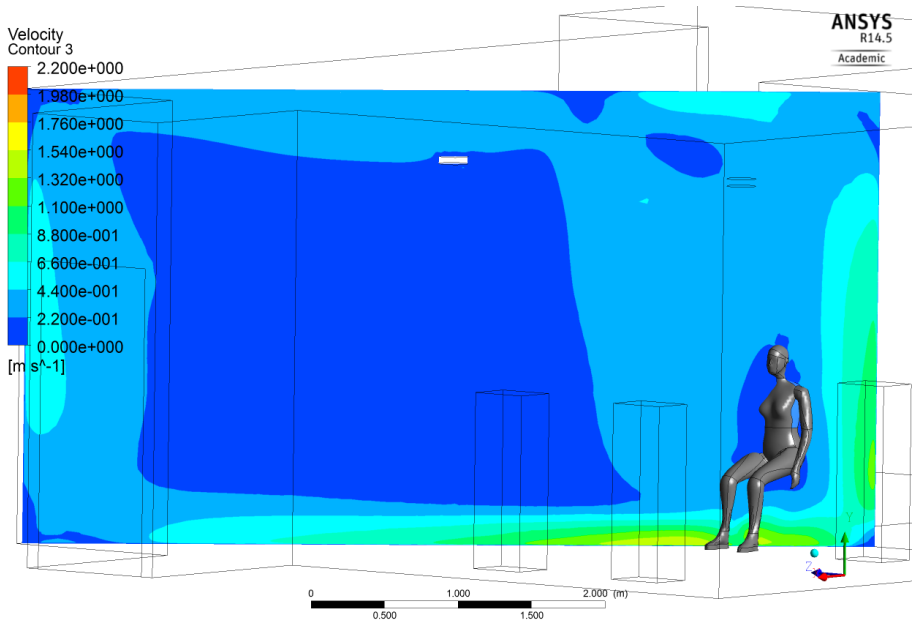

Figure 5.7: *Air speed field - plane passing for F2 (OFF - simulation 10) and M2.*

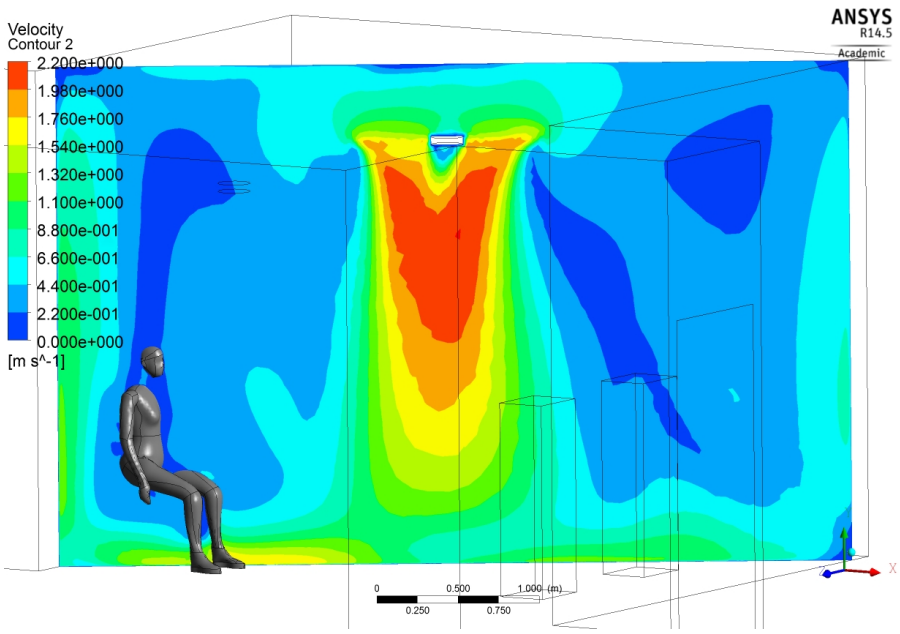

Figure 5.8: *Air speed field - plane passing for F1 (ON - simulation 10) and M2.*

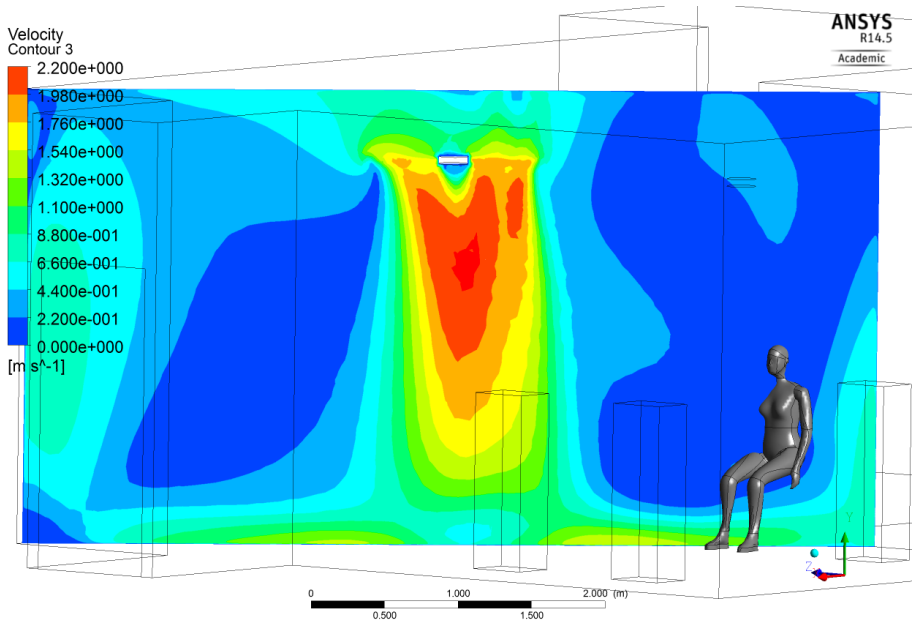

Figure 5.9: *Air speed field - plane passing for F2 (ON - simulation 11) and M2.*

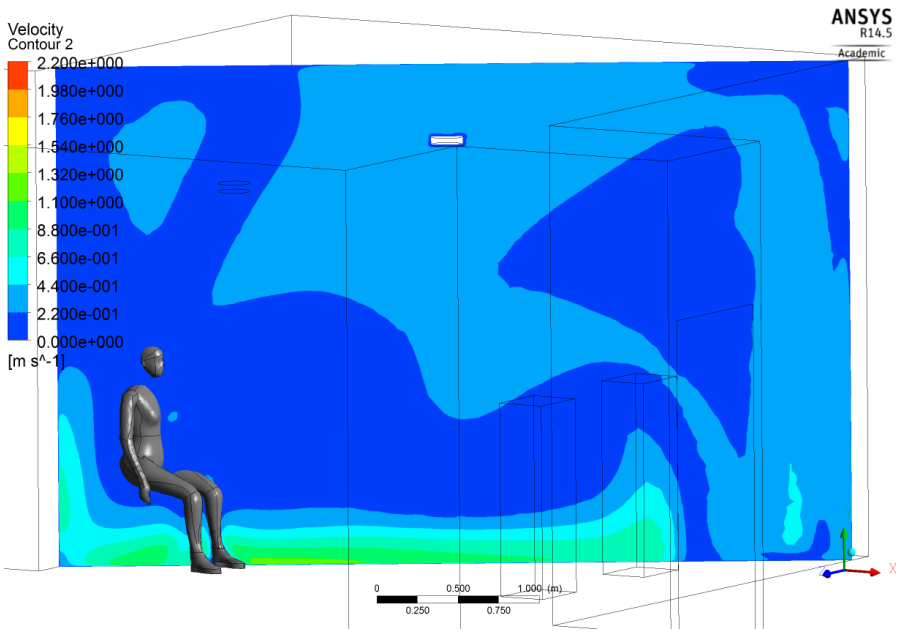

Figure 5.10: *Air speed field - plane passing for F1 (OFF - simulation 11) and M2.*

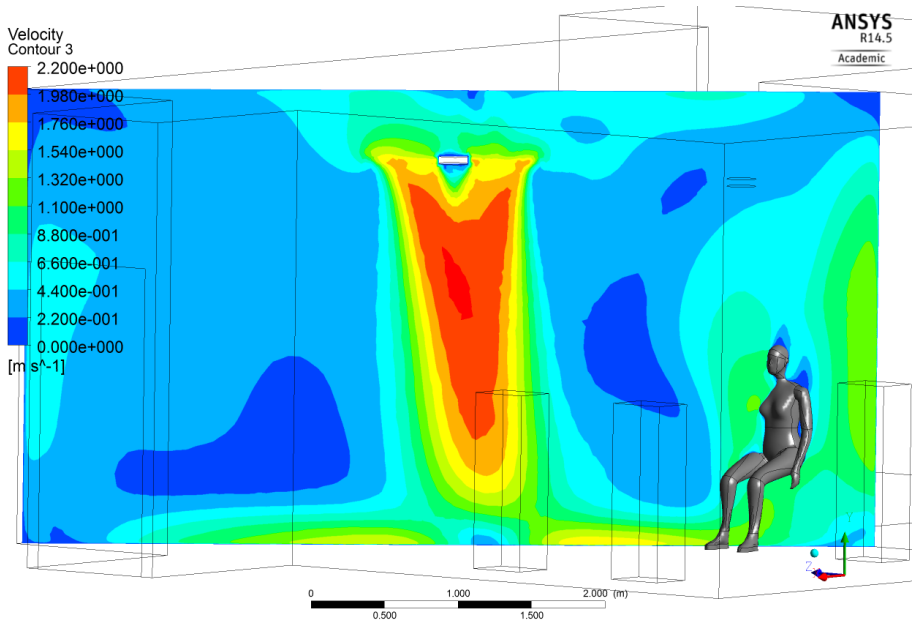

Figure 5.11: *Air speed field - plane passing for F2 (ON - simulation 12) and M2.*

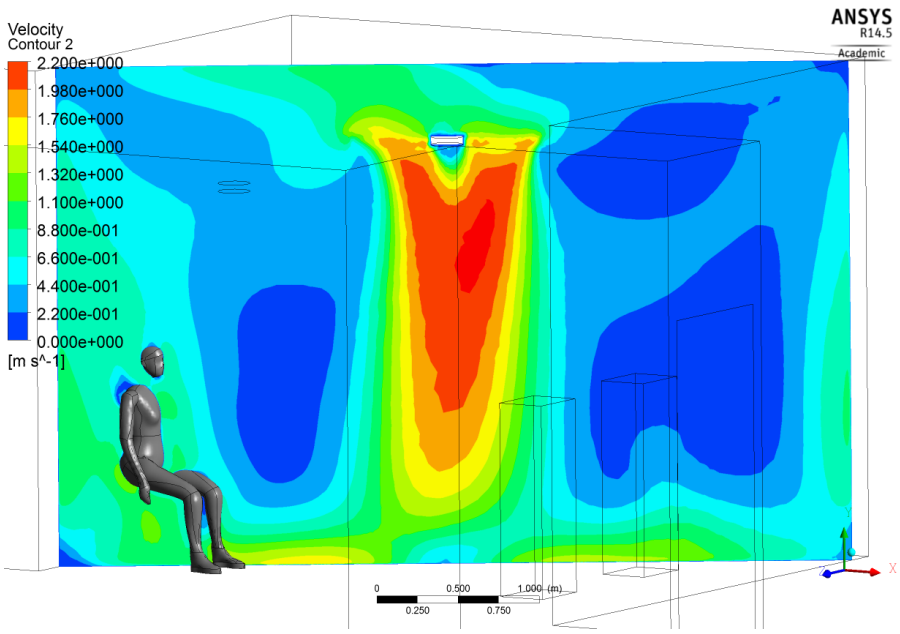

Figure 5.12: *Air speed field - plane passing for F1 (ON - simulation 12) and M2.*

5.2.2 Thermal comfort results

Thermal comfort results are presented in the following three sections, whose aim is to compare the IESD-Fiala model predictions with actual thermal sensation votes reported in the literature (section 5.2.2), to show the effect of different temperature and relative humidity on the IESD-Fiala model predictions (section 5.2.2), and to highlight the sensitivity of these predictions to metabolic rate, clothing and pre exposure time variations (section 5.2.2), respectively.

Comparison between DTS and actual thermal sensation votes reported in the literature (Scenarios 1 to 8)

The DTS in the first eight simulation scenarios is illustrated in Figures 5.13 and 5.14. In the former (Figure 5.13), the full 7-point ASHRAE thermal sensation scale from -3 to +3 has been used in order to be able to immediately see in which thermal sensation band the subject is (e.g. warm, cool, etc.) and to able to compare cases that have very different DTS results. In order to be able to distinguish between the outputs of each simulation and to focus on the details, in the latter (Figure 5.14), the same DTS figures have also been reported using an enlarged scale on the vertical axis. The same approach has then been used throughout this chapter to allow for both direct inter-scenario comparison and analysis of the small variations.

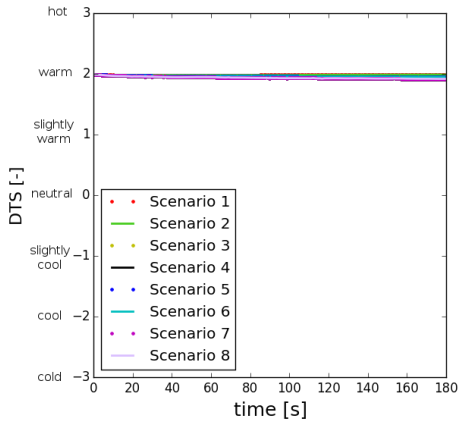

Figure 5.13: *DTS in the first eight simulation scenarios (y-axis: full 7-point thermal sensation scale from -3 to +3).*

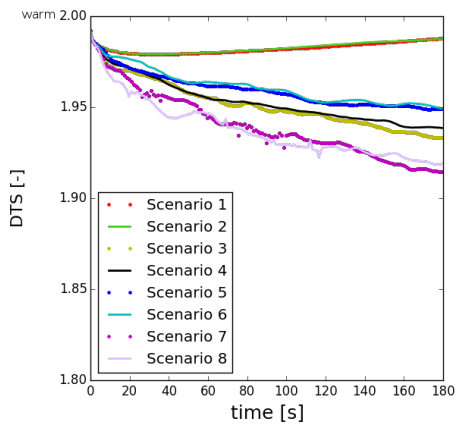

Figure 5.14: *DTS in the first eight simulation scenarios (y-axis: enlarged scale).*

The analysis of the thermal comfort results in these eight scenarios, whose key metric is the DTS, offers the opportunity to make some initial considerations on the coupled system developed, and on its capabilities defined as the capability of the model of providing realistic results.

Firstly, these results suggest that there is no noticeable difference between the two virtual subjects, represented by the computational manikins placed in position M1 and M2. As shown earlier in this chapter, the air speed near them assumes similar figures, and therefore it was likely that the two DTS outputs were very close.

Secondly, the results are in agreement with what could have been expected based on which ceiling fan was active and the distance between fan and manikin. In simulations 1 and 2, where no fan was active, the DTS increases during the simulation. On the other hand, it decreases in all other cases. In simulation 7 and 8 both ceiling fans were operating, and indeed the DTS is lower than in any other case. In simulations 3 and 4, only the fan that is closer to both manikins was active, and indeed the DTS is lower than in simulations 5 and 6, where only the other ceiling fan was blowing air.

Thirdly, the effect of air movement on the DTS is very limited in all six cases in which at least one fan was active, suggesting that, under these environmental con-

ditions, using a ceiling fan was not an effective solution to improve thermal comfort. This is due to the significantly elevated air temperature and mean radiant temperature, and it is in good agreement with previous research. In a study about the demand for air movement in warm environments (Huang et al., 2013), it was noticed that 34°C was out of the suitable application range of fans. In other words, when the air temperature is equal to 34°C or higher, air movement does not provide with any benefits regardless the higher or lower air speed. Based on these simulation results, it can be concluded that the coupled system accurately represents this real phenomenon.

Lastly, the simulated DTS is nearly 2 (that means "warm") on the 7-point ASHRAE thermal sensation scale, while the actual thermal sensation vote as reported by Indraganti (2010c) under the same environmental conditions is 1.8. Since this is a mean value calculated based on hundreds of responses from participants, and DTS assumes an average person, then the coupled system met its aim, proving to be accurate not only about the effect of air movement on thermal comfort, but only on the overall thermal sensation vote. Moreover, the calculated DTS value is much more realistic than the Fanger PMV, which is 3.9 as calculated by Indraganti (2010c).

Thus, in relation to the research hypothesis, the results of the first eight simulations showed that the coupled system gives accurate and realistic thermal comfort predictions in warm conditions and in the presence of air movement, being in this regard superior to the traditional PMV model. As stated in section 1.2, the key criterion to say whether the coupled system is superior to the traditional models is indeed to verify whether its predictions, compared with the values calculated by traditional models, are closer to the actual votes of participants.

The effect of different temperature and relative humidity on DTS (Scenarios 9 to 20)

The DTS calculated by the IESD-Fiala model for simulation scenarios 9 to 16 is reported in Figures 5.15 to 5.18. In all graphs presented in this section, the green

line refers to the no-active-fan condition, the blue line to the most-distant-active fan condition (thus, only F2 was active), the black line to the nearest-active fan condition (thus, F1 was active), and the pink line to the both-active fan condition (thus, both F1 and F2 were active).

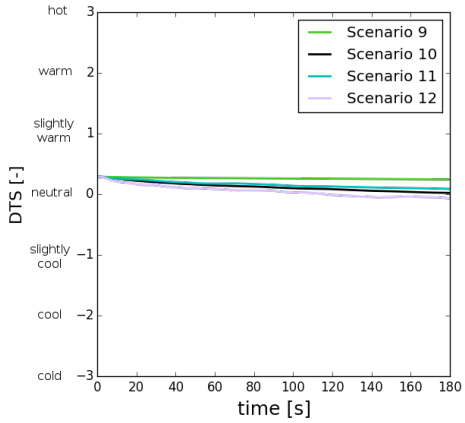

Figure 5.15: *DTS in scenarios 9 to 12: $T_{air} = MRT = 30.0°C$, RH = 30% (y-axis: full 7-point thermal sensation scale from -3 to +3).*

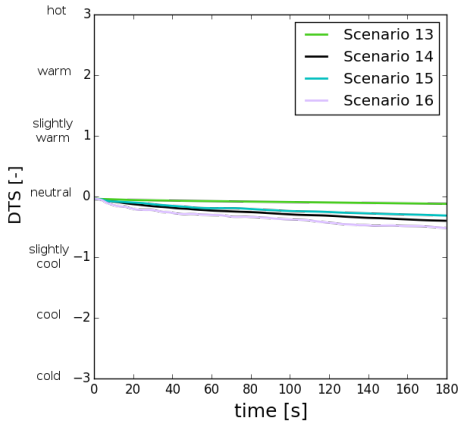

Figure 5.16: *DTS in scenarios 13 to 16: $T_{air} = MRT = 28.0°C$, RH = 30% (y-axis: full 7-point thermal sensation scale from -3 to +3).*

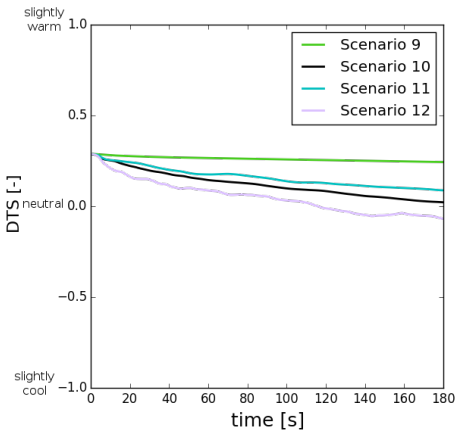

Figure 5.17: *DTS in scenarios 9 to 12: $T_{air} = MRT = 30.0°C$, RH = 30% (y-axis: enlarged scale).*

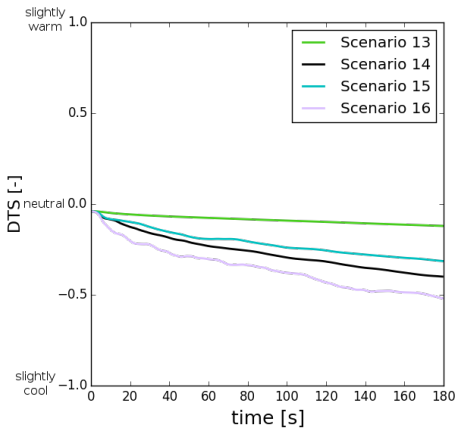

Figure 5.18: *DTS in scenarios 13 to 16: $T_{air} = MRT = 28.0°C$, RH = 30% (y-axis: enlarged scale).*

In the 28-30°C temperature range, the DTS is almost stable during the simulated period when no air moment was available (simulations 9 and 13), while it decreases in all other cases (Figure 5.17 and 5.18). However, the effect of air movement on

the thermal sensation is higher at 28°C (Figure 5.18) than at 30°C (Figure 5.17). In the former case, the DTS fell by up to 0.5 point (simulation 16), while in the latter there is only an up to 0.25 point reduction (simulation 12). Most importantly, at the end of the simulated period, the DTS in simulations 12 and 13 is almost identical. In scenario 13, no fan was operating and the temperature was 28°C. In scenario 12, two fans were operating and the temperature was two degrees higher, being equal to 30°C. Thus, the model shows that the set-point temperature can be increased without jeopardising human thermal comfort by using ceiling fans, but also it shows which is the most effective ceiling fan configuration.

The coupled system, via the IESD-Fiala model, proved to be less sensitive to relative humidity variations than to temperature variations. Keeping the temperature at 30°C, the relative humidity was increased from 30% to 50% (Figure 5.19 and 5.20). Comparing the DTS in these two relative humidity conditions (Figure 5.17 with Figure 5.20), the results at the end of the simulated periods are fairly similar. At 50% relative humidity, the DTS dropped quicker than at 30% relative humidity in the first part of the simulated period, and it is slightly higher in all four possible fan configurations at the end of the simulations. However, the difference with the drier scenarios is negligible.

Thus, this group of simulation scenarios showed the sensitivity of the DTS to temperature and relative humidity variations under the different possible fan configurations, highlighting that the coupled system, via its thermal comfort component, is more sensitive to temperature than to relative humidity variations within the range of warm conditions tested in this study.

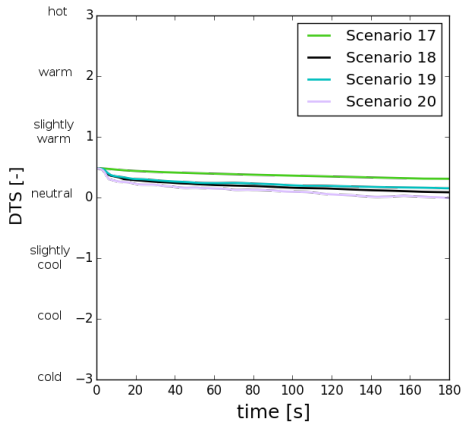

Figure 5.19: *DTS in scenarios 17 to 20: $T_{air} = MRT = 50.0°C$, RH = 30% (y-axis: full 7-point thermal sensation scale from -3 to +3).*

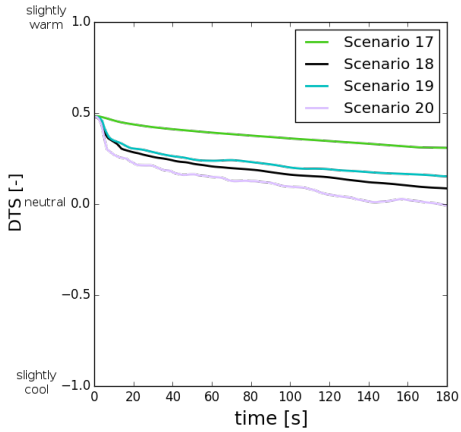

Figure 5.20: *DTS in scenarios 17 to 20: $T_{air} = MRT = 30.0°C$, RH = 50% (y-axis: enlarged scale).*

The effect of metabolic rate, clothing and pre exposure time on DTS (Scenarios 21 to 23)

Considering the environmental boundary conditions, scenarios 21 to 23 are based on scenario 10, which means temperature (air temperature and mean radiant temperature) equal to 30°C, relative humidity equal to 30%, and only one active fan (F1). In other words, the initial boundary conditions in the CFD model are identical in these four cases, since, as explained in the methodology (section 5.1), metabolic rate, clothing and pre exposure time are specified only within the IESD-Fiala model.

In the following paragraphs, the analysis of the thermal comfort results starts with the scenarios characterised by a different metabolic rate (simulation 21), and a different pre exposure time (simulation 23), respectively. It then focuses on the scenario in which a different clothing option was tested (simulation 22). The reasons for this order are that, firstly, this third variation (clothing) had a larger effect on the DTS than the other two (metabolic rate and pre exposure time), and, secondly, the clothing affects the surface of the virtual manikin. Since the two components of the coupled system, namely the CFD software and the IESD-Fiala model are linked via the 59 parts of the body surface, a more accurate analysis of the phenomena affecting

this element is essential.

Within this range of environmental conditions, the impact of a different pre exposure time (simulation 23) on the DTS is negligible, while the model is more sensitive to a different metabolic rate (simulation 21) (fig. 5.21 and 5.22). In both these cases, the difference depends on the algorithm used by the IESD-Fiala model.

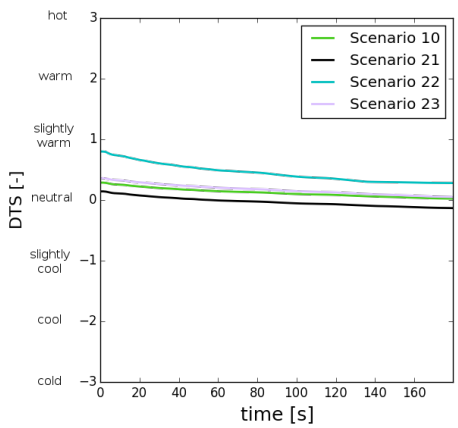

Figure 5.21: *DTS in scenarios 10 and 21 to 23: T_{air} = MRT = 30.0°C, RH = 30% (y-axis: full 7-point thermal sensation scale from -3 to +3).*

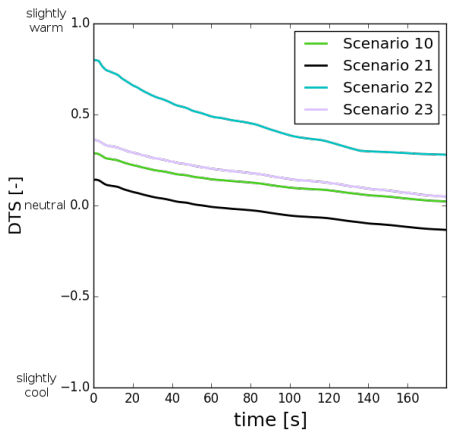

Figure 5.22: *DTS in scenarios 10 and 21 to 23: T_{air} = MRT = 30.0°C, RH = 30% (y-axis: enlarged scale).*

As said earlier, the biggest difference is noted when a different clothing option is used (simulation 22). This is also the most interesting and relevant aspect since the two components of the coupled system, namely CFD and IESD-Fiala model, are linked through the surface of the virtual manikin. For this reason, this difference can be explained by looking at the virtual manikin surface temperature in both cases. It is important to highlight that the temperature fields displayed within the CFD model on each part of the body surface are the values of the outermost layer. In the naked parts such as the face, this is the skin temperature. In the covered areas, this is the external temperature of the relative garment. When the sari option is used (Figure 5.23), the temperature of upper part of arms and legs, of the torso and of the feet is clearly more elevated than when the other clothing option is used (Figure 5.24). Air permeability is not one of the parameters used to the define the clothing within the

IESD-Fiala model (see Table 5.4 at page 121). Therefore, a possible explanation for this difference is that the Indian sari simply allows for a better dissipation of the heat produced by the human body.

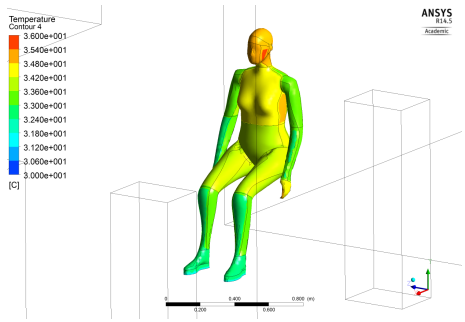

Figure 5.23: *Virtual manikin surface temperature - Indian sari.*

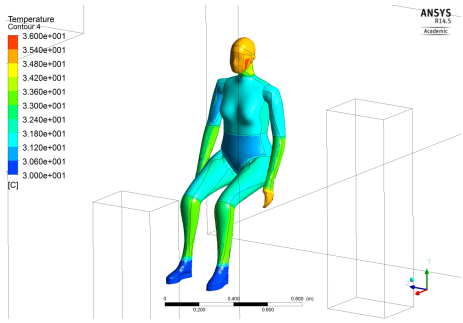

Figure 5.24: *Virtual manikin surface temperature - Western summer clothing.*

5.2.3 Required computational power

The required computational power is a key element in relation to the usability of the coupled system, and it sets the limit for the number of configurations that can be tested and for the choice of the total simulated period of time.

Simulations were run on the High Performance Computer System at Loughborough University, a 2460-core 64-bit Intel Xeon cluster. 12 or 20 cores were used in these simulations (Table 5.7) in order to make efficient use of the cluster architecture. In theory, the larger the number of cores is, the shorter the time required to achieve a converged solution becomes. However, there is no simple linear relationship between number of cores and CPU time for two reasons. Firstly, at the very beginning of each run, a certain amount of time is required to split the job among the different cores, and this increases with the number of cores. The second point is that a single core of the 20-core nodes is faster than a single core of the 12-core nodes. This applies only to this particular High Performance Computer System, and it means that 20-core nodes not only have more cores, but also that their basic components are more powerful.

Table 5.7: *Duration of the simulations*

Scenario ID	Number of cores	CPT time
1	12	07 h, 52 m
2	12	08 h, 04 m
3	12	1 d, 13 h, 25 m
4	12	1 d, 12 h, 00 m
5	12	1 d, 06 h, 58 m
6	12	1 d, 10 h, 28 m
7	12	1 d, 21 h, 58 m
8	12	1 d, 23 h, 22 m
9	20	14 h, 55 m
10	20	14 h, 51 m
11	20	16 h, 00 m
12	20	1 d, 02 h, 25 m
13	20	15 h, 28 m
14	20	15 h, 36 m
15	20	15 h, 55 m
16	20	1 d, 02 h, 46 m
17	20	14 h, 52 m
18	20	14 h, 43 m
19	20	16 h, 07 m
20	20	1 d, 02 h, 25 m
21	20	14 h, 46 m
22	20	14 h, 33 m
23	20	14 h, 45 m

In this research, 12 or 20 cores were used depending exclusively on the availability of licences and nodes. The CPU time ranges from nearly eight hours to almost two days depending on the complexity of environmental conditions and on the number of cores used (Table 5.7). The sum of these 23 CPU time is 510.37 hours, that is 21 days, 6 hours and 22 minutes. This is a significant amount of time, that could have been only slightly reduced if all simulations would have been performed using 20-core nodes. Pre- and post- processing were done using the same computers used for the same purpose in the CFD studies presented in the previous chapters.

5.3 Summary

This chapter illustrates the results obtained using the coupled system to investigate how the use of ceiling fans affects human thermal comfort in real residential buildings in India. Having developed and validated the CFD model typical Indian ceiling fan, the coupled system was used to model a typical Indian drawing room. In total, 23 scenarios were modelled varying the environmental conditions (air temperature, mean radiant temperature, and relative humidity), the status (on/off) of the fans, the position of the coupled manikin (and therefore the distance between fan and this manikin), the metabolic rate, the clothing, and the pre-exposure time (the time in which the person was exposed to the same environmental conditions before running the test).

In this chapter, there is no direct comparison of measured and simulated air speed values because the key component of the CFD model, namely the ceiling fan, was fully validated in the previous chapter. Moreover, other elements, such as the mesh requirements near the surface of the virtual manikin and the sensitivity of the dynamic thermal sensation to slight variations of the air speed hitting the victual manikin, had been investigated in the initial testing and validation of the coupled system. Therefore, the focus of this chapter is on the thermal comfort results generated in these real residential configurations in India.

The analysis of the results begins with the description of the air flow generated by one or more ceiling fans around the virtual manikin. When all fans were switched off, the simulated air speed values were very low in all monitored points within the room, as expected in a buoyancy driven flow (especially if air temperature, surfaces' temperature, and manikin's surface temperature were all very similar). When only one fan was active, regardless of which fan active, the air flow pattern is qualitatively similar to the pattern described in the previous chapter (entirely dedicated to the ceiling fan CFD model), with higher values near the floor (0.1 m above the floor) and lower speed at higher level. A direct numerical comparison between the simulated

values presented in this chapter and the measured values used in the previous chapter is not possible since the monitoring points were placed in different locations within the model. When two fans were operating at the same time, the most noticeable difference was a general increase in the air speed figures at mid (0.6 m above the floor) and high (1.1 m above the floor) level in all locations.

The thermal comfort results of the first eight simulations showed that the coupled system accurately modelled the effect that the air movement generated by the ceiling fans has on the occupants. Without the use of fans, in warm conditions the dynamic thermal sensation increased during the simulated period. When ceiling fans were operating, the dynamic thermal sensation decreased during the simulated period in all scenarios tested. Moreover, the shorter the distance between fan and manikin was, the higher the effect of the elevated air speed was. Similarly, the simultaneous use of two fans led to a further reduction, and therefore to higher thermal comfort.

The environmental boundary conditions such as temperature and relative humidity used in these first eight simulations were taken from published field studies on Indian dwellings. In agreement with actual thermal sensation votes reported by participants, the coupled system predicted that air movement has little impact on human thermal comfort if the air temperature is above 34°C. Moreover, the simulated dynamic thermal sensation is nearly +2 on the 7-point ASHRAE thermal sensation scale, while the actual thermal sensation vote as reported in previous studies under the same environmental conditions is +1.8. Thus, the coupled system gives accurate and realistic thermal comfort predictions in warm conditions and in the presence of air movement, being in this regard superior to the traditional PMV model.

The second group of simulations evaluated scenarios characterised by lower temperature and higher relative humidity, and showed that the set-point temperature of the air conditioning can be increased without jeopardising human thermal comfort by using ceiling fans to generate elevated air movement, but also highlighted which is the most effective ceiling fan configuration. Moreover, this set of results showed that

the coupled system, via the IESD-Fiala model, is less sensitive to relative humidity variations than to temperature variations.

There are three parameters that are set only in the IESD-Fiala model, namely the metabolic rate, the clothing, and the pre exposure time (the time in which the person was exposed to the same environmental conditions before running the test). The results of the last group of simulations highlighted that, within the warm conditions tested in this study, the dynamic thermal sensation is much more influenced by the clothing than by the other two. This research showed that two ensembles with similar overall clo value, but different distribution of the garments on the body parts, lead to very different prediction of the human thermal sensation. This is another aspect in which the coupled system is superior to the PMV model, where only the overall clo value is used as input parameter.

Lastly, simulations were run on the High Performance Computer System. The number of cores used ranged from 12 to 20, and the total CPU time from 8 hours to 2 days (the simulated time was 3 minutes in all simulations). The actual total CPU time of each simulation depended on the level of complexity of the simulated environments (for instance, scenarios in which two fans are active are more complex, and therefore the simulated time is higher). In general, the elevated computational power required to run this model is compensated by the quality of the results obtained.

Chapter 6

ESTIMATE OF THE POTENTIAL ENERGY SAVINGS IN A TYPICAL INDIAN HOUSE

The aim of this part of the work was to develop and test a new methodology based on the adaptive theory to quantify the energy savings achievable in mixed mode buildings due to air movement. In other words, assuming that people can be kept thermally comfortable in non-uniform warm thermal environments using air movement, this chapter answered two questions. How much energy can be saved if the cooling set point temperature is increased due to the simultaneous usage of fans? Which is the most accurate method to make this estimate? Thus, in this chapter, there is no direct test of the research hypothesis, but there is evidence to say that the additional technical and computational effort required to use the coupled model is justified because the benefit (in terms of energy savings) achieved by creating non-uniform, but thermally comfortable, environments is noticeable.

6.1 Methodology

In this study, computer simulations have been used to test the new methodology, and the analysis focused on the energy demand for space cooling and the indoor environmental conditions predicted using this methodology. The core of this methodological approach is the way in which the cooling set-point is defined. The proposed method has been initially applied to an apartment in Ahmedabad, India, which is a typical example of a mixed mode building with ceiling fans. The analysis has then been extended to other locations to include the full range of Indian climatic conditions.

6.1.1 Cooling set-point definition

Indian Model of Adaptive Comfort (IMAC) (Manu et al., 2016) was specifically developed from Indian data, but its equations implicitly incorporate the effect of air speed. Thus, using this model for estimating the energy savings due to the use of fans is not possible. The ASHRAE (ASHRAE, 2013a) adaptive model was therefore used in this study.

According to ASHRAE 55-2013 (point 5.4.1 (ASHRAE, 2013a)), the adaptive model is applicable when all the following conditions are met:

a) There is no mechanical cooling system installed. No heating system is in operation

b) Metabolic rates range from 1.0 to 1.3 met

c) Occupants are free to adapt their clothing to the indoor and/or outdoor thermal conditions within a range at least as wide as 0.5-1.0 clo

d) The prevailing mean outdoor temperature is greater than 10°C and less than 33.5°C

Considering the Ahmedabad climate and the Indian typical domestic environment, all conditions are met, with the partial exception of the first condition for the case

of a mixed mode building. However, based on recent previous works by Indraganti (2010b) and Manu et al. (2016), in this study it has been assumed that the ASHRAE adaptive model is applicable also if air conditioning is available.

Moreover, the acceptable operative temperature limit in occupant-controlled spaces can be increased by 1.2°C 1.8°C and 2.2°C due air speed equal to 0.6 m/s, 0.9 m/s and 1.2 m/s, respectively (ASHRAE 55-2013, Table 5.4.2.4 (ASHRAE, 2013a)). In warm and hot conditions, an elevated air speed can improve the thermal sensation of the occupants, rather than being cause of an undesired draught.

In this research, for a chosen mixed mode building in which there are also fans, a dynamic thermal model was created. In the initial simulation, the cooling set-point for temperature was varied monthly according to the ASHRAE 55-2013 adaptive model, considering the 90 per cent acceptability upper limits. In the subsequent three simulations, these monthly set-points were increased according to ASHRAE 55-2013 for air speeds up to 1.2 m/s.

The Ahmedabad weather file used in this study to calculate the monthly cooling set-point (Table 6.1) was created by ISHRAE in Typical Meteorological Year 2 (TMY2) format for use with building energy performance simulation programs (EnergyPlus weather data, 2016). T_{comf} comfort temperature, which is neutral operative temperature where the lowest total percentage of people are expected to be either too hot or too cold (Borgeson and Brager, 2011), and $T_{max(90\%)}$ 90 per cent temperature upper limit, are calculated based on T_m monthly arithmetic mean of the daily average outdoor dry bulb temperatures:

$$T_{comf} = 17.88°\mathrm{C} + 0.31 \times T_m \tag{6.1}$$

$$T_{max(90\%)} = T_{comf} + 2.5°\mathrm{C} \tag{6.2}$$

Table 6.1: *Dynamic cooling set-point*

	JAN	FEB	MAR	APR	MAY	JUN
T_m	20	22	27	31	33	32
T_{comf}	24.0	24.6	26.2	27.4	28	27.7
$T_{max(90\%)}$	26.5	27.1	28.7	29.9	30.5	30.2
$T_{maxAirSpeed(0.6m/s)}$	27.7	28.3	29.9	31.1	31.7	31.4
$T_{maxAirSpeed(0.9m/s)}$	28.3	28.9	30.5	31.7	32.3	32
$T_{maxAirSpeed(1.2m/s)}$	28.7	29.3	30.9	32.1	32.7	32.4
	JUL	AUG	SEP	OCT	NOV	DEC
T_m	29	28	29	28	25	20
T_{comf}	26.8	26.5	26.8	26.5	25.6	24.0
$T_{max(90\%)}$	29.3	29	29.3	29	28.1	26.5
$T_{maxAirSpeed(0.6m/s)}$	30.5	30.2	30.5	30.2	29.3	27.7
$T_{maxAirSpeed(0.9m/s)}$	31.1	30.8	31.1	30.8	29.9	28.3
$T_{maxAirSpeed(1.2m/s)}$	31.5	31.2	31.5	31.2	30.3	28.7

6.1.2 Dynamic cooling set-point implementation

Once the four sets of monthly cooling set-points were calculated (Table 6.1), these were implemented in DesignBuilder/EnergyPlus using an advanced feature called Energy Management System (EMS), which is available in DesignBuilder from the recently (September 2016) realised version 5 (EMS, 2016).

In EMS, a simple programming language called EnergyPlus Runtime Language (Erl) is used to describe the control algorithms. EnergyPlus interprets and executes the Erl program as the model is being run (EMS Application Guide, 2016).

In this study, an Erl script has been written to specify a different cooling set-point per month using an IF and ELSEIF structure. Erl currently supports up to 199 ELSEIF statements, which means that by using Erl the cooling set-point could not be changed every day of the year as would be required by the IMAC or EN15251 adaptive model. This is the technical reason why the ASHRAE adaptive model was chosen in this study rather than IMAC.

Four scripts have been developed, one for each simulation. These were used only to specify the set-point value, while the ON/OFF control strategy has been defined in DesignBuilder.

6.1.3 The case study building

The dynamic cooling set-point method has been tested on a typical Indian apartment, this being one of the apartments in the international project on thermal comfort and air movement in residential buildings (Loveday et al., 2016) which has already been mentioned earlier in this thesis (section 4.1). The project involves UK, Indian, and American partners.

This apartment (Figure 6.1) has a floor surface area of 145 m^2, internal height 3.2 m, and is surrounded by other apartments above, below, and to the side. Thus, ceiling, floor and party-wall have been assumed to be adiabatic (Figure 6.2). Typical construction elements of the Ahmedabad region have been used (Table 6.2, and Figure 6.3, 6.4 and 6.5). Due to the hot climate, there are no insulation layers, all windows have single glazing, and there is no heating system installed. The balconies have been added in DesignBuilder to simulate shading effect, and the internal doors have been assumed to be opened 50 per cent of the time.

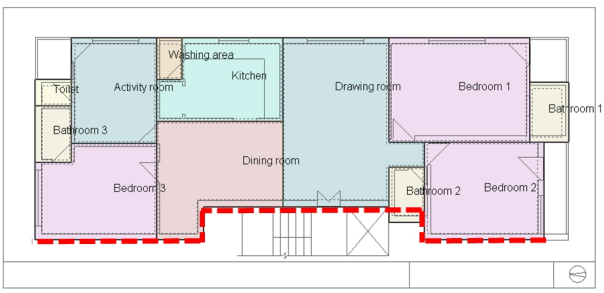

Figure 6.1: *Floor plan (the red dashed line indicates an adiabatic party-wall).*

Figure 6.2: *Schematic section view (the red dashed line indicates adiabatic surfaces).*

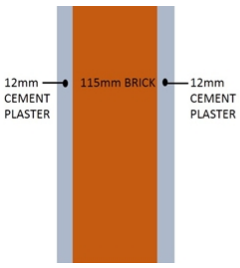

Figure 6.3: *Internal wall.*

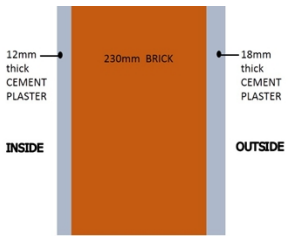

Figure 6.4: *External wall.*

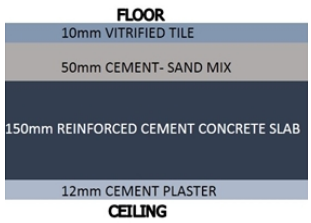

Figure 6.5: *Floor and ceiling.*

Physical partitions have been used to create a zone for each room of the apartment, and an additional virtual partition has been placed between the dining room and the drawing room. Although this is a unique open space, the former is used for having meals, while the latter is a living room. Therefore, their use is significantly different.

Table 6.2: *Characteristics of construction elements*

Element	Layers	U-value [W/m$_2$K]
Internal partitions	12 mm cement plaster 115 mm brick 12mm cement plaster	1.98
External walls	From inside: 12mm cement plaster 230mm brick 18mm cement plaster	1.59
Ceiling and floor	From the top: 10mm vitrified tile 50mm cement – sand mix 150mm reinforced cement concrete slab 12mm cement plaster	2.17

Since the aim of this work was to model a typical house, the occupancy schedule and relative internal heat gains have been chosen from the available standard templates based on the type of each room.

Within DesignBuilder, the chosen method for natural ventilation is "calculated", which uses the EnergyPlus AIRNET method to calculate the ventilation rates using wind and buoyancy-driven pressure, openings' size and operation, and crack sizes. This option slows the simulation down, but it is preferable if a reasonable estimate of the natural ventilation rates and infiltration rates in the building is not available (EnergyPlus documentation, 2016). The "medium" crack template was used.

The "mixed-mode" option has also been selected, and, for any given cooling set-point temperature, the air conditioning system was ON if:

a) The space was occupied

b) The indoor air temperature was above set point temperature

c) The outdoor air temperature was above indoor air temperature

Moreover, the air-conditioning was installed only in two rooms, namely "bedroom 1" and "bedroom 2". In an on-going field study (Loveday et al., 2016), the author has observed that in Indian apartments there is often air conditioning only in a few rooms, not everywhere in the house. Within DesignBuilder, the modelled system is a typical residential mini-split system, whose coefficient of performance is 4.5. This type of air conditioners dominates air conditioner sales in most parts of the world including Asia and Europe (Shah et al., 2013).

In order to compare E_{nofan} energy demand for space cooling of the first simulation and the values of the subsequent three $E_{withfan}$, the energy used by the fan must also be taken into account. Considering that a higher set-point could have been chosen due to the use of a fan, n total number of hours in which this was ON in the subsequent three simulations must be equal to the total number of cooling hours in the first simulation. The fan energy consumption E_{fan} is obtained by multiplying n for the average power of the fan, which for a typical Indian ceiling fan is 50W (BEE, 2016):

$$E_{fan} = n \times 50W/1000 \tag{6.3}$$

Since the air conditioning is available in two rooms, in a real scenario two fans may be operating at the same time, doubling E_{fan}. Therefore, this second possible scenario was also considered.

This value is then added to E_{AC} energy used by the air conditioning system:

$$E_{withfan} = E_{AC} + E_{fan} \tag{6.4}$$

The energy savings achievable using ceiling fans are therefore:

$$E_{savings} = E_{nofan} - E_{withfan} \tag{6.5}$$

Both air temperature and operative temperature set-points have been simulated to assess savings' benefits using both approaches.

6.1.4 Extension of the analysis to other locations in India

In order to select other appropriate locations in India, the first step was the analysis of the Indian climate. According to the Indian Energy Conservation Building Code (ECBC, 2009), the different climates that are present in India can be categorised into five groups (Figure 6.6) which are usually called "hot and dry", "warm and humid", "composite", "temperate", and "cold", respectively.

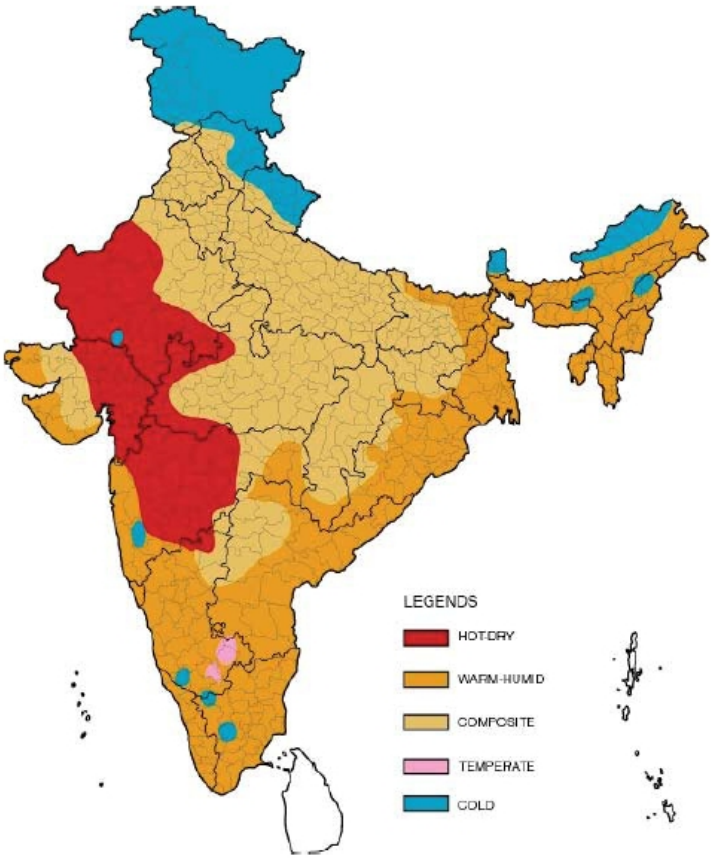

Figure 6.6: *Map of Indian climatic regions (ECBC, 2009).*

The "hot and dry" region is characterised by high temperatures (up to 45°C at midday in summer), low humidity (25-40%) and rainfall (less than 500mm/year), intense solar radiation and a generally clear sky, and hot winds during the day and cooler wind at night (ECBC, 2009).

In the "warm and humid" region (ECBC, 2009), the temperature is moderately high during day and night (30 to 35°C), both humidity and rainfall are extremely high (70-90% and more than 1200mm/year, respectively), there is diffused solar radiation when the cloud cover is high, and intense solar radiation when the sky is clear, and wind speed goes from very low to very high.

As its name suggests, the "temperate" region is characterised by moderate temperature (30 to 34°C during the day, 17 to 24°C during the night), moderate humidity and rainfall (60-85% and more than 1000mm/year, respectively), and the solar radiation is quite stable during the year and the sky is usually clear (ECBC, 2009).

The "cold" region is the coldest Indian climatic zone (ECBC, 2009). Temperatures are moderate in summer during the day (17 to 30°C), but can go down to 4°C during the summer nights, and down to -14°C in winter. The humidity is usually low in sunny conditions (10-50%), while it increases in cloudy conditions (70-80%). Similarly, the solar radiation decreases when the sky is cloudy. Rainfall ranges between low and moderate.

The fifth zone is called "composite", and it applies when at least six months do not fall within any of the other categories (ECBC, 2009). The temperature is high in summer (up to 43°C) and low in winter (down to 4°C), the humidity is lower in summer (20-50%) and much higher during the monsoons (50-95%), and the direct solar radiation is usually very high in all seasons apart from the monsoon period, when it is diffused.

This code (ECBC, 2009) also explicitly highlights that the significant difference in the climatic data across these zones defines unique thermal comfort requirements for buildings located in different zones. This statement can be considered a support

to the use of a method, such as the one developed in this research, in which the cooling set-point is defined in relation to the climate of the region in which a building is located.

In order to select other appropriate locations in India for the application of the developed simulation approach, the second step was the analysis of the distribution of the Indian population across the five climatic regions. India has a population of 1.21 billion people and a geographical area of 3.29 million km^2 (Census, 2011). Although the climatic regions are five, 93% of the population lives in three climatic zones, namely "warm and humid", "composite", and "hot and dry" (Figure 6.7). Moreover, 95% of the geographical area falls into these three categories (Figure 6.8). 9 out of 10 of the most populated Indian cities are in these three zones, and the only exception is Bangalore (Table 6.3), which is in the "temperate" region. The Indian Energy Conservation Building Code (ECBC, 2009) gives the climatic zone for the 50 major cities, and only two of them are in "cold" region, namely Gauhati and Sundernagar. However, the population of both of them is well below a million people. In particular, the latter has only nearly 24,000 inhabitants (Census, 2011).

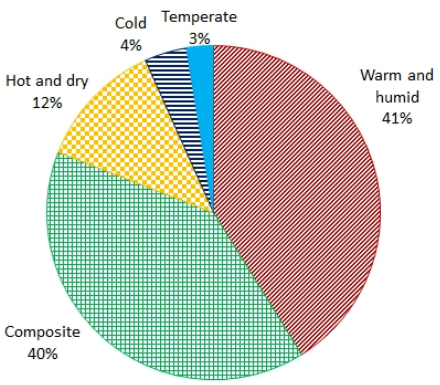

Figure 6.7: *Distribution of the Indian population across the five climatic regions (Census, 2011).*

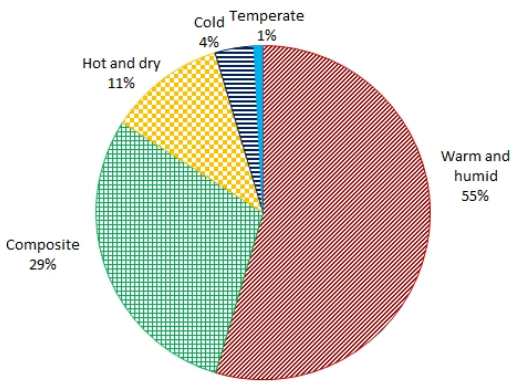

Figure 6.8: *Distribution of the Indian geographical area across the five climatic regions (Census, 2011).*

Table 6.3: *Population of the 10 most populated cities in India and their respective climatic zones (Census, 2011).*

City	Climatic zone	Population
Mumbai	Warm and humid	12,442,373
Delhi	Composite	11,034,555
Bangalore	Temperate	8,443,675
Hyderabad	Composite	6,993,262
Ahmedabad	Hot and dry	5,577,940
Chennai	Warm and humid	4,656,732
Kolkata	Warm and humid	4,496,694
Surat	Hot and dry	4,467,797
Pune	Warm and humid	3,124,458
Jaipur	Composite	3,046,163

Based on climatic regions and population distribution, three other cities have been selected to extend the analysis of the potential energy savings due to the use of ceiling fan as a means to reduce the use of air conditioners. The three cities are Mumbai ("warm and humid"), Delhi ("composite") and Bangalore ("temperate"), which are the largest cities of their respective climatic regions. Ahmedabad is the biggest city of the "hot and dry". No city has been included to represent the fifth region because, due to the much colder climatic conditions, it is unlikely that air conditioning is used in this zone.

It is sensible to focus the analysis on the largest cities since these are the locations in which air conditioners are more likely to be used. Given the complexity of the Indian society, in smaller cities and rural areas the context is likely to be very different and therefore the results obtained by analysing these zones might be unrealistic or at least not comparable with those calculated for large cities.

The weather files used in this study to calculate the monthly cooling set-points for the three cities were also created by ISHRAE in TMY2 format for use with building energy performance simulation programs (EnergyPlus weather data, 2016). Thus, the source is the same of the Ahmedabad weather file. The cooling set-points for Mumbai, Delhi, and Bangalore are reported in Table 6.4, 6.5, and 6.6, respectively. The procedure used to define and implement them into DesignBuilder is exactly the

same method used for Ahmedabad.

It is worth reminding that the ASHRAE adaptive model is applicable only if the prevailing mean outdoor temperature is greater than 10°C and less than 33.5°C (ASHRAE, 2013a). This condition is met in all these three additional locations.

Table 6.4: *Dynamic cooling set-point - Mumbai.*

	JAN	FEB	MAR	APR	MAY	JUN
T_m	24	24	26	28	30	28
T_{comf}	25.2	25.2	25.9	26.5	27.1	26.5
$T_{max(90\%)}$	27.7	27.7	28.4	29.0	29.6	29.0
$T_{maxAirSpeed(0.6m/s)}$	28.9	28.9	29.6	30.2	30.8	30.2
$T_{maxAirSpeed(0.9m/s)}$	29.5	29.5	30.2	30.8	31.4	30.8
$T_{maxAirSpeed(1.2m/s)}$	29.9	29.9	30.6	31.2	31.8	31.2
	JUL	AUG	SEP	OCT	NOV	DEC
T_m	27	27	27	28	26	24
T_{comf}	26.2	26.2	26.2	26.5	25.9	25.2
$T_{max(90\%)}$	28.7	28.7	28.7	29.0	28.4	27.7
$T_{maxAirSpeed(0.6m/s)}$	29.9	29.9	29.9	30.2	29.6	28.9
$T_{maxAirSpeed(0.9m/s)}$	30.5	30.5	30.5	30.8	30.2	29.5
$T_{maxAirSpeed(1.2m/s)}$	30.9	30.9	30.9	31.2	30.6	29.9

Table 6.5: *Dynamic cooling set-point - Delhi.*

	JAN	FEB	MAR	APR	MAY	JUN
T_m	14	16	21	28	31	33
T_{comf}	22.1	22.8	24.3	26.5	27.4	28.0
$T_{max(90\%)}$	24.6	25.3	26.8	29.0	29.9	30.5
$T_{maxAirSpeed(0.6m/s)}$	25.8	26.5	28.0	30.2	31.1	31.7
$T_{maxAirSpeed(0.9m/s)}$	26.4	27.1	28.6	30.8	31.7	32.3
$T_{maxAirSpeed(1.2m/s)}$	26.8	27.5	29.0	31.2	32.1	32.7
	JUL	AUG	SEP	OCT	NOV	DEC
T_m	31	29	29	25	19	14
T_{comf}	27.4	26.8	26.8	25.6	23.7	22.1
$T_{max(90\%)}$	29.9	29.3	29.3	28.1	26.2	24.6
$T_{maxAirSpeed(0.6m/s)}$	31.1	30.5	30.5	29.3	27.4	25.8
$T_{maxAirSpeed(0.9m/s)}$	31.7	31.1	31.1	29.9	28.0	26.4
$T_{maxAirSpeed(1.2m/s)}$	32.1	31.5	31.5	30.3	28.4	26.8

Table 6.6: *Dynamic cooling set-point - Bangalore.*

	JAN	FEB	MAR	APR	MAY	JUN
T_m	20	23	26	27	26	23
T_{comf}	24.0	24.9	25.9	26.2	25.9	24.9
$T_{max(90\%)}$	26.5	27.4	28.4	28.7	28.4	27.4
$T_{maxAirSpeed(0.6m/s)}$	27.7	28.6	29.6	29.9	29.6	28.6
$T_{maxAirSpeed(0.9m/s)}$	28.3	29.2	30.2	30.5	30.2	29.2
$T_{maxAirSpeed(1.2m/s)}$	28.7	29.6	30.6	30.9	30.6	29.6
	JUL	AUG	SEP	OCT	NOV	DEC
T_m	23	22	23	22	21	20
T_{comf}	24.9	24.6	24.9	24.6	24.3	24.0
$T_{max(90\%)}$	27.4	27.1	27.4	27.1	26.8	26.5
$T_{maxAirSpeed(0.6m/s)}$	28.6	28.3	28.6	28.3	28.0	27.7
$T_{maxAirSpeed(0.9m/s)}$	29.2	28.9	29.2	28.9	28.6	28.3
$T_{maxAirSpeed(1.2m/s)}$	29.6	29.3	29.6	29.3	29.0	28.7

Similarly to what has been done for the first location (Ahmedabad), both air temperature and operative temperature set-points have been simulated to assess savings' benefits using both approaches also for Mumbai, Delhi, and Bangalore. Thus, in total other 24 cases have been simulated (three locations, four level of air sped, and two types of temperature control).

6.2 Results and discussion

This results's section initially focuses on the effect that the choice between air temperature and operative temperature, as control parameter, has on the energy predictions calculated using DTM. It then reports the demand for space cooling and the energy savings that can be achieved in a typical Indian residential building using ceiling fans to generate air movement and therefore increasing the cooling set-point temperature without jeopardising occupants' thermal comfort. As explained in the methodology (section 6.1), a dynamic cooling set-point was used. The results are firstly presented for Ahmedabad, and then for the other three cities.

6.2.1 Effect of using air temperature or operative temperature

As explained in the methodology (section 6.1), when the operation of an element of the building such as the cooling system or the openings is controlled by temperature set-points, in DesignBuilder/EnergyPlus these values can be either operative temperature or air temperature. In this research, both air temperature and operative temperature set-points have been simulated to assess savings benefits using both approaches.

There is a noticeable difference in the energy consumption depending on whether air temperature or operative temperature was chosen as the control parameter. In the initial case where no fan was used, the total number of cooling hours (Table 6.7 and Figure 6.9) is 1482 when air temperature is used, but it reaches 2527 with the other control type, which is a 70% increase due only to a change in this setting within the simulation program. As the fan speed goes up to 0.6 m/s, 0.9 m/s and 1.2 m/s, this percentage grows to 111%, and 133 per cent and 152%, respectively. The respective energy consumption expressed in kWh (Table 6.7 and Figure 6.10) are relative low using both air temperature and operative temperature, but should these predictions be used to scale up the energy saving estimates to a regional scale, then these differences would make a bigger impact.

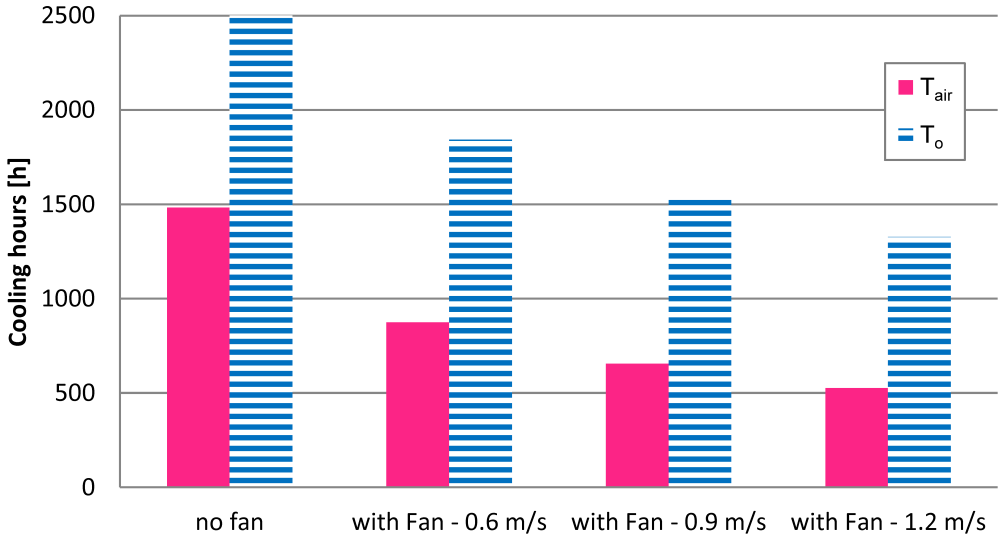

Figure 6.9: *Total number of hours in which the air conditioning system is ON.*

Table 6.7: *Energy saving (without including energy used by the fan).*

Simulation	Cooling hours [h]	Energy for space cooling [kWh]	Energy for space cooling [kWh/m^2]	Savings without including the fan energy consumption [kWh]	Savings without including the fan energy consumption [%]
Control type: T_{air}					
no fan	1482	1381	9.52	0	0
with Fan - 0.6 m/s	873	691	4.76	690	50
with Fan - 0.9 m/s	654	469	3.23	912	66
with Fan - 1.2 m/s	526	359	2.47	1022	74
Control type: T_o					
no fan	2527	2827	19.49	0	0
with Fan - 0.6 m/s	1843	1655	11.41	1172	41
with Fan - 0.9 m/s	1524	1235	8.52	1592	56
with Fan - 1.2 m/s	1327	1011	6.98	1815	64

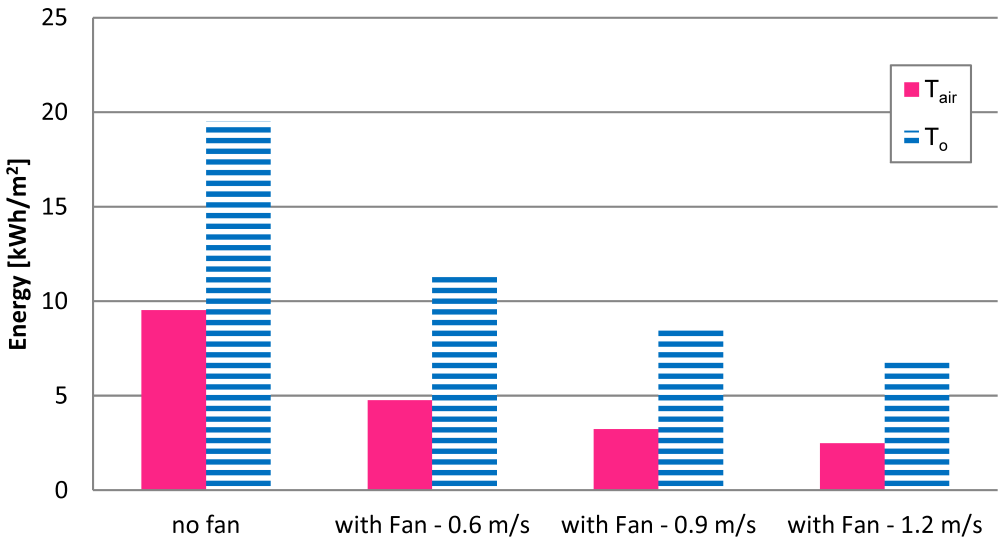

Figure 6.10: *Energy used by the air conditioning system.*

In general, the operative temperature is a function of the air temperature and the mean radiant temperature. For low air speeds, smaller than 0.2 m/s, the operative temperature is the arithmetic mean of the air temperature and the mean radiant temperature. Then, as the air speed increases, the relative weight of the mean radiant temperature decreases (Niu and Burnett, 1998). This relative weight can be calculated for different air speeds using the following equation from ISO7726 (ISO, 2001):

$$T_o = \frac{T_{air} \times \sqrt{10 \times S_{air}} + MRT}{1 + \sqrt{10 \times S_{air}}} \tag{6.6}$$

At air speeds equal to 0.6 m/s, 0.9 m/s, and 1.2 m/s, the the relative weight of the mean radiant temperature is 29%, 25%, and 22%, respectively.

International standards on thermal comfort usually refer to operative temperature when a certain temperature limit is given, and this is the case also for the ASHRAE adaptive model (ASHRAE, 2013a) on which the cooling set-points used in this study are based. Indeed, the operative temperature gives a better indication of the temperature that a person is feeling in a certain environment.

On the other hand, real-word room air-conditioners are controlled by a simple

thermostat, which is likely to be sensing the air temperature nearby its location, but far less influenced by the radiant component. In a real scenario, this means that a user would simply decrease the set-point if uncomfortably warm. However, if the model uses air temperature as a control, this behaviour is not captured.

It is important to highlight that in the two conditioned bedrooms (floor plan shown in Figure 6.1 at page 145), air temperature and operative temperature are almost identical when no air conditioning is used. As the air conditioning is turned on, the air temperature decreases faster (Figure 6.11), with the difference (operative temperature – air temperature) being within 1.6°C in over 85% of the hours in which the air conditioning is used.

Previous research on Indian offices (Jain et al., 2011) also noticed that the energy demand for space cooling obtained using the air temperature, as control parameter, is significantly lower than when the operative temperature is used in EnergyPlus simulations. The difference was found to go up to 29%, which at first sight might look much smaller than the figures mentioned earlier in this chapter. However, in that case the chosen set-point temperature was 24°C, which means that the cooling load in kWh was very high using either air temperature or operative temperature. Therefore the relative difference was smaller. Similarly, in this study, the percentage difference grows as the set-point is increased due to the higher air speed.

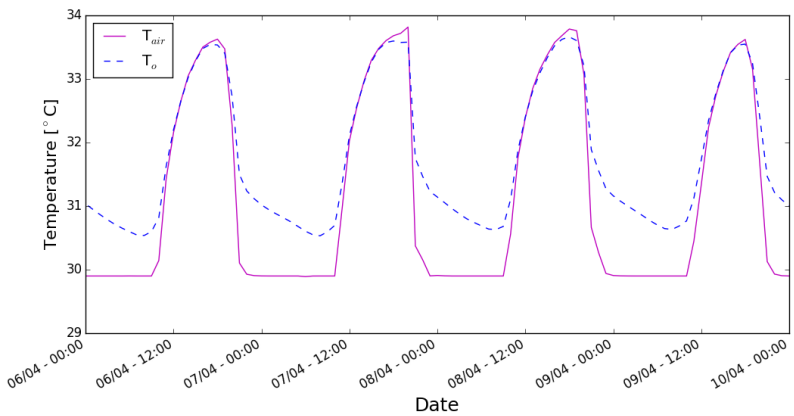

Figure 6.11: *Example of T_{air} and T_o profiles in a bedroom over four generic days in April (Control type: T_{air}).*

Therefore, whenever in a given space the air temperature and mean radiant temperature are different, the energy load for space cooling is more realistic if calculated using operative temperature when the users have total direct control over the set-point, and using the air temperature when they do not. When air conditioning is used in bedrooms overnight, it is likely to be in between these two extreme conditions.

Moreover, it is important to focus on how DTMs calculate the operative temperature. During a simulation, both air temperature for each node and the surfaces' temperature are calculated, and then the operative temperature is calculated as the arithmetic mean of the other two values. However, the fans are not explicitly included in this type of models, but only their effect is taken into account. In the models developed in this research, this has been done by increasing the cooling set-point. Using the arithmetic mean is fine only if air speed is very low, that is the case without active fans. In the other cases, the actual operative temperature that would be felt by a person is closer to the simulated air temperature. Thus, the energy load for space cooling is more realistic if calculated using operative temperature when there is no air movement. However, when there is elevated air movement, the energy load for space cooling is likely to be overestimated if calculated using operative temperature as control parameter. This aspect cannot be modelled in a DTM software since the air speed is not uniform in a room, but should be taken into consideration while looking at the energy results and their link to the level of comfort.

For all these reasons, in this study both control types have been used and the respective results reported.

6.2.2 Energy savings - Ahmedabad

Regardless of whether the operative temperature or the air temperature is used as control parameter, a significant reduction in energy consumption is achievable if ceiling fans are used to increase the set-point temperature (Table 6.8). The figures go up to 69 and 60% or 948 and 1689 kWh using the air temperature and the operative

temperature as a control temperature, respectively.

Table 6.8: *Energy saving (including the energy used by the fan).*

Simulation	n [h]	Fan average power [W]	E_{fan} [kWh]	$E_{savings}$ [kWh]	$E_{savings}$ [%]	Fan only hours [h]
Control type: T_{air}						
no fan	0	0	0	0	0	0
with Fan - 0.6 m/s	1482	50	74	616	45	609
with Fan - 0.9 m/s	1482	50	74	838	61	828
with Fan - 1.2 m/s	1482	50	74	948	69	956
Control type: T_{or}						
no fan	0	0	0	0	0	0
with Fan - 0.6 m/s	2527	50	126	1046	34	684
with Fan - 0.9 m/s	2527	50	126	1466	52	1003
with Fan - 1.2 m/s	2527	50	126	1689	60	1200

As shown in Figures 6.12 and 6.13, this reduction is due to the decrease in air conditioning usage. Due to the elevated air movement generated by the ceiling fan, the same level of thermal comfort can be guaranteed using an higher set-point temperature for the cooling system, and therefore using less energy. The higher the air speed assumed to be available to the occupants is, the more significant this reduction becomes. Furthermore, these two graphs (Figures 6.12 and 6.13) visually highlight that, changing the control type from air temperature to operative temperature, there is a small increase in the number of hours in which air movement alone can deliver the required cooling (in the graphs, part called "Fan only"). However, there is a significant growth in the usage of the air conditioning alongside the fan. With the air temperature used as control parameter and assuming that 0.9 m/s or 1.2 m/s air speed is available, then the air conditioning system is used in less than 45, or 35 %, of the hours in which some cooling is required, respectively (see also Table 6.8). With T_o as control parameter, regardless of the available air speed, the air conditioning system is always used in more than 50 of the cooling hours.

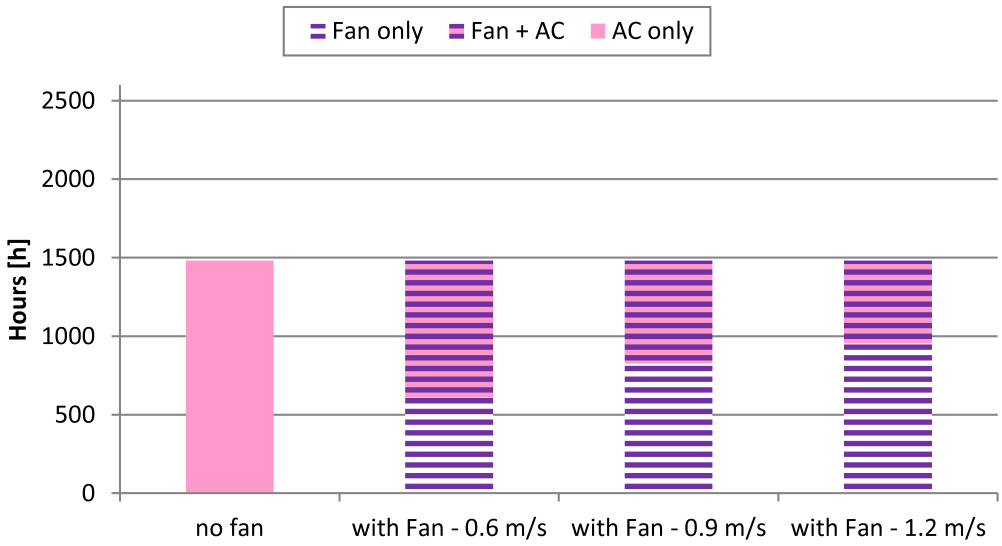

Figure 6.12: *Number of hours in which the air conditioning system, the fan, or both are ON (Control type: T_{air}).*

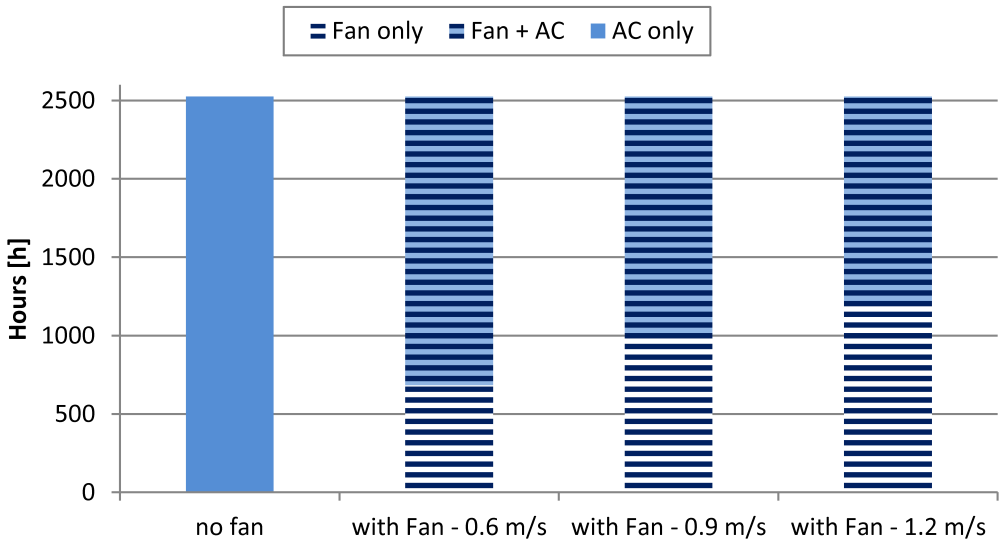

Figure 6.13: *Number of hours in which the air conditioning system, the fan, or both are ON (Control type: T_o).*

The simultaneous use of a second ceiling fan only slightly reduces the energy savings (Table 6.9). For both operative temperature and air temperature based estimates, the energy savings would be negligible only if nine ceiling fans were to be operating at the same time, which is not a realistic scenario. This significant margin has also another positive consequence. In a typical Indian apartment, there are small fluctuations in the electricity supply, and also different speed settings lead to slightly different power usage. Both variations depend on the specific house and fan, but having such a significant margin ensures that ceiling fans are clearly an effective way to improve thermal comfort while saving energy.

Table 6.9: *Energy saving including the energy used by two fans.*

Simulation	$E_{savings}$ [kWh]	$E_{savings}$ [%]
Control type: T_{air}		
no fan	0	0
with Fan - 0.6 m/s	542	39
with Fan - 0.9 m/s	764	55
with Fan - 1.2 m/s	874	63
Control type: T_o		
no fan	0	0
with Fan - 0.6 m/s	919	33
with Fan - 0.9 m/s	1339	47
with Fan - 1.2 m/s	1563	55

6.2.3 Energy savings - extension of the analysis to Mumbai, Delhi, and Bangalore

The energy loads and relative saving are fairly different in the three locations. In Delhi, there is the highest energy demand for space cooling (Table 6.12), with figures reasonably similar to Ahmedabad's loads (Table 6.7). The energy demand for space cooling is significantly lower in Mumbai (Table 6.10), and almost negligible in Bangalore (Table 6.14).

The dynamic cooling set-point method is based on temperatures, and therefore

it was likely that the loads were more relevant in those areas, such as Ahmedabad and Delhi, in which the outdoor temperature may exceed 40°C, and the monthly arithmetic mean of the daily average outdoor dry bulb temperatures is higher than 30°C in some months. On the other hand, in Bangalore the loads are so low that it is possible that most of the people would choose not to purchase and install an air conditioning system, but would prefer to accept a slightly uncomfortable environment for a very few hours (down to 7, assuming an air speed of 1.2 m/s) of the year (Table 6.14). In other words, in the climatic conditions of Bangalore ceiling fans alone are capable to deliver the required level of comfort, and the saving calculated in this study would become virtual (Table 6.15) if no air conditioners was used.

In the two driest locations, namely Ahmedabad and Delhi, the fans alone cannot be sufficient to provide the required cooling, but a significant reduction of the energy demand for space cooling is still achievable due to the use of air movement. In Delhi, this can be up to 60% of the energy used by the air conditioning if no fan was used (Table 6.13). However, it is worth remembering that, in warm and hot conditions, the use of fans has two positive effects: it increases both the convective and evaporative heat exchange between a person and the surrounding thermal environment. The former depends on a temperature difference, the latter on a water vapour pressure difference. With the same temperature difference, if the surrounding thermal environment is drier, then the same air speed has an higher cooling effect than in a more humid environment. This method, based on the ASHRAE adaptive theory, does not take humidity into account, but only temperatures. Thus, in these dry locations, the cooling effect of air speed is likely to be a little higher than what expected. In other words, this means that a person might choose to use a sightly higher set-point with the same air speed, and this would lead to higher energy savings.

Table 6.10: *Energy saving (without including energy used by the fan) - Mumbai.*

Simulation	Cooling hours [h]	Energy for space cooling [kWh]	Energy for space cooling [kWh/m^2]	Savings without including the fan energy consumption [kWh]	Savings without including the fan energy consumption [%]
Control type: T_{air}					
no fan	1068	609	4.20	0	0
with Fan - 0.6 m/s	326	115	0.79	494	81
with Fan - 0.9 m/s	148	33	0.23	576	95
with Fan - 1.2 m/s	80	14	0.10	595	98
Control type: T_o					
no fan	1966	1814	12.51	0	0
with Fan - 0.6 m/s	954	598	4.12	1216	67
with Fan - 0.9 m/s	567	256	1.77	1558	86
with Fan - 1.2 m/s	371	124	0.86	1690	93

Table 6.11: *Energy saving (including the energy used by the fan) - Mumbai.*

Simulation	n [h]	Fan average power [W]	E_{fan} [kWh]	$E_{savings}$ [kWh]	$E_{savings}$ [%]	Fan only hours [h]
Control type: T_{air}						
no fan	0	0	0	0	0	0
with Fan - 0.6 m/s	1068	50	53	441	72	742
with Fan - 0.9 m/s	1068	50	53	523	86	920
with Fan - 1.2 m/s	1068	50	53	542	89	988
Control type: T_{or}						
no fan	0	0	0	0	0	0
with Fan - 0.6 m/s	1966	50	98	1118	62	1012
with Fan - 0.9 m/s	1966	50	98	1460	80	1399
with Fan - 1.2 m/s	1966	50	98	1592	88	1595

Table 6.12: *Energy saving (without including energy used by the fan) - Delhi.*

Simulation	Cooling hours [h]	Energy for space cooling [kWh]	Energy for space cooling [kWh/m^2]	Savings without including the fan energy consumption [kWh]	Savings without including the fan energy consumption [%]
Control type: T_{air}					
no fan	1371	1545	10.66	0	0
with Fan - 0.6 m/s	1060	1026	7.08	519	34
with Fan - 0.9 m/s	731	661	4.56	884	57
with Fan - 1.2 m/s	623	542	3.74	1003	65
Control type: T_o					
no fan	1893	2555	17.62	0	0
with Fan - 0.6 m/s	1594	1948	13.43	607	24
with Fan - 0.9 m/s	1186	1293	8.92	1262	49
with Fan - 1.2 m/s	1022	1087	7.50	1468	57

Table 6.13: *Energy saving (including the energy used by the fan) - Delhi.*

Simulation	n [h]	Fan average power [W]	E_{fan} [kWh]	$E_{savings}$ [kWh]	$E_{savings}$ [%]	Fan only hours [h]
Control type: T_{air}						
no fan	0	0	0	0	0	0
with Fan - 0.6 m/s	1371	50	69	450	29	311
with Fan - 0.9 m/s	1371	50	69	815	53	640
with Fan - 1.2 m/s	1371	50	69	934	60	748
Control type: T_{or}						
no fan	0	0	0	0	0	0
with Fan - 0.6 m/s	1893	50	95	512	20	299
with Fan - 0.9 m/s	1893	50	95	1167	46	707
with Fan - 1.2 m/s	1893	50	95	1373	54	871

Table 6.14: *Energy saving (without including energy used by the fan) - Bangalore.*

Simulation	Cooling hours [h]	Energy for space cooling [kWh]	Energy for space cooling [kWh/m^2]	Savings without including the fan energy consumption [kWh]	Savings without including the fan energy consumption [%]
Control type: T_{air}					
no fan	169	66	0.46	0	0
with Fan - 0.6 m/s	50	9	0.06	57	86
with Fan - 0.9 m/s	19	2	0.01	64	97
with Fan - 1.2 m/s	7	1	0.00	66	99
Control type: T_o					
no fan	447	286	1.97	0	0
with Fan - 0.6 m/s	209	114	0.79	172	60
with Fan - 0.9 m/s	140	61	0.42	225	79
with Fan - 1.2 m/s	96	35	0.24	251	88

Table 6.15: *Energy saving (including the energy used by the fan) - Bangalore.*

Simulation	n [h]	Fan average power [W]	E_{fan} [kWh]	$E_{savings}$ [kWh]	$E_{savings}$ [%]	Fan only hours [h]
Control type: T_{air}						
no fan	0	0	0	0	0	0
with Fan - 0.6 m/s	169	50	8	49	74	119
with Fan - 0.9 m/s	169	50	8	56	84	150
with Fan - 1.2 m/s	169	50	8	57	86	162
Control type: T_{or}						
no fan	0	0	0	0	0	0
with Fan - 0.6 m/s	447	50	22	150	52	238
with Fan - 0.9 m/s	447	50	22	203	71	307
with Fan - 1.2 m/s	447	50	22	229	80	351

The opposite situation happens in Mumbai. In this case, the humidity levels are so elevated that the benefit provided by the elevated air movement depends almost only on the increase of the convective heat flux. In Mumbai (Table 6.11), a reduction of up to 89% in the energy demand for space cooling can be achieved using ceiling fans (but also other sources of elevated air speeds) taking into account also the energy used by the fan. However, the case of Mumbai highlights one possible limitation of the developed method to define dynamically the cooling set-point. This method is based on temperature only, and does not consider the possibility that the air conditioning is used to dehumidify the indoor air. In the Indian context, this is unlike to happen since people are used to very humid conditions. However, should this approach be used in Western countries, or should the Indian habits change, then this should be somehow included into the developed method.

The energy predictions presented in this chapter are calculated using the new approach which is based on the dynamic cooling set-point that varies each month. If the methods used in previous research on office buildings (Schiavon and Melikov, 2008) had been applied, then the set-points would have been constant throughout the year. Considering category II (EN 15251-2007 (EN, 2007)), in which case 10% of people are considered to be dissatisfied, the temperature thresholds would have been 26.0°C, 27.7°C and 28.5°C for 0.2 m/s or less, 0.5 m/s and 0.8 m/s, respectively. These values are lower than those used in this study , both for the cases without and with air movement, and therefore the annual energy consumption calculated with these set-points would be higher.

However, research by Indraganti (2010b) showed that the comfort band in Indian residential buildings can be extended by up to 32.5°C, which is much closer to the highest set-point used in this work, that is 32.7°C in Ahmedabad (in May) and Delhi (in June) with air speed equal to 1.2 m/s, than the values used in previous research. Moreover, the same study highlighted how complex the domestic environment is, that users are heavily influenced by the outdoor conditions, and that the different adaptive

solutions such as ceiling fans and air conditioners are widely used and combined. Therefore, energy savings predictions calculated with the proposed methodology are lower than those calculated with traditional methods for fully air-conditioned buildings, but they are likely to be more realistic for the situation of Indian residential mixed-mode buildings.

6.3 Summary

This last experimental chapter illustrates the likely energy saving that can be achieved in a typical Indian apartment if ceiling fans are used to increase the set-point temperature of the air conditioning system while maintaining the same level of thermal comfort. In other words, while the focus of the previous chapter was on the coupled system and on the effect of air movement on thermal comfort in warm conditions, this chapter focuses on the energy demand side of the problem. A novel method to vary the set-point temperature of the air-conditioning system according to the ASHRAE 55 adaptive model of thermal comfort was developed as part of this research.

In dynamic thermal modelling, whenever the use of a component such as the air conditioning depends on temperature values, these may refer to air temperature or operative temperature values. In this study, a noticeable difference in the energy consumption was found depending on whether air temperature or operative temperature was chosen as the control parameter. The reason is that, when the air conditioner was turned on, the air temperature decreased faster than the operative temperature. As a result, the energy consumption was lower when air temperature was chosen as the control parameter. When air conditioning is used only in bedrooms overnight as in the apartment modelled in this study, it is likely that the most realistic energy predictions are in between the values calculated with the two approaches.

Using ceiling fans to limit the use of the air conditioner led to a significant reduction of the energy demand for space cooling. Taking into account the energy used by

a common ceiling fan, a reduction of up to 89% in the annual energy demand can be achieved. In other words, the same level of thermal comfort can be guaranteed by the use of a combination of elevated air movement and air conditioning, but using only 11% of the energy that would be required to provide this level of thermal comfort using only an air conditioner. The simultaneous use of a second fan only slightly reduced the energy savings.

Lastly, in this study, a dynamic set-point for the air conditioning system was used: the set-point temperature varied each months based on the ASHRAE 55 adaptive model of thermal comfort. The indoor environmental conditions simulated using this approach are closer to those noted by field-based research, and this further supports the accuracy of the energy estimates.

Chapter 7

CONCLUSIONS

The research presented in this thesis has developed a better understanding of human thermal comfort in non-uniform indoor environments, focusing especially on residential buildings and warm thermal conditions, and to improve the capability of prediction of occupants' thermal comfort in these conditions.

Due to global warming, and the rapid growth in population and disposable income in developing counties such as India, the energy demand for space cooling is dramatically increasing world-wide, and therefore focusing on alternative and low-energy techniques for space cooling is essential. For these reasons, this research has identified which low-energy techniques and devices, such as ceiling fans, are already in use in residential buildings, and improved the capability of prediction of their effect of thermal comfort. As a result of this work, designers will be able to accurately predict the performance of these alternative solutions with confidence, and will be better informed to support their use.

In this research, data from field studies in residential buildings in India and in the UK was used to identify the most common techniques and devices used by the occupants to achieve thermally comfortable conditions during the warm season. Computer simulations were used to model these scenarios with two main purposes: predicting the likely human thermal sensation in these non-uniform conditions, and comparing

the energy consumed by different systems to provide the same level of thermal comfort. The former was achieved by using a coupled CFD-thermophysiological model, and involved the accurate definition of all boundary conditions such as the ceiling fans, and the validation of the models with data collected using experimental facilities. The latter was achieved by means of dynamic thermal simulations.

This chapter is divided into three main sections. The first presents the key findings and conclusions of this research, showing how the aim and objectives have been addressed, and highlights the contribution to knowledge made by this research. The second section describes the wider significance of this work, which means summarising the impact of this study on academia, industry, and policy. The final part states the limitations of this research, and provides directions and ideas that may become the basis for future work that could address these limitations.

7.1 Key findings of this research and contribution to knowledge

This research has shown that the coupled model is able to predict human thermal comfort in complex non-uniform indoor configurations, as long as the environment around the human body is accurately modelled. In particular, the DTS is superior to the traditional PMV calculation as both temporal and spatial variation and non-uniform conditions can be taken into account. Therefore, the higher required computational power is compensated by more accurate thermal sensation predictions.

The initial testing and validation of the coupled system showed that this coupled system can accurately model the effect that elevated air movement has on the human thermal sensation. However, the model has a very low sensitivity to small variations in air speed. In other words, a very small inaccuracy in the modelling of the air speed hitting the person does not affect the dynamic thermal sensation. This is relevant because, in real buildings, it is often impossible to control and measure all

the environmental variables as done in a controlled experimental set-up, and therefore small modelling inaccuracies are likely to occur, but impossible to detect.

The analysis of the field data collected in UK and Indian residential buildings highlighted that, in UK houses, people rely on opening windows to improve their thermal sensation during the warm season. On the other hand, ceiling fans are widely used in Indian flats as cooling devices, and therefore are by far the most common means to generate non-uniform thermal environmental conditions in these houses. Due to the nature of the air flow generated by a ceiling fan, the mutual position of fan and person is crucial for assessing thermal comfort.

The detailed work completed to develop and validate a transient three-dimensional model of a typical Indian ceiling fan showed that a simple implicit CFD model, that combines accuracy with efficient computation, can be used for accurate thermal comfort studies. The model developed is able to accurately, qualitatively and quantitatively, predict the air flow generated by a typical Indian ceiling fan in a room. When using the SST k-ω turbulence model, 83% of the simulated values are within the error bars of the respective measured value, and both the swirling and downward air movements are effectively modelled. Due to the small number of input parameters required, the relatively low CPU time required, and the use of an unstructured mesh, this model can be effectively used in any study in which it is important to accurately model the air movement generated by the fan, such as thermal comfort or air quality and contaminant distribution research. The choice of the most appropriate turbulence model is essential, and the best results have been achieved using the SST k-ω turbulence model, which is available in most of the CFD packages.

When the coupled system was used to model real Indian apartments, the thermal comfort results showed that the coupled system accurately models the effect that the air movement generated by the ceiling fans has on the occupants. The shorter the distance between fan and manikin and the higher the number of active ceiling fans were, the more significant the effect of the elevated air speed was. Moreover, in

agreement with actual thermal sensation votes reported by participants, the coupled system predicted that air movement has little impact on human thermal comfort if the air temperature is above 34°C. The DTS calculated by the model is nearly +2 on the 7-point ASHRAE thermal sensation scale, and the actual thermal sensation vote is +1.8.

Modelling real scenarios using the coupled system showed not only that the set-point temperature of the air conditioning can be increased without jeopardising human thermal comfort by using ceiling fans to generate elevated air movement, but also demonstrated which is the most effective configuration of ceiling fans. In addition, the results highlighted that the coupled system can accurately model complex clothing ensembles, being in this regard superior to the traditional PMV model.

The more the environmental conditions are non-uniform, the longer the time required to calculate the DTS. This is due to the fact that more time is required to accurately replicate these environmental conditions, such as the fan effect, within the CFD model, and also the duration of each simulation is usually longer. Furthermore, this research gives indications about mesh type and resolution, turbulence models, and numerical schemes that can be used to generate a realistic model of the environment around a human body. This is not only applicable to thermal comfort research, but also to any other situation in which CFD is used to study the interaction between people and the surrounding environment.

Lastly, the estimate of the energy savings achievable due to air movement in mixed mode buildings showed that the dynamic cooling set-point led to more realistic simulation scenarios since it captures the existing connection between the users of mixed-mode buildings and the outdoor temperature. The energy demand for space cooling can be reduced by as much as 90% by using ceiling fans, without jeopardising occupants' thermal comfort, and the simultaneous use of two fans slightly reduces the energy savings. Moreover, using the operative or air temperature as control parameters in the dynamic thermal simulation significantly affects the results. Since

the air temperature decreases faster when the air conditioning is turned on, estimates based on it may be excessively low.

Thus, in summary, this research contributed to the existing body of knowledge by providing:

- Comprehensive guidelines about what the coupled IESD-Fiala and CFD model is and what it can be used for, how to proceed in order to apply it, and its strengths and limitations,
- An accurate and validated transient three-dimensional CFD model of a typical Indian ceiling fan, that can be used for any study that requires the air flow generated by a ceiling fan to be modelled in CFD; and
- An innovative method, based on a dynamic cooling set-point, for estimation of the energy savings achievable due to air movement in mixed model buildings.

7.2 Wider significance of this research: impact on academia, industry, and policy

The findings of this research enable some wider considerations. In particular, the focus may be broadened, and the impact of this work on academia, industry and policy may be highlighted.

Firstly, the major impact of this research on academia is clearly the contribution to knowledge summarised in the previous section. However, the overall positive outcome of this study goes beyond that, and it includes the fact that this research strengthened the cooperation between some of the world leading energy-related research universities, namely Loughborough University and De Montfort University in the UK, CEPT University in India, and University of California Berkeley in the USA. This cooperation has been sealed by joint publications, both conference and journal

papers, as a tangible sign of the positive team effort. Moreover, this cooperation set the basis for future joint research projects involving these institutions.

Secondly, this research has a positive impact on industry. The coupled system has computational requirements that, in 2017, are more compatible with the typical time scale of academic research, than with the tighter deadlines of the private sector. However, this simply means that the coupled system is not suitable for replacing simpler models, such as the PMV, in all circumstances, but it can be used, for consultancy purposes, to investigate the most relevant and complex scenarios. Moreover, the methods presented in this research enable a calculation of the discretization error. Thus, if a consultant used a more coarse mesh to speed up the process, they could calculate their discretization error, and then decide whether it is acceptable for their specific case. Lastly, the available computational power is growing significantly year after year, and cloud-based high-performance computing systems can be used to increase the computational resources only when required, minimizing the capital and maintenance costs of the hardware. Within CFD industry, using "cloud-based" usually means that pre- and post- processing are done mainly on a local average PC, while the simulation is run remotely on resources made available to users on demand via the Internet from a cloud computing provider. This is very important for firms which do not need (or cannot afford) to have high-performance computing systems in-house for their day-to-day work (for instance, a firm which usually performs dynamic thermal simulations of buildings, but not CFD analyses). Indeed if they want to conduct a CFD analysis (and minimize the computational time), they can hire cloud-based resources only when required. Thus, the main limitation is likely to be cost of the licences, which might be overcome in the near future by switching to open-source CFD codes.

Lastly, this research did not suggest any specific changes in the current international standards and regulations in this area. However, some indications may be given at this stage. Policy makers should promote the use of more advanced models,

such as the IESD-Fiala model coupled with CFD, if they lead to the use of more energy-efficient solutions to achieve the same level of thermal comfort. Then, from a policy maker point of view, the most relevant output of this research is the method developed for the estimate of the energy savings achievable due to air movement in mixed model buildings. The use of a dynamic cooling set-point, as opposed to a fixed annual value (which is that is usually stated in standards and regulations), and the considerations on the control parameter (operative or air temperature) used in dynamic thermal simulation leave a scope for discussion and, perhaps, changes. In general, for instance, if the energy use predictions of a region were based on incorrect assumptions (such as an unrealistic cooling set-point), than polices built on them would have little, if not negative, impact.

7.3 Limitations of this research

Firstly, the IESD-Fiala model was validated by previous studies, but the validation dataset only included studies with adult real human participates from Western countries. Since specific groups such as school children or elderly are likely to perceive thermal sensation differently, research is needed to adapt the model to those particular groups.

The coupled system currently works only with one coupled virtual manikin. If thermal comfort has to be assessed in different locations within a room, the virtual manikin has to be moved each time to the required spot. Other occupants can be represented only as passive uncoupled elements. Further work is needed to be able to couple two or more virtual manikins at the same time. Since this implies the modification of the code of the functions that link IESD-Fiala model and CFD, this enhancement could be combined with an overall computational improvement of the coupled system. This may include the move from a commercial CFD code to an open source one, eliminating the limitations due to the cost of the licences. A major

advantage of rewriting the coupled system (with or without moving to an open-source CFD code) is that this would enable a much easier usability of this coupled system. As it is now, its installation is complicated and must be completed by its original developers, making modifications (for instance, the addition of a new type of clothing such as the Indian sari) has similar problems, and even the access to the data and functions already implemented is very limited.

In the developed CFD model of the ceiling fan, due to the use of a simplified implicit model and RANS turbulence models, the major differences between measurements and simulated values occur in the narrow region below the perimeter of the fan, where there are rapid temporal and spatial variations in the flow field. Further work is required to investigate the possibility of using more advanced Reynolds stress turbulence models and LES, balancing the accuracy of the results and the computational effort required to achieve a reliable converged solution. More advanced measurement techniques such as particle image velocimetry could be used in the future to provide a better understanding of the flow field generated by the ceiling fan and better validation data, including data for lower fan rotational speeds. This would also ease the use of more advanced turbulence models.

Further work is needed also to improve the accuracy of the energy predictions. The currently available field-based research on mixed mode buildings supports the idea that users of these buildings are affected by the outdoor conditions, and therefore a method based on the adaptive model is likely to be closer to real-world scenarios.

However, these studies also show two other important things. Firstly, when air conditioning is available, even if only in certain rooms or at a certain time, then the occupants of a building tend to be less tolerant than people in fully naturally ventilated buildings. The second point is that in mixed mode buildings the use of air-conditioners depends on a range of factors that are not related to the outdoor temperature, such as noise, pollution and disposable income, and the situation is even more complex in domestic buildings.

Thus, further studies based on real field data are needed to properly address mixed mode buildings. The economies of developing countries such as India are growing fast, and represent the main market for air conditioners. Moreover, in these fast-developing countries, mixed mode buildings are extremely common since the air conditioning is often made available only in certain rooms or areas of a building. Therefore over- or under- estimating their energy requirement for space cooling would heavily affect the global figures for energy demand.

It will then be possible to say whether the most suitable method for estimating energy savings due to air movement in mixed mode buildings is the one proposed in this thesis and based on ASHRAE adaptive model, one based on IMAC, or a different one that has not yet been developed.

References

Aarti, N., Anamika, P., and Tanmay, T. HVAC Market Assessment and Transformation Approach for India. Technical report, U.S. Agency for International Development, Washington DC, 2014.

Ackerly, K. and Brager, G. Window signalling systems: control strategies and occupant behaviour. *Building Research and Information*, 41(January 2015):342–360, 2013. doi: 10.1080/09613218.2013.772044.

Adeeb, E., Maqsood, A., and Mushtaq, A. Effect of Number of Blades on Performance of Ceiling Fans. *MATEC Web of Conferences*, 28:02002, 2015. doi: 10.1051/matecconf/20152802002.

Afaq, M. A., Maqsood, A., Parvez, K., and Mushtaq, A. Study on the Design Improvement of an Indoor Ceiling Fan. In *2014 11th International Bhurban Conference on Applied Sciences & Technology (IBCAST) Islamabad, Pakistan, 14th-18th January*, pages 279–283, Islamabad, Pakistan, 2014. IEEE.

ANSYS. CFX - Solver Modeling Guide. Technical report, 2015a.

ANSYS. CFX - Solver Theory Guide. Technical report, 2015b.

ANSYS CFX, 2015. http://www.ansys.com/Products/Simulation+Technology/Fluid+Dynamics/Fluid+Dynamics+Products/ANSYS+CFX, last access 01.02.2017.

Arens, E., Xu, T., Miura, K., Hui, Z., Fountain, M., and Bauman, F. A study of occupant cooling by personally controlled air movement. *Energy and Buildings*, 27: 45–59, 1998. doi: 10.1016/S0378-7788(97)00025-X.

Arens, E., Turner, S., Zhang, H., and Paliaga, G. Moving air for comfort. *ASHRAE Journal*, 51:18–28, 2009.

Arens, E., Zhang, H., and Pasut, W. Thermal comfort and perceived air quality of a PEC system. In *Indoor Air 2011, June 5-10*, Austin, 2011.

ASHRAE. *Handbook - Fundamentals*. American Society of Heating, Refrigerating and Air-Conditioning Engineers, Inc., Atlanta, 2009.

ASHRAE. Standard 55-2010: Thermal Environmental Conditions for Human Occupancy, 2010.

ASHRAE. Standard 55-2013: Thermal Environmental Conditions for Human Occupancy, 2013a.

ASHRAE. *Handbook - Fundamentals*. American Society of Heating, Refrigerating and Air-Conditioning Engineers, Inc., Atlanta, 2013b.

ASHRAE. Standard 113-2013: Method of Testing for Room Air Diffusion, 2013c.

Barlow, S. and Fiala, D. Occupant comfort in UK offices-How adaptive comfort theories might influence future low energy office refurbishment strategies. *Energy and Buildings*, 39:837–846, 2007. doi: 10.1016/j.enbuild.2007.02.002.

Bassiouny, R. and Korah, N. S. Studying the features of air flow induced by a room ceiling-fan. *Energy and Buildings*, 43(8):1913–1918, 2011. doi: 10.1016/j.enbuild.2011.03.034.

Becker, R. and Paciuk, M. Thermal comfort in residential buildings - Failure to predict by Standard model. *Building and Environment*, 44(5):948–960, 2009. doi: 10.1016/j.buildenv.2008.06.011.

BEE, 2016. https://www.bijlibachao.com/top-ten-appliances/best-ceiling-fan-khaitan-havells-usha-crompton-greaves-orient-in-india-electricity-consumption.html, last access 10.10.2016.

Beizaee, A., Lomas, K., and Firth, S. National survey of summertime temperatures and overheating risk in English homes. *Building and Environment*, 65:1–17, 2013. doi: 10.1016/j.buildenv.2013.03.011.

Borgeson, S. and Brager, G. Comfort standards and variations in exceedance for mixed-mode buildings. *Building Research & Information*, 39(January 2015):118–133, 2011. doi: 10.1080/09613218.2011.556345.

Brager, G. Mixed-mode cooling. *ASHRAE Journal*, 48:30–37, 2006.

Brager, G. and de Dear, R. A Standard for Natural Ventilation. *ASHRAE Journal - Envelope Systems*, 2000.

Brager, G., Zhang, H., and Arens, E. Evolving opportunities for providing thermal comfort. *Building Research & Information*, 43(February):274–287, 2015. doi: 10.1080/09613218.2015.993536.

Broday, E. E., Augusto, A., Xavier, D. P., and de Oliveira, R. Comparative analysis of methods for determining the metabolic rate in order to provide a balance between man and the environment. *International Journal of Industrial Ergonomics*, 44(4): 570–580, 2014. doi: 10.1016/j.ergon.2014.05.006.

Buratti, C. and Ricciardi, P. Adaptive analysis of thermal comfort in university classrooms: Correlation between experimental data and mathematical models. *Building and Environment*, 44(4):674–687, April 2009. doi: 10.1016/j.buildenv.2008.06.001.

Cândido, C., de Dear, R., Lamberts, R., and Bittencourt, L. Air movement accept-

ability limits and thermal comfort in Brazil's hot humid climate zone. *Building and Environment*, 45:222–229, 2010. doi: 10.1016/j.buildenv.2009.06.005.

Cândido, C., Lamberts, R., de Dear, R., Bittencourt, L., and de Vecchi, R. Towards a Brazilian standard for naturally ventilated buildings: guidelines for thermal and air movement acceptability. *Building Research & Information*, 39:145–153, 2011. doi: 10.1080/09613218.2011.557858.

Cao, X., Liu, J., Jiang, N., and Chen, Q. Particle image velocimetry measurement of indoor airflow field: A review of the technologies and applications. *Energy and Buildings*, 69:367–380, 2014a. doi: 10.1016/j.enbuild.2013.11.012.

Cao, X., Liu, J., Pei, J., Zhang, Y., Li, J., and Zhu, X. 2D-PIV measurement of aircraft cabin air distribution with a high spatial resolution. *Building & Environment*, 82: 9–19, 2014b. doi: 10.1016/j.buildenv.2014.07.027.

Celik, I. Procedure for Estimation and Reporting of Uncertainty Due to Discretization in CFD Applications. *Journal of fluids engineering -Transactions of the ASME*, 130 (7):na, 2008. doi: 0.1115/1.2960953.

Census, 2011. http://www.censusindia.gov.in/2011census/dchb/DCHB.html, last access 15.06.2017.

Chen, Q. Ventilation performance prediction for buildings: A method overview and recent applications. *Building and Environment*, 44(4):848–858, 2009. doi: 10.1016/j.buildenv.2008.05.025.

Cheng, Y., Niu, J., and Gao, N. Thermal comfort models: A review and numerical investigation. *Building and Environment*, 47:13–22, 2012. doi: 10.1016/j.buildenv.2011.05.011.

Choi, J. I. and Edwards, J. R. Large-eddy simulation of human-induced contaminant

transport in room compartments. *Indoor Air*, 22(2005):77–87, 2012. doi: 10.1111/j.1600-0668.2011.00741.x.

Chris, W. and Megan, G. Measuring progress - Preparing for climate change through the UK Climate Impacts Programme, 2005.

CIBSE. Guide A: Environmental Design, 2005.

Cook, M., Ji, Y., and Hunt, G. CFD modelling of buoyancy-driven natural ventilation opposed by wind. In *9th International IBPSA Conference*, pages 207–214, Montreal, Canada, 2005.

Cook, M., Zitzmann, T., and Pfrommer, P. Dynamic thermal building analysis with CFD – modelling radiation. *Journal of Building Performance Simulation*, 1(2): 117–131, 2008. doi: 10.1080/19401490802250421.

Cook, M., Yang, T., and Cropper, P. Thermal comfort in naturally ventilated classrooms: application of coupled simulation models. In *Proceedings of Building Simulation 2011: 12th Conference of International Building Performance Simulation Association*, pages 2257–2262, Sydney, 2011.

Cropper, P., Yang, T., Cook, M., Fiala, D., and Yousaf, R. Exchange of simulation data between CFD program and a multi-segmented human thermal comfort model. In *5th Windsor Conference, Air Conditioning and the Low Carbon Cooling Challenge, Cumberland Lodge, Windsor, UK*, London, 2008. Network for Comfort and Energy Use in Buildings.

Cropper, P., Yang, T., Cook, M., Fiala, D., and Yousaf, R. Simulating the effect of complex indoor environmental conditions on human thermal comfort. In *Eleventh International IBPSA Conference, (Building Simulation 2009), 27-30 July, Glasgow, Scotland*, pages 1367–1373, Glasgow, 2009.

Cropper, P., Yang, T., Cook, M., Fiala, D., and Yousaf, R. Coupling a model of human thermoregulation with computational fluid dynamics for predicting human–environment interaction. *Journal of Building Performance Simulation*, 3(3): 233–243, September 2010. doi: 10.1080/19401491003615669.

de Dear, R. A global database of thermal comfort field experiments. *ASHRAE Transactions*, 104(1b):1141–1152, 1998.

de Dear, R. Revisiting an old hypothesis of human thermal perception: alliesthesia. *Building Research & Information*, 39(2):108–117, 2011. doi: 10.1080/09613218.2011.552269.

de Dear, R. and Brager, G. Developing an adaptive model of thermal comfort and preference. *ASHRAE Transactions*, 104:1–18, 1998.

de Dear, R., Akimoto, T., Arens, E., Brager, G., Candido, C., Cheong, D., Li, B., Nishihara, N., Sekhar, C., Tanabe, S., Toftum, J., Zhang, H., and Zhu, Y. Progress in thermal comfort research over the last twenty years. *Indoor Air*, 23:442–461, 2013. doi: 10.1111/ina.12046.

de Dear, R. J., Arens, E., Hui, Z., and Oguro, M. Convective and radiative heat transfer coefficients for individual human body segments. *International Journal of Biometeorology*, 40(3):141–156, 1997.

de Wilde, P. and Tian, W. The role of adaptive thermal comfort in the prediction of the thermal performance of a modern mixed-mode office building in the UK under climate change. *Journal of Building Performance Simulation*, 3(January 2015): 87–101, 2010. doi: 10.1080/19401490903486114.

Derbez, M., Berthineau, B., Cochet, V., Lethrosne, M., Pignon, C., Riberon, J., and Kirchner, S. Indoor air quality and comfort in seven newly built, energy-efficient houses in France. *Building and Environment*, 72:173–187, February 2014. doi: 10.1016/j.buildenv.2013.10.017.

Deuble, M. P. and de Dear, R. Mixed-mode buildings: A double standard in occupants' comfort expectations. *Building and Environment*, 54:53–60, 2012. doi: 10.1016/j.buildenv.2012.01.021.

Djongyang, N., Tchinda, R., and Njomo, D. Thermal comfort: A review paper. *Renewable and Sustainable Energy Reviews*, 14(9):2626–2640, December 2010. doi: 10.1016/j.rser.2010.07.040.

DSLDC. Hourly Demand Data from the State Load Dispatch Center. Technical report, Delhi State Load Dispatch Center, 2012.

Dynamics Dantec. ComfortSense, 2015. http://www.dantecdynamics.com/ comfort-sense, last access 15.06.2015.

ECBC. *Energy Conservation Building Code User Guide*. Bureau of Energy Efficiency, New Delhi, India, 2009.

EMS, 2016. https://designbuilder.co.uk/helpv5.0/Content/Energy_Management_System_EMS.htm, last access 05.10.2016.

EMS Application Guide, 2016. https://energyplus.net/sites/all/modules/custom/nrel_custom/pdfs/pdfs_v8.6.0/EMSApplicationGuide.pdf, last access 05.10.2016.

EN. 15251: Indoor environmental input parameters for design and assessment of energy performance of buildings addressing indoor air quality, thermal environment, lighting and acoustics, 2007.

EnergyPlus documentation, 2016. https://energyplus.net/documentation, last access 01.10.2016.

EnergyPlus weather data, 2016. https://energyplus.net/weather-region/asia_wmo_region_2/IND%20%20, last access 01.10.2016.

Eurostat. Manual for statistics on energy consumption in households, 2013.

Fanger, P. *Thermal Comfort*. McGraw-Hill, New York, USA, 1970.

Fanger, P. and Christensen, N. K. Perception of draught in ventilated spaces. *Ergonomics*, 29(August 2012):215–235, 1986. doi: 10.1080/00140138608968261.

Fanger, P., Melikov, A., Hanzawa, H., and Ring, J. Air turbulence and sensation of draught. *Energy and Buildings*, 12:21–39, 1988. doi: 10.1016/0378-7788(88)90053-9.

Faragher, J. Probabilistic Methods for the Quantification of Uncertainty and Error in Computational Fluid Dynamics Simulations. Technical report, Australian Government - Department of Defence, 2004.

Feng, L., Yao, S., Sun, H., Jiang, N., and Liu, J. TR-PIV measurement of exhaled flow using a breathing thermal manikin. *Building and Environment*, 94:683–693, 2015. doi: 10.1016/j.buildenv.2015.11.001.

Fiala, D., Lomas, K., and Stohrer, M. A computer model of human thermoregulation for a wide range of environmental conditions: the passive system. *Journal of Applied Physiology*, 87:1957–1972, 1999.

Fiala, D., Lomas, K., and Stohrer, M. Computer prediction of human thermoregulatory and temperature responses to a wide range of environmental conditions. *International Journal of Biometeorology*, 45(3):143–159, 2001. doi: 10.1007/s004840100099.

Fiala, D., Havenith, G., Bröde, P., Kampmann, B., and Jendritzky, G. UTCI-Fiala multi-node model of human heat transfer and temperature regulation. *International Journal of Biometeorology*, 56:429–441, 2012. doi: 10.1007/s00484-011-0424-7.

Foda, E., Almesri, I., Awbi, H. B., and Sirén, K. Models of human thermoregulation and the prediction of local and overall thermal sensations. *Building and Environment*, 46(10):2023–2032, 2011. doi: 10.1016/j.buildenv.2011.04.010.

Frontczak, M. and Wargocki, P. Literature survey on how different factors influence human comfort in indoor environments. *Building and Environment*, 46(4):922–937, 2011. doi: 10.1016/j.buildenv.2010.10.021.

Frontczak, M., Andersen, R. V., and Wargocki, P. Questionnaire survey on factors influencing comfort with indoor environmental quality in Danish housing. *Building and Environment*, 50:56–64, 2012. doi: 10.1016/j.buildenv.2011.10.012.

Fu, M., Yu, T., Zhang, H., Arens, E., Weng, W., and Yuan, H. A model of heat and moisture transfer through clothing integrated with the UC Berkeley comfort model. *Building and Environment*, 80:96–104, 2014. doi: 10.1016/j.buildenv.2014.05.028.

Gagge, A. P., Stolwijk, J., and Hardy, J. Comfort and thermal sensations and associated physiological responses at various ambient temperatures. *Environmental research*, 1(1):1–20, 1967.

Gagge, A. P. A new physiological variable associated with sensible and insensible perspiration. *American Journal of Physiology-Legacy Content*, 120(2):277–287, 1937.

Gagge, A., Stolwijk, J., and Nishi, Y. An Effective Temperature Scale Based on a Simple Model of Human Physiological Regulatiry Response. *ASHRAE Transactions*, 77:247–262, 1971.

Gandhi, P., Brager, G., and Dutton, S. Mixed Mode Simulation Tools. Technical report, 2014.

Gao, N. and Niu, J. CFD study on micro-environment around human body and personalized ventilation. *Building and Environment*, 39:795–805, 2004. doi: 10.1016/j.buildenv.2004.01.026.

Gao, N. and Niu, J. CFD Study of the Thermal Environment around a Human

Body: A Review. *Indoor and Built Environment*, 14(1):5–16, 2005. doi: 10.1177/1420326X05050132.

Gao, N., Niu, J., and Zhang, H. Coupling CFD and Human Body Thermoregulation Model for the Assessment of Personalized Ventilation. *HVAC&R Research*, 12 (January 2015):497–518, 2006. doi: 10.1080/10789669.2006.10391191.

Gao, N., Zhang, H., and Niu, J. Investigating Indoor Air Quality and Thermal Comfort Using a Numerical Thermal Manikin. *Indoor and Built Environment*, 16(1):7–17, 2007. doi: 10.1177/1420326X06074667.

Gossauer, E. and Wagner, A. Post-occupancy Evaluation and Thermal Comfort: State of the Art and New Approaches. *Advances in Building Energy Research*, 1 (1):151–175, 2007. doi: 10.1080/17512549.2007.9687273.

Guedes Correia, M., Matias, L., and Santos, C. P. Thermal comfort criteria and building design: Field work in Portugal. *Renewable Energy*, 34(11):2357–2361, November 2009. doi: 10.1016/j.renene.2009.03.004.

Hajdukiewicz, M., Geron, M., and Keane, M. M. Formal calibration methodology for CFD models of naturally ventilated indoor environments. *Building and Environment*, 59:290–302, 2013a. doi: 10.1016/j.buildenv.2012.08.027.

Hajdukiewicz, M., Geron, M., and Keane, M. M. Calibrated CFD simulation to evaluate thermal comfort in a highly-glazed naturally ventilated room. *Building and Environment*, 70:73–89, 2013b. doi: 10.1016/j.buildenv.2013.08.020.

Haldi, F. and Robinson, D. Modelling occupants' personal characteristics for thermal comfort prediction. *International journal of biometeorology*, 55(5):681–94, September 2011. doi: 10.1007/s00484-010-0383-4.

Hamza, N., Setaih, K., Hamza, N., Lecturer, S., Mohammed, M. A., Dudek, S., Townshend, T., and Lecturer, S. CFD modeling as a tool for assessing outdoor

thermal comfort in urban settings in hot arid climates. *Journal of Information Technology in Construction*, 19:248–269, 2014.

Hanzawa, H., Melikov, A., and Fanger, P. Airflow Characteristics in the Occupied Zone of Ventilated Spaces. *ASHRAE Transactions*, 93:524–539, 1987.

Havenith, G., Holmér, I., and Parsons, K. Personal factors in thermal comfort assessment: Clothing properties and metabolic heat production. *Energy and Buildings*, 34:581–591, 2002. doi: 10.1016/S0378-7788(02)00008-7.

Hong, S. H., Gilbertson, J., Oreszczyn, T., Green, G., and Ridley, I. A field study of thermal comfort in low-income dwellings in England before and after energy efficient refurbishment. *Building and Environment*, 44:1228–1236, 2009. doi: 10.1016/j.buildenv.2008.09.003.

Horikiri, K., Yao, Y., and Yao, J. Numerical optimisation of thermal comfort improvement for indoor environment with occupants and furniture. *Energy and Buildings*, 88:303–315, 2015. doi: 10.1016/j.enbuild.2014.12.015.

Hoyt, T., Arens, E., and Zhang, H. Extending air temperature setpoints : Simulated energy savings and design considerations for new and retro fit buildings. *Building and Environment*, xxx:1–8, 2014. doi: 10.1016/j.buildenv.2014.09.010.

Huang, L., Ouyang, Q., Zhu, Y., and Jiang, L. A study about the demand for air movement in warm environment. *Building and Environment*, 61:27–33, 2013. doi: 10.1016/j.buildenv.2012.12.002.

Huang, L., Arens, E., Zhang, H., and Zhu, Y. Applicability of whole-body heat balance models for evaluating thermal sensation under non-uniform air movement in warm environments. *Building and Environment*, 75:108–113, 2014. doi: 10.1016/j.buildenv.2014.01.020.

Huizenga, C., Hui, Z., and Arens, E. A model of human physiology and comfort for assessing complex thermal environments. *Building and Environment*, 36(6): 691–699, 2001. doi: 10.1016/S0360-1323(00)00061-5.

ICEM CFD, 2015. http://www.ansys.com/Products/Other+Products/ ANSYS+ICEM+CFD, last access 01.02.2017.

Indraganti, M. Thermal comfort in naturally ventilated apartments in summer: Findings from a field study in Hyderabad, India. *Applied Energy*, 87(3):866–883, 2010a. doi: 10.1016/j.apenergy.2009.08.042.

Indraganti, M. Behavioural adaptation and the use of environmental controls in summer for thermal comfort in apartments in India. *Energy and Buildings*, 42(7): 1019–1025, 2010b. doi: 10.1016/j.enbuild.2010.01.014.

Indraganti, M. Adaptive use of natural ventilation for thermal comfort in Indian apartments. *Building and Environment*, 45(6):1490–1507, 2010c. doi: 10.1016/j.buildenv.2009.12.013.

Indraganti, M. Thermal comfort in apartments in India: Adaptive use of environmental controls and hindrances. *Renewable Energy*, 36(4):1182–1189, 2011. doi: 10.1016/j.renene.2010.10.002.

Indraganti, M. and Rao, K. D. Effect of age, gender, economic group and tenure on thermal comfort: A field study in residential buildings in hot and dry climate with seasonal variations. *Energy and Buildings*, 42(3):273–281, 2010. doi: 10.1016/j.enbuild.2009.09.003.

Indraganti, M., Lee, J., Zhang, H., and Arens, E. a. Thermal adaptation and insulation opportunities provided by different drapes of Indian saris. *Architectural Science Review*, 58(1):87–92, 2014a. doi: 10.1080/00038628.2014.976540.

Indraganti, M., Lee, J., Zhang, H., and Arens, E. A. Versatile Indian sari : Clothing insulation with different drapes of typical sari ensembles. *8th Windsor Conference: Counting the Cost of Comfort in a changing world*, (April):10–13, 2014b.

ISO. 7726: Ergonomics of the Thermal Environment, Instruments for Measuring Physical Quantities, 2001.

ISO. 8996: Ergonomics of the thermal environment - Determination of metabolic heat production, 2004.

ISO. 7730: Ergonomics of the thermal environment - Analytical determination and interpretation of thermal comfort using calculation of the PMV and PPD indices and local thermal comfort criteria, 2005.

ISO. 9920: Ergonomics of the thermal environment — Estimation of thermal insulation and water vapour resistance of a clothing ensemble, 2007.

Ito, K. Integrated numerical approach of computational fluid dynamics and epidemiological model for multi-scale transmission analysis in indoor spaces. *Indoor and Built Environment*, 23(7):1029–1049, 2014. doi: 10.1177/1420326X13516658.

Jain, A., Upadhyay, R. R., Chandra, S., Saini, M., and Kale, S. Experimental investigation of the flow field of a ceiling fan. In American Society of Mechanical Engineers, editor, *ASME 2004 Heat Transfer/Fluids Engineering Summer Conference*, pages 93–99, 2004.

Jain, V., Garg, V., Mathur, J., and Dhaka, S. Effect of operative temperature based thermostat control as compared to air temperature based control on energy consumption in highly glazed buildings. In *Building Simulation 2011: 12th Conference of International Building Performance Simulation Association, Sydney, 14-16 November.*, pages 2688–2695, Sydney, Austarlia, 2011. IBPSA.

Karava, P., Athienitis, A. K., Stathopoulos, T., and Mouriki, E. Experimental study of the thermal performance of a large institutional building with mixed-mode cooling and hybrid ventilation. *Building and Environment*, 57:313–326, 2012. doi: 10.1016/j.buildenv.2012.06.003.

Karjalainen, S. Thermal comfort and use of thermostats in Finnish homes and offices. *Building and Environment*, 44(6):1237–1245, 2009. doi: 10.1016/j.buildenv.2008.09.002.

Kumar, A., Hancke, G. P., and Member, S. An Energy-Efficient Smart Comfort Sensing System Based on the IEEE 1451 Standard for Green Buildings. *IEEE sensors journal*, 14(12):4245–4252, 2014.

Lai, A. C. K. and Yik, F. W. H. Perception of importance and performance of the indoor environmental quality of high-rise residential buildings. *Building and Environment*, 44:352–360, 2009. doi: 10.1016/j.buildenv.2008.03.013.

Lai, A. C. K., Mui, K. W., Wong, L. T., and Law, L. Y. An evaluation model for indoor environmental quality (IEQ) acceptance in residential buildings. *Energy and Buildings*, 41:930–936, 2009. doi: 10.1016/j.enbuild.2009.03.016.

Launder, B. and Spalding, D. The numerical computation of turbulent flows. *Computer methods in applied mechanics and engineering*, 3(2):269–289, 1974.

Licina, D., Melikov, A., Sekhar, C., and Tham, K. W. Human convective boundary layer and its interaction with room ventilation flow. *Indoor Air*, 25(1):21–35, 2015. doi: 10.1111/ina.12120.

Licina, D., Pantelic, J., Melikov, A., Sekhar, C., and Tham, K. W. Experimental investigation of the human convective boundary layer in a quiescent indoor environment. *Building and Environment*, 75:79–91, 2014. doi: 10.1016/j.buildenv.2014.01.016.

Limbachiya, V., Vadodaria, K., Loveday, D., and Haines, V. Identifying a suitable method for studying thermal comfort in people's homes. *Proceedings of the 7th Windsor Conference*, page 15, 2012.

Liu, W., Mazumdar, S., Zhang, Z., Poussou, S. B., Liu, J., Lin, C. H., and Chen, Q. State-of-the-art methods for studying air distributions in commercial airliner cabins. *Building and Environment*, 47(1):5–12, 2012. doi: 10.1016/j.buildenv.2011.07.005.

Lomas, K. and Kane, T. Summertime temperatures and thermal comfort in UK homes. *Building Research and Information*, 41(3):259–280, 2013. doi: 10.1080/09613218.2013.757886.

Lomas, K., Cook, M., and Fiala, D. Low energy architecture for a severe US climate: Design and evaluation of a hybrid ventilation strategy. *Energy and Buildings*, 39: 32–44, 2007. doi: 10.1016/j.enbuild.2006.03.032.

Loveday, D., Webb, L., Verma, P., Cook, M., Rawal, R., Vadodaria, K., Cropper, P., Brager, G., Zhang, H., Foldavary, V., Arens, E., Babich, F., Bobb, R., Ariffin, R., Kaam, S., and Toledo, L. The Role of Air Motionfor Providing Thermal Comfort in Residential / Mixed Mode Buildings: aMulti-partner Global Innovation Initiative (GII) Project. In *Proceedings of 9th Windsor Conference: MakingComfort Relevant*, 2016.

Manu, S., Shukla, Y., Rawal, R., Thomas, L. E., de Dear, R., Dave, M., and Vakharia, M. Assessment of Air Velocity Preferences and Satisfaction for Naturally Ventilated Office Buildings in India. In *PLEA 2014: 30th Conference on Passive and Low Energy Architecture*, number December, pages 1–8, 2014.

Manu, S., Shukla, Y., Rawal, R., Thomas, L. E., and de Dear, R. Field studies of thermal comfort across multiple climate zones for the subcontinent: India Model

for Adaptive Comfort (IMAC). *Building and Environment*, 98:55–70, 2016. doi: 10.1016/j.buildenv.2015.12.019.

Martinho, N., Lopes, A., and Gameiro da Silva, M. Evaluation of errors on the CFD computation of air flow and heat transfer around the human body. *Building and Environment*, 58:58–69, 2012. doi: 10.1016/j.buildenv.2012.06.018.

Matias, L., Almeida, S., Pina Santos, C., Rebelo, M., and Guedes Correia, M. Adaptive Thermal Comfort for Buildings in Portugal based on Occupants ' Thermal Perception. In *PLEA2009 - 26th Conference on Passive and Low Energy Architecture*, number June, Quebec City, 2009.

McLeod, R. S., Hopfe, C. J., and Kwan, A. An investigation into future performance and overheating risks in Passivhaus dwellings. *Building and Environment*, 70:189–209, 2013. doi: 10.1016/j.buildenv.2013.08.024.

Melikov, A. and Kaczmarczyk, J. Air movement and perceived air quality. *Building and Environment*, 47:400–409, 2012. doi: 10.1016/j.buildenv.2011.06.017.

Melikov, A., Hanzawa, H., and Fanger, P. Airflow characteristics in the occupied zone of heated spaces without mechanical ventilation. *ASHRAE Transactions*, 94(1):52 – 70, 1988.

Menter, F. R. Improved two-equation k–omega turbulence models for aerodynamic flows - NASA Technical Memorandum TM-103975. Technical report, NASA, Ames, CA, 1992a.

Menter, F. R. Performance of Popular Turbulence Models for Attached and Separated Adverse Pressure Gradient Flow. *AIAA journal*, 30:2066–2072, 1992b.

Menter, F. R. Zonal two equation k-turbulence models for aerodynamic flows. *AIAA journal*, 2906, 1993.

Menter, F. R. Two-equation eddy-viscosity turbulence model for engineering applications. *AIAA journal*, 32:1598–1605, 1994.

Menter, F. R. Eddy-viscosity transport equations and their relation to the k–epsilon model. *Journal of fluids engineering -Transactions of the ASME*, 119:876–884, 1997.

Menter, F. R., Kuntz, M., and Langtry, R. Ten years of industrial experience with the SST turbulence model. In *Proceedings of the Fourth International Symposium on Turbulence, Heat and Mass Transfer*, Begell House, Redding, CT, 2003.

MeshLab, 2016. http://meshlab.sourceforge.net/, last access 15.02.2016.

Mishra, A. K. and Ramgopal, M. Field studies on human thermal comfort — An overview. *Building and Environment*, 64:94–106, June 2013. doi: 10.1016/j.buildenv.2013.02.015.

Momoi, Y., Sagara, K., Yamanaka, T., and Kotani, H. Modeling of Ceiling Fan Based on Velocity Measurement for CFD Simulation of Airflow in Large Room. In *Proceedings of 9th international conference on air distribution in rooms*, volume 1, Coimbra, Portugal, 2004.

Momoi, Y., Sagara, K., Yamanaka, T., and Kotani, H. Modeling of prescribed velocity generated by ceiling fan based on velocity measurement for CFD simulation. In *Proceedings of 10th international conference on air distribution in rooms*, volume 1, Helsinki, Finland, 2007.

Nevins, R., Rohles, F., Springer, W., and Feyerherm, A. Temperature-humidity chart for thermal comfort of seated persons. *Ashrae Trans.*, 72:283–291, 1966.

Nicol, F. and Humphreys, M. Derivation of the adaptive equations for thermal comfort in free-running buildings in European standard EN15251. *Building and Environment*, 45(1):11–17, 2010. doi: 10.1016/j.buildenv.2008.12.013.

Nicol, F. and Wilson, M. A critique of European Standard EN 15251: strengths, weaknesses and lessons for future standards. *Building Research & Information*, 39 (2):183–193, 2011. doi: 10.1080/09613218.2011.556824.

Nicol, J. F. and Humphreys, M. A. Adaptive thermal comfort and sustainable thermal standards for buildings. *Energy and buildings*, 34(6):563–572, 2002.

Nielsen, P. V. Computational fluid dynamics and room air movement. *Indoor air*, 14 (Suppl 7):134–143, 2004. doi: 10.1111/j.1600-0668.2004.00282.x.

Nielsen, P. V. Fifty Years of CFD for Room Air Distribution. *Building and Environment*, 91:78–90, 2015. doi: 10.1016/j.buildenv.2015.02.035.

Niu, J. and Burnett, J. Integrating Radiant/Operative Temperature Controls into Building Energy Simulations. *ASHRAE Transactions*, 104(2):210, 1998.

Onset. HOBO U12 sensors, 2015. http://www.onsetcomp.com/products/data-loggers/u12-013, last access 15.06.2015.

Oseland, N. A. Predicted and reported thermal sensation in climate chambers, offices and homes. *Energy and Buildings*, 23:105–115, 1995. doi: 10.1016/0378-7788(95)00934-5.

Parsons, K. *Human Thermal Environments*. CRC Press - Taylor & Francis Group, Oxon, 3rd edition, 2014.

Pasut, W. and De Carli, M. Evaluation of various CFD modelling strategies in predicting airflow and temperature in a naturally ventilated double skin facade. *Applied Thermal Engineering*, 37:267–274, 2012. doi: 10.1016/j.applthermaleng.2011.11.028.

Pasut, W., Arens, E., Zhang, H., and Zhai, Y. Enabling energy-efficient approaches to thermal comfort using room air motion. *Building and Environment*, 79:13–19, 2014. doi: 10.1016/j.buildenv.2014.04.024.

Patel, V. C., Rodi, W., and Scheuerer, G. Turbulence models for near-wall and low Reynolds number flows-a review. *AIAA journal*, 23(9):1308–1319, 1985.

Pathan, A., Young, A., and Oreszczyn, T. UK domestic air conditioning: a study of occupant use and energy efficiency. In *Air Conditioning and the Low Carbon Cooling Challenge*, number July, 2008.

Peeters, L., de Dear, R., Hensen, J., and D'haeseleer, W. Thermal comfort in residential buildings: Comfort values and scales for building energy simulation. *Applied Energy*, 86(5):772–780, 2009. doi: 10.1016/j.apenergy.2008.07.011.

Prakash, D. and Ravikumar, P. Analysis of thermal comfort and indoor air flow characteristics for a residential building room under generalized window opening position at the adjacent walls. *International Journal of Sustainable Built Environment*, 2015. doi: 10.1016/j.ijsbe.2015.02.003.

Pt-teknik, 2017. http://pt-teknik.dk/ last access 15.06.2017.

Raja, I., Nicol, F., McCartney, K. J., and Humphreys, M. Thermal comfort: Use of controls in naturally ventilated buildings. *Energy and Buildings*, 33:235–244, 2001. doi: 10.1016/S0378-7788(00)00087-6.

Rhino, 2016. https://www.rhino3d.com/, last access 15.02.2016.

Rijal, H. B., Humphreys, M., and Nicol, F. Understanding occupant behaviour: the use of controls in mixed-mode office buildings. *Building Research & Information*, 37:381–396, 2009. doi: 10.1080/09613210902904221.

Schellen, L., Loomans, M., De Wit, M., Olesen, B., and van Marken Lichtenbelt, W. D. Effects of different cooling principles on thermal sensation and physiological responses. *Energy and Buildings*, 62:116–125, 2013a. doi: 10.1016/j.enbuild.2013.01.007.

Schellen, L., Loomans, M., Kingma, B. R. M., De Wit, M., Frijns, A. J. H., and van Marken Lichtenbelt, W. D. The use of a thermophysiological model in the built environment to predict thermal sensation: Coupling with the indoor environment and thermal sensation. *Building and Environment*, 59:10–22, 2013b. doi: 10.1016/j.buildenv.2012.07.010.

Schiavon, S. and Melikov, A. Energy saving and improved comfort by increased air movement. *Energy and Buildings*, 40:1954–1960, 2008. doi: 10.1016/j.enbuild.2008.05.001.

Schiavon, S., Hoyt, T., and Piccioli, A. Web application for thermal comfort visualization and calculation according to ASHRAE Standard 55. *Building Simulation*, 7:321–334, 2014a. doi: 10.1007/s12273-013-0162-3.

Schiavon, S., Rim, D., Pasut, W., and Nazaroff, W. Sensation of draft at ankles for displacement ventilation and underfloor air distribution systems. In *13th International Conference Indoor Air 2014*, Hong Kong, 2014b.

Seo, J., Park, J., and Choi, Y. Numerical study on human model shape and grid dependency for indoor thermal comfort evaluation. *Journal of Mechanical Science and Technology*, 27(2):397–405, 2013. doi: 10.1007/s12206-012-1252-3.

Sevilgen, G. and Kilic, M. Numerical analysis of air flow, heat transfer, moisture transport and thermal comfort in a room heated by two-panel radiators. *Energy and Buildings*, 43(1):137–146, January 2011. doi: 10.1016/j.enbuild.2010.08.034.

Shah, N., Paul, W., and Amol, P. Cooling the Planet: Opportunities for Deployment of Superefficient Room Air conditioners. Technical report, Lawrence Berkeley National Laboratory and Navigant consulting, Inc., 2013.

Shikder, S., Mourshed, M., and Price, A. Summertime impact of climate change on multi-occupancy British dwellings. *Open House International*, 37(4):50–60, 2012.

Spalart, P., Jou, W., Strelets, M., and Allmaras, S. Comments on the feasibilty of les for wings and on the hybrid rans/les approach, advances in dns/les, 1st afosr int. conf. on dns/les, 1997.

Spindler, H. C. and Norford, L. K. Naturally ventilated and mixed-mode buildings-Part II: Optimal control. *Building and Environment*, 44(4):750–761, 2009. doi: 10.1016/j.buildenv.2008.05.018.

Stolwijk, J. Mathematical model of thermoregulation. physiological and behavioral temperature regulation, 1970.

Stolwijk, J. A mathematical model of physiological temperature regulation in man. Technical report, NASA CR-1855, Washington, DC, 1971.

Stolwijk, J. and Hardy, J. Temperature regulation in man—a theoretical study. *Pflügers Archiv European Journal of Physiology*, 291(2):129–162, 1966.

Teixeira, S., Falcao, E., Rodrigues, N., and Teixeira, J. C. Sensibility Studies on a Transient Thermal Model of the Human Body. In *14th International Conference on Computational Science and Its Applications*, pages 176–180, 2014. doi: 10.1109/ICCSA.2014.40.

Versteeg, H. K. and Malalasekera, W. *An introduction to computational fluid dynamics: the finite volume method*. Pearson Education, 2007.

Wallin, S. and Johansson, A. An explicit algebraic Reynolds stress model for incompressible and compressible turbulent flows. *Journal of Fluid Mechanics*, 403: 89–132, 2000.

Wang, M., Lin, C. H., and Chen, Q. Advanced turbulence models for predicting particle transport in enclosed environments. *Building and Environment*, 47(1): 40–49, 2012. doi: 10.1016/j.buildenv.2011.05.018.

Wang, Z., Zhang, L., Zhao, J., and He, Y. Thermal comfort for naturally ventilated residential buildings in Harbin. *Energy and Buildings*, 42(12):2406–2415, 2010. doi: 10.1016/j.enbuild.2010.08.010.

Wang, Z., Zhang, L., Zhao, J., He, Y., and Li, A. Thermal responses to different residential environments in Harbin. *Building and Environment*, 46(11):2170–2178, 2011. doi: 10.1016/j.buildenv.2011.04.029.

Wilcox, D. C. Reassessment of the Scale-determining Equation for Advanced Turbulence Models. *AIAA journal*, 26(11):1299–1310, 1988.

Wilcox, D. C. Comparison of Two-equation Turbulence Models for Boundary Layers with Pressure Gradients. *AIAA journal*, 31(8):1414–1421, 1993a.

Wilcox, D. C. Turbulence Modelling for CFD. Technical report, DCW Industries Inc., La Canada, CA, 1993b.

Wilcox, D. C. Simulating Transition with a Two-equation Turbulence Model. *AIAA journal*, 32:247–255, 1994.

Willmott, C. J. and Matsuura, K. Advantages of the mean absolute error (mae) over the root mean square error (rmse) in assessing average model performance. *Climate research*, 30(1):79–82, 2005.

Wissler, E. H. A mathematical model of the human thermal system. *Bulletin of Mathematical Biology*, 26(2):147–166, 1964.

Yang, B., Schiavon, S., Sekhar, C., Cheong, D., Wai, K., and Nazaroff, W. Cooling effi ciency of a brushless direct current stand fan. *Building and Environment*, 85: 196–204, 2015. doi: 10.1016/j.buildenv.2014.11.032.

Yang, L., Ye, M., and He, B.-J. CFD simulation research on residential indoor air quality. *The Science of the total environment*, 472:1137–44, February 2014. doi: 10.1016/j.scitotenv.2013.11.118.

Yousaf, R., Wood, D., Cook, M., Yang, T., Hodder, S., and Passmore, M. CFD and PIV based investigation of indoor air flows dominated by buoyancy effects generated by human occupancy and equipment. In *12th Conference of International Building Performance Simulation Association*, pages 1465–1472, Sydney, 2011.

Zhai, Y., Zhang, H., Zhang, Y., Pasut, W., Arens, E., and Meng, Q. Comfort under personally controlled air movement in warm and humid environments. *Building and Environment*, 65:109–117, 2013. doi: 10.1016/j.buildenv.2013.03.022.

Zhai, Y., Zhang, Y., Zhang, H., Pasut, W., Arens, E., and Meng, Q. Human comfort and perceived air quality in warm and humid environments with ceiling fans. *Building and Environment*, 90:178–185, 2015. doi: 10.1016/j.buildenv.2015.04.003.

Zhai, Z. J., Zhang, Z., Zhang, W., and Chen, Q. Y. Evaluation of various turbulence models in predicting airflow and turbulence in enclosed environments by CFD: part 1 - Summary of prevalent turbulence models. *Hvac&R Research*, 13:853–870, 2007. doi: 10.1080/10789669.2007.10391459.

Zhang, H., Arens, E., Huizenga, C., and Han, T. Thermal sensation and comfort models for non-uniform and transient environments, part III: Whole-body sensation and comfort. *Building and Environment*, 45(2):399–410, February 2010a. doi: 10.1016/j.buildenv.2009.06.020.

Zhang, H., Arens, E., Huizenga, C., and Han, T. Thermal sensation and comfort models for non-uniform and transient environments, part II: Local comfort of individual body parts. *Building and Environment*, 45(2):389–398, February 2010b. doi: 10.1016/j.buildenv.2009.06.015.

Zhang, H., Arens, E., Huizenga, C., and Han, T. Thermal sensation and comfort models for non-uniform and transient environments: Part I: Local sensation of individual body parts. *Building and Environment*, 45(2):380–388, February 2010c. doi: 10.1016/j.buildenv.2009.06.018.

Zhang, R., Lam, K. P., Yao, S.-c., and Zhang, Y. Coupled EnergyPlus and computational fluid dynamics simulation for natural ventilation. *Building and Environment*, 68:100–113, 2013. doi: 10.1016/j.buildenv.2013.04.002.

Zhang, Z., Zhang, W., Zhai, Z. J., and Chen, Q. Y. Evaluation of Various Turbulence Models in Predicting Airflow and Turbulence in Enclosed Environments by CFD: Part 2—Comparison with Experimental Data from Literature. *HVAC&R Research*, 13(6):871–886, 2007. doi: 10.1080/10789669.2007.10391460.

Zhao, Y., Zhang, H., Arens, E., and Zhao, Q. Thermal sensation and comfort models for non-uniform and transient environments, part IV: Adaptive neutral setpoints and smoothed whole-body sensation model. *Building and Environment*, 72:300–308, February 2014. doi: 10.1016/j.buildenv.2013.11.004.

Zhu, Q., Yi, J., Sheng, S., Wen, C., and Hu, H. A Computer-Aided Modeling and Measurement System for Environmental Thermal Comfort Sensing. *IEEE transactions on instrumentation and measurement*, 64(2):478–486, 2015a.

Zhu, S., Srebric, J., Rudnick, S. N., Vincent, R. L., and Nardell, E. A. Numerical modeling of indoor environment with a ceiling fan and an upper-room ultraviolet germicidal irradiation system. *Building and Environment*, 72:116–124, 2014. doi: 10.1016/j.buildenv.2013.10.019.

Zhu, Y., Luo, M., Ouyang, Q., Huang, L., and Cao, B. Dynamic characteristics and comfort assessment of airflows in indoor environments: A review. *Building and Environment*, 2015b. doi: 10.1016/j.buildenv.2015.03.032.